



**University of
Sunderland**

Yeo, Li Key (2022) Evaluation of niosome formulations containing methylene blue and cinnarizine manufactured by thin film hydration and microfluidic methods. Doctoral thesis, University of Sunderland.

Downloaded from: <http://sure.sunderland.ac.uk/id/eprint/14697/>

Usage guidelines

Please refer to the usage guidelines at <http://sure.sunderland.ac.uk/policies.html> or alternatively contact sure@sunderland.ac.uk.

Evaluation of Niosome Formulations Containing
Methylene Blue and Cinnarizine Manufactured by
Thin Film Hydration and Microfluidic Methods

Li Key Yeo

A thesis submitted in partial fulfilment of the requirements of the
University of Sunderland for the degree of Doctor of Philosophy

PhD

March 2022

Abstract of Research

Enabling formulations has been emerging in formulation development owing to their characteristics to improve critical quality attributes of the drug delivery systems. This study focused on the preparation of niosome formulation as nanocarrier drug delivery system for the delivery of small drug molecules. This study was aimed to prepare niosome formulations to encapsulate cinnarizine, a poorly water-soluble drug with narrow absorption window in the stomach using the conventional thin film hydration (TFH) method and microfluidic (MF) method. Small drug molecule methylene blue was used as a model hydrophilic drug for optimisation of manufacturing and formulation parameters in order to pave the way for cinnarizine-containing niosome formulations.

The self-assembled niosomes were based on a 45/45/10 molar ratio of Span® 60 surfactant, cholesterol, and co-surfactant, respectively. Different drug-exciipient ratios and different co-surfactant types (i.e. Cremophor® ELP, Cremophor® RH40 and Solutol® HS15) were investigated. Manufacturing variables in thin film hydration method were investigated, such as the hydration time and hydration volume. The effect of sonication on TFH-based niosomes was investigated. On the other hand, in microfluidic method, investigated manufacturing variables were total flow rate (mL/min) and flow rate ratio of the aqueous to organic solvents of the system parameters. Formulation parameters were drug concentration and total surfactant/lipid concentration. Differential scanning calorimetry (DSC) and Fourier transform infrared spectroscopy (FTIR) were used to analyse the interactions between the model drug and formulation excipients. Additionally, the shape and size of all prepared niosome formulations were analysed using transmission electron microscopy (TEM) and dynamic light scattering (DLS) techniques. The drug release characteristics of the formulations were evaluated using dialysis technique in 0.1M hydrochloric acid (pH1.2) at 37±1 °C under agitation. Determination and quantification of drug were obtained using high-performance liquid chromatography (HPLC) for encapsulation efficiencies and release data. Release data were analysed by fitting to release kinetic model to describe drug release behaviour. Stability studies of niosome formulations at a refrigeration temperature (2-8 °C) and room temperature (21-25 °C) for one month were evaluated for their size and distribution. The incorporation of different mucoadhesive polymers (chitosan solution and alginate-based Gaviscon® suspension) with MF-based niosomes were prepared to study their feasibility to adhere to gastric mucosa for prolonged retention of the formulation system containing drug with an absorption window in the stomach, in order to enhance drug absorption and bioavailability. A modified HPLC with evaporative light scattering detection (HPLC-ELSD) method was employed in the direct quantification of Span® 60 and cholesterol recovery of the MF-based niosomes before and after purification process (gel chromatography filtration), in order to understand the applicability on preparation of niosomes using microfluidics.

Generally, based on the size and distribution data, it was found that TFH-based niosome formulations showed large and highly polydisperse, comparing to MF-based niosome formulations. Niosome formulations released entrapped drug in a slow release pattern, offering a more consistent drug absorption with a prolonged gastric retention time. At the same time, mucoadhesive formulations have shown adhesion to the stomach mucosa, showing retentive potential for drug absorption. This study demonstrated and evaluated both the conventional TFH-based niosome and advanced MF-based niosome formulations encapsulating small drug molecules – cinnarizine (poorly water-soluble) and methylene blue (hydrophilic), offers insights on controlling manufacturing parameters to produce niosome formulations for their applicability as dosage forms.

Keywords: Niosome, methylene blue, cinnarizine, thin film hydration, microfluidics

Research activity

Publications

Yeo, L.K., Olusanya, T.O.B., Chaw, C.S. and Elkordy, A.A. (2018) Brief effect of a small hydrophobic drug (cinnarizine) on the physicochemical characterisation of niosomes produced by thin film hydration and microfluidic methods. *Pharmaceutics*, 10, 185.

Yeo, L.K.; Chaw, C.S.; Elkordy, A.A. The Effects of Hydration Parameters and Co-Surfactants on Methylene Blue-Loaded Niosomes Prepared by the Thin Film Hydration Method. *Pharmaceutics* 2019, 12, 46.

Yeo, L.K.; Chaw, C.S.; Elkordy, A.A. Effects of preparation methods on the characteristics of niosomes. *British Journal of Pharmacy* 2019.

Yeo, L.K.; Chaw, C.S.; Elkordy, A.A. Non-ionic surfactant-based drug delivery system for oral delivery of poorly water-soluble drug for dissolution and bioavailability enhancement. *International Journal of Pharmacy Practice* 2020, 28, S2.

Conferences with poster presentations

1. University of Sunderland Research Conference, University of Sunderland (05/06/2017) Title: Novel niosomal formulations for entrapment of cinnarizine as a model of poorly water-soluble drug.
2. EPSRC EHDA Network 2nd Pharm. Tech. Conference, University College London (14/07/2017) Title: Novel niosomal formulations for entrapment of cinnarizine as a model of poorly water-soluble drug.
3. The Great North Pharmacy Research Conference, University of Sunderland (21/07/2017) Title: Novel niosomal formulations for entrapment of cinnarizine as a model of poorly water-soluble drug.

4. North East Postgraduate (NEPG) Conference, Newcastle (30/10/2017) Title: Microfluidic-based preparations of novel niosomal formulations for entrapment of cinnarizine as a model poorly water-soluble drug.
5. 11th PBP World Meeting on Pharmaceutics, Biopharmaceutics and Pharmaceutical Technology, Granada, Spain (21/3/2018) Title: Microfluidic-based preparations of novel niosomal formulations for entrapment of cinnarizine as a model poorly water-soluble drug.
6. APS PharmSci 2018 Conference, Glasgow (07/09/2018) Title: Effects of preparation methods on the characteristics of niosomes.
7. 9th Chemical Nanoscience Symposium Newcastle 2019, Newcastle Uni (04/04/2019) Title: Novel microfluidic-based niosomes to target narrow absorption drug (cinnarizine).
8. 10th APS International PharmSci Conference 2019, University of Greenwich, London (11/09/2019-13/09/2019) Title: Analysis of novel mucoadhesive microfluidic-based niosomes.

Oral presentation

Faculty research seminar (13/03/2019)

Title: Vesicular systems for a small drug molecule (cinnarizine).

Faculty research seminar (24/11/2021)

Title: Characterisation of niosome formulations manufactured by thin film hydration and microfluidic methods

Acknowledgements

Firstly, I would like to express my gratitude to my supervisors Professor Amal Ali Elkordy and Dr Cheng Shu Chaw for their guidance, advice and support throughout this project.

I would like to thank Paul Neesam, Maria Barry, Paul Stronach and Kayleigh Ironside for all their technical assistance.

I would like to thank all my colleagues at the University of Sunderland for their support.

I would like to thank the graduate research team, library support team and the researcher development team for all their assistance, support and guidance.

Finally, I would like to thank my family for their never-ending support and encouragement to me for completing this research degree and making them proud.

Table of contents

<i>Abstract of Research</i>	<i>ii</i>
<i>Research activity</i>	<i>iii</i>
<i>Acknowledgements</i>	<i>vi</i>
<i>Table of contents</i>	<i>vii</i>
<i>List of tables</i>	<i>xiii</i>
<i>List of figures</i>	<i>xvii</i>
<i>List of abbreviations</i>	<i>xxii</i>
<i>List of equations</i>	<i>xxiv</i>
1. Introduction	2
1.1. Drug solubility and dissolution	3
1.2. Drug absorption	6
1.2.1. Oral drug absorption from the gastrointestinal (GI) tract	7
1.2.2. Factors affecting gastric drug absorption	8
1.2.3. Solubility and dissolution enhancement approaches	8
1.3. Niosomes as drug delivery system	14
1.3.1. Niosome component: Spans	19
1.3.2. Niosome component: Cholesterol	21
1.3.3. Niosome component: Co-surfactants	23
1.4. Niosomes manufacturing methods	24
1.4.1. Reverse phase evaporation method	25
1.4.2. Heating method	25

1.4.3.	Ether injection method.....	26
1.4.4.	Thin film hydration method.....	27
1.4.5.	Microfluidic method	28
1.5.	Microfluidic method	28
1.5.1.	NanoAssemblr® Benchtop system.....	30
1.6.	Encapsulation efficiency, drug loading and drug release	39
1.7.	Gastric physiology (stomach)	41
1.7.1.	Gastric mucus layer as physiological barrier.....	42
1.7.2.	Mucus composition and structure.....	42
1.8.	Mucoadhesion.....	47
1.9.	Analysis of non-ionic surfactant-based drug delivery system	49
1.10.	Posed research questions	51
1.11.	Aim and objectives	52
1.12.	Novelty of the research	53
1.13.	Thesis structure	53
2.	<i>Materials and methods</i>.....	57
2.1.	Materials.....	57
2.1.1.	Model drugs.....	57
2.1.2.	Non-ionic surfactant and co-surfactants	58
2.1.3.	Lipids.....	62
2.1.4.	Polymers for mucoadhesion study	63
2.1.5.	Reagents, buffers and solvents.....	65
2.2.	Methods.....	66
2.2.1.	Manufacturing of niosomes: Thin film hydration method (TFH).....	66

2.2.2.	Manufacturing of niosomes: Microfluidic method (MF)	68
2.3.	Calibrations	74
2.3.1.	Calibration plot: Cinnarizine	74
2.3.2.	Calibration plot: Methylene blue.....	81
2.3.3.	Calibration plot: Mucin	82
2.3.4.	Calibration plot: Coumarin-6	83
2.4.	Purification of niosomes: Gel chromatography filtration.....	85
2.4.1.	Determination of encapsulation efficiency (EE) and drug loading into niosomes (for actual and expected loading).....	86
2.4.2.	Freeze-drying of purified niosomes	87
2.5.	Preparation of mucoadhesive niosomes	88
2.5.1.	Mucin adsorption study.....	88
2.5.2.	Period Acid Schiff (PAS) mechanism	89
2.5.3.	Viscosity measurement of mucoadhesive biopolymers	89
2.5.4.	Mucoadhesion study using mucoadhesive niosomes entrapped with coumarin-6	91
2.6.	Microfluidic-based niosome component recovery	92
2.6.1.	After preparation (Span® 60/cholesterol recovery) and after purification (niosome recovery) ..	92
2.6.2.	Preparation of niosome component standards for calibration using high performance liquid chromatography with evaporative light scattering detection (HPLC-ELSD).....	92
2.6.3.	Niosome component calibration using high performance liquid chromatography with evaporative light scattering detection (HPLC-ELSD)	93
2.7.	Characterisation of niosomes	94
2.7.1.	Niosomes morphology: optical microscopy.....	94
2.7.2.	Niosomes morphology: transmission electron microscopy (TEM)	95
2.7.3.	Particle size, distribution and zeta potential measurements	95
2.7.4.	Fourier-transform infrared (FTIR) spectroscopy	96
2.7.5.	Differential scanning calorimetry (DSC).....	96

2.7.6.	<i>In vitro</i> drug release study	97
2.8.	Statistical analysis	98
3.	<i>Manufacturing of niosomes containing methylene blue as a model hydrophilic drug</i>	99
3.1.	Overview	100
3.2.	Aims and Objectives	104
3.3.	Results and Discussion.....	105
3.3.1.	Effect of thin film hydration process and formulation parameters on niosome characteristics	105
3.3.2.	Influence of manufacturing methods and formulation compositions on niosome characteristics	109
3.3.3.	Effect of storage on niosome size	112
3.4.	Conclusion.....	116
4.	<i>Manufacturing of niosomes containing cinnarizine as a model poorly water-soluble drug</i>	118
4.1.	Overview	119
4.2.	Aims and Objectives	124
4.3.	Results and Discussion.....	125
4.3.1.	Vesicle size distribution and encapsulation efficiency: Effect of surfactant/lipid concentrations and sonication on niosomes manufactured by thin film hydration method	125
4.3.2.	Vesicle size distribution and encapsulation efficiency: Effect of TFR and FRR on the vesicle size and distribution of MF niosomes	127
4.3.3.	Vesicle size distribution and encapsulation efficiency: Effect of loading drug on microfluidic-based niosome characteristics	130
4.3.4.	Vesicle size distribution and encapsulation efficiency: Effect of manufacturing methods and formulation compositions on niosome characteristics.....	132

4.3.5.	Vesicle size distribution and encapsulation efficiency: Effect of manufacturing methods and total surfactant/lipid concentrations on niosome characteristics	135
4.3.6.	Effect of manufacturing method on drug release	136
4.3.7.	Morphological properties of niosome vesicles	137
4.3.8.	Fourier-transform infrared (FTIR) spectroscopy	139
4.3.9.	Differential scanning calorimetry (DSC).....	142
4.3.10.	Effect of hydrophilic and hydrophobic drugs loading on niosome characteristics	144
4.4.	Conclusion.....	145
5.	<i>Mucoadhesion study.....</i>	147
5.1.	Overview.....	148
5.2.	Aim and Objectives.....	153
5.3.	Results and Discussion.....	154
5.3.1.	Bulk behaviour of mucoadhesive biopolymer solution: viscosity.....	154
5.3.2.	Bulk behaviour: Influence of the mucoadhesive biopolymer on zeta potential of mucin dispersion and manufactured niosomes.....	157
5.3.3.	Adsorption of mucin on manufactured mucoadhesive niosomes.....	160
5.3.4.	Adsorption of mucoadhesive niosomes on gastric mucosa.....	163
5.4.	Conclusion.....	167
6.	<i>Recovery study.....</i>	169
6.1.	Overview.....	169
6.2.	Aim and Objectives.....	171
6.3.	Results and Discussion.....	172
6.3.1.	Span® 60 calibration	175
6.3.2.	Cholesterol calibration.....	177

6.3.3.	Component recovery: Cholesterol recovery from surfactant/lipid mixture with presence of drug	178
6.3.4.	Component recovery: Cholesterol recovery from lipid mixture with presence of Cremophor® ELP as co-surfactant.....	179
6.3.5.	Formulation recovery: Cholesterol recovery from microfluidic-based niosomes	180
6.3.6.	Evaluation of microfluidics manufacturing: process and formulation recovery.....	182
6.4.	Conclusion.....	184
7.	<i>General conclusions and future work</i>	188
7.1.	Effect of niosome manufacturing methods on characteristics of niosomes encapsulated with methylene blue and cinnarizine	188
7.2.	Mucoadhesion.....	189
7.3.	Recovery study for microfluidic-based niosomes	190
7.4.	Potential future works.....	190
8.	<i>References</i>	192

List of tables

Table 1-1: Description of solubility terms (Part II - British Pharmacopoeia, 2020).....	3
Table 1-2: Niosome vesicle types, vesicle size ranges and their structures.....	16
Table 1-3: Examples of Span® niosomes that have been investigated as oral drug delivery system.	20
Table 2-1: Physicochemical properties of cinnarizine (CIN), methylene blue (MB) and coumarin-6 (C-6).	57
Table 2-2: Physicochemical properties of Span® 60.....	59
Table 2-3: Physicochemical properties of co-surfactants.	61
Table 2-4: Physicochemical properties of lipids.	62
Table 2-5: Compositions of niosomal formulations (total surfactant/lipid content of 200mg and drug content of 0.5 mg/mL).	67
Table 2-6: General experimental details on system and formulation parameters.....	70
Table 2-7: Experimental details and formulation compositions (component concentrations) in determining the effect of total flow rate (mixing speed).	71
Table 2-8: Experimental details and formulation compositions (component concentrations) in determining the effect of flow rate ratio (aqueous: organic).	71
Table 2-9: Evaluation of %RSD and recovery during the assessment of accuracy..	81
Table 2-10: Gradient elution.....	84
Table 2-11: polymer solutions used in viscosity measurement study with parameters used.	90
Table 2-12: Gradient elution.....	94
Table 3-1: Effect of hydration volumes on niosome characteristics for before and after sonication process. Final concentration of MB expected was 0.5 mg/mL.	107

Table 3-2: Effect of hydration times on niosome characteristics for before and after sonication process. Final concentration of MB expected was 0.5 mg/mL.	108
Table 3-3: Effect of methylene blue concentrations on niosome characteristics for before and after sonication process. The final concentration of MB expected was 0.5 mg/mL.	109
Table 3-4: Effect of manufacturing methods and formulation compositions on niosome characteristics. (All post-G50 measurements. TFH after sonication measurements. All final surfactant/lipid concentration at 20mg/mL. Final concentration of MB expected was 0.5 mg/mL.....	110
Table 3-5: Effect of manufacturing methods and different final surfactant/lipid concentrations on niosome characteristics. Final concentration of MB expected was 0.5 mg/mL. (All post-G50 measurements. TFH after sonication measurements.)..	111
Table 4-1: Effect of different final surfactant/lipid concentrations used on niosome size and distribution in TFH-based niosomes comprised of different formulation compositions, without sonication as post-preparation processing technique for size reduction.	126
Table 4-2: Niosome characteristics for sonicated TFH-niosome formulations at different final total surfactant/lipid concentrations before purification process.....	127
Table 4-3: Effect of total flow rate on niosome size and distributions post-cartridge.	129
Table 4-4: Effect of flow rate ratio (aqueous: organic) on niosome size and distribution post-cartridge; encapsulation efficiency post-purification.	129
Table 4-5: Effect of cinnarizine loading characteristics of microfluidic-based niosomes.	131

Table 4-6: Effect of manufacturing methods and formulation compositions on niosome characteristics.	133
Table 4-7: Niosome characteristics for sonicated TFH-based niosomes and microfluidic-based niosomes at different final total surfactant/lipid concentrations.	136
Table 4-8: Principal peaks with respective assignments of pure cinnarizine in its free base form.	140
Table 4-9: Physicochemical properties of niosomes encapsulated with cinnarizine (CIN) and methylene blue (MB).....	145
Table 5-1: Rheological data of mucoadhesive biopolymer dispersions based on Hershel Bulkley model ($n = 3 \pm SD$).	157
Table 5-2: Zeta potential measurement data of mucin dispersion (1 mg/mL), mucin-biopolymer mixtures and biopolymer-niosomes suspensions at pH 4.5. Preparation details shown in Section 2-5.....	160
Table 5-3: Mucin binding efficiency (%) of mucoadhesive niosomes.	162
Table 5-4: Summary of the physicochemical properties of microfluidic-based niosomes (without and with coumarin-6 entrapped). Niosome formulation studied was comprised of Span® 60: cholesterol: Cremophor® ELP.....	163
Table 6-1: Evaluation of %RSD and recovery during calibration of Span® 60.	176
Table 6-2: Evaluation of %RSD and recovery of cholesterol during calibration of cholesterol standard solutions.	178
Table 6-3: Evaluation of %RSD and recovery of cholesterol in the surfactant/lipid mixture of Span® 60 (S60) and cholesterol (CHO) at a total concentration of 2.0 mg/mL. Known drug (cinnarizine) concentration at 0.05 mg/mL.	179
Table 6-4: Evaluation of %RSD and recovery of cholesterol in the lipid mixture of Span® 60 (S60, cholesterol (CHO) and Cremophor® ELP (ELP) at a total lipid	

concentration of 2.0 mg/mL. Known drug (cinnarizine) concentration at 0.05 mg/mL.
..... 180

Table 6-5: Evaluation of recovery of cholesterol within microfluidic-based niosomes without drug encapsulation. Calculated theoretical total composition/cholesterol concentrations based on the initial total lipid concentration, the flow rate ratio for mixing, and dilution factor on filtration process and sample preparation. The total composition was Span® 60: cholesterol (1:1). 182

Table 6-6: Physicochemical characteristics of microfluidic-based niosomes and their percentage recovery of cholesterol before and after gel filtration. For this study, microfluidic-based niosomes without drug were studied. The niosome composition was Span® 60: cholesterol (1:1). 184

List of figures

Figure 1-1: Critical Packing Parameter (CPP) of surfactant where v is lipophilic tail volume, l_c is the critical lipophilic tail length, and a_0 is the polar head surface area per molecule at the hydrocarbon-water interface.	17
Figure 1-2: Chemical structure of sorbitan monostearate (Span® 60; C ₂₄ H ₄₆ O ₆). Drawn by ChemDraw.	20
Figure 1-3: Chemical structures of Span® 60 and cholesterol showing the hydrogen bonding interaction between the two molecules drawn by ChemDraw. [Adapted from Nasser, 2005]	23
Figure 1-4: Schematic illustration for niosome preparation by reverse phase evaporation method.....	25
Figure 1-5: Schematic illustration of niosome preparation by heating method.	26
Figure 1-6: Schematic illustration for niosome preparation by ether injection method.	26
Figure 1-7: Schematic diagram for niosome preparation using thin film hydration method.	28
Figure 1-8: Schematic diagrams of microfluidic platforms: (A) a hydrodynamic flow focusing; (B) a microfluidic micro-mixer; and (C) staggered herringbone micro-mixer. Figure adapted from Damiani et al., (2018).....	29
Figure 1-9: The stomach (adapted from Wilson and Washington, 1989).	42
Figure 2-1: Chemdraw chemical structures of (A) cinnarizine, (B) methylene blue, and (C) coumarin-6. All drawn by ChemDraw.	58
Figure 2-2: Chemdraw chemical structure of Span® 60.....	59

Figure 2-3: Chemdraw chemical structures of (A) Cremophor® ELP; (B) Cremophor® RH40; (C) Solutol® HS15; and (D) Lauroglycol® 90 (C ₁₅ H ₃₀ O ₃).	61
Figure 2-4: Chemdraw chemical structures of (A) cholesterol ;(B) glycerol monostearate (GMS); and (C) dipamitoylphosphatidylcholine (DPPC).	63
Figure 2-5: Alginic acid structure from Liang et al. (2015).	64
Figure 2-6: Process overview of thin film hydration method for niosome preparation.	67
Figure 2-7: NanoAssemblr® Benchtop instrumental system (image was taken in our laboratory, Fleming 107, University of Sunderland).	68
<i>Figure 2-8: NanoAssemblr® microfluidic cartridge back (left) and front (right).</i>	68
Figure 2-9: Inner view of the Benchtop instrument showing the syringe pump system and the outlets (sample and waste collection).	69
Figure 2-10: Schematic diagram for the mechanism of action of NanoAssemblr™ microfluidic cartridge in the niosome preparation to encapsulate cinnarizine. Mixing of two fluids occurs at the staggered herringbone micromixer (SHM) feature. Niosome encapsulation of methylene blue prepared from the mixing between MB-containing aqueous buffer and dissolved excipients-containing organic solvent.	69
<i>Figure 2-11: Diagram depicting two fluids mixing in a NanoAssemblr™ microfluidic cartridge (adapted from Precision Nanosystems Inc.).</i>	73
Figure 2-12: Calibration plot for cinnarizine measured using UV spectrophotometry.	75
Figure 2-13: Gradient elution.	76
Figure 2-14: Calibration plot of cinnarizine (0.01 to 10 µg/mL) measured using HPLC - linearity assessment of the method. The known cinnarizine concentrations were 0.01,	

0.05, 0.1, 0.5, 1, 2, 5 and 10 µg/mL. Calibration curve was plotted starting from 0.01 µg/mL.....	77
Figure 2-15: (A) drug-free formulation (baseline); (B) cinnarizine-containing formulation.....	78
Figure 2-16: Cinnarizine quantification – method precision assessment (top) intraday and (below) interday linearity plots with linear regression coefficients.....	80
Figure 2-17: Methylene blue calibration curve.....	81
Figure 2-18: Calibration curve of mucin.....	83
Figure 2-19: Calibration curve of coumarin-6 standard solutions.....	84
Figure 2-20: Pararosaniline hydrochloride (colourless on the left and magenta colour on the right).....	89
Figure 3-1: Graphical abstract for manufacturing of niosomes containing methylene blue as a model hydrophilic drug.....	99
Figure 3-2: Graphs showing average vesicle sizes of Span® 60: cholesterol: Cremophor® ELP niosomes of different total surfactant/lipid concentrations prepared by thin film hydration method without sonication, stored at room temperature (top) and at fridge temperature (bottom). Initial concentration of MB used was 0.5 mg/mL. Different independent batches of niosomes prepared for room temperature and refrigerated storage.....	113
Figure 3-3: Graphs showing average vesicle sizes of thin-film hydration niosomes without sonication (top) and with sonication (bottom). Error bars were omitted for the clarity of the plot. Both niosome suspensions were stored at fridge temperature 4°C. Non-sonicated niosomes were prepared independently from the niosome batches prepared shown in Figure 3-1. Initial concentration of MB used was 0.5 mg/mL.	115

Figure 3-4: Graph showing particle size of microfluidic-based niosomes were stored at fridge temperature 4°C. Formulations of Span® 60: cholesterol: Cremophor® ELP at different total surfactant/lipid concentrations. 116

Figure 4-1: Graphical abstract for manufacturing of niosomes containing cinnarizine as a model poorly water-soluble drug..... 118

Figure 4-2: Structure of cinnarizine (C₂₆H₂₈N₂) in free base and salt forms (Chemdraw).
..... 120

Figure 4-3: Line curves showed size changes upon refrigerated storage for Span® 60: cholesterol: Cremophor® ELP niosomes prepared by using microfluidic at different flow rate ratios (FRR) and the same formulation prepared using thin film hydration followed by sonication (n=3)..... 130

Figure 4-4: Line curves showed size changes upon room temperature (23±2 °C) and refrigerated storage (4±2 °C) for purified microfluidic-based niosomes comprised of different formulation compositions..... 134

Figure 4-5: In vitro drug release plot shows the cumulative drug release over 24 hours period in simulated gastric fluid without enzymes (pH 1.2 and 37 °C) for cinnarizine-loaded S60:Cho:ELP niosomes manufactured by thin film hydration and microfluidic methods. Initial drug concentration used was 0.5 mg/mL. Error bars have been omitted intentionally for the clarity of the graph..... 137

Figure 4-6: Transmission electron microscopy images obtained of (left) S60: Cho MF-niosomes (TFR12 mL/min, FRR4:1); (right) S60: Cho: ELP MF-niosomes (TFR 12mL/min, FRR 1:1)..... 138

Figure 4-7: Transmission electron microscopy images obtained of (left) S60: Cho: ELP sonicated TFH-niosomes; (right) S60: Cho: RH40 sonicated TFH-niosomes. 139

Figure 4-8: FTIR spectra for (A) individual pure ingredient: cholesterol (green), Cremophor® ELP (blue), Cremophor® RH40 (purple), Solutol® HS15 (black) and Span® 60 (red); (B) pure cinnarizine base.....	141
Figure 4-9: DSC thermograms (heat flow as a function of temperature; exothermic up) for (A) pure raw ingredients of niosome formulation composition; (B) S60: Cho: ELP TFH-niosomes; (C) S60: Chol: RH40 TFH-niosomes; and (D) S60: Cho: HS15 TFH-niosomes.....	143
Figure 4-10: DSC thermograms for (a) pure main raw formulation ingredients; and (b) freeze-dried S60: Cho: ELP MF-niosomes with the addition of mannitol as lyoprotectant.....	143
Figure 5-1: Graphical abstract for mucoadhesion study.....	147
Figure 5-2: Herschel Bulkley flow curves for 0.6 % w/v CS LMW (top left); 1.25 % w/v CS HV (top right); and Gaviscon® alginate suspension (bottom). Raw data shown in red and fitted curve shown in blue.....	156
Figure 5-3: Flow curves for different types of non-Newtonian fluid behaviours. (Adapted from Chhabra, 2010).....	157
Figure 5-4: Calibration of mucin standard dispersions (25 to 150 µg/mL) using PAS colorimetric method (colourless to magenta) by ultraviolet spectrophotometer at 555 nm.....	161
Figure 5-5: Chromatogram of coumarin-6 (10 µg/mL) detected at 5.2 min (fluorescence detection: excitation wavelength at 440 nm and emission wavelength at 460 nm, top) and at 5 min (ultraviolet detection: wavelength at 250 nm, bottom). .	164
Figure 5-6: Calibration plot for coumarin-6 standard concentration (0.5 to 10 µg/mL) based on fluorescence detection. (Luminescence unit per second, LU*s)	165

Figure 5-7: Percentage recovery of coumarin-6 at predetermined time intervals. Plot showed average of percentage of coumarin-6 recovered from two independent batches..... 166

Figure 6-1: Chromatogram showing distinctive peaks for glyceryl monostearate (GMS), cholesterol, and dipalmitoyl phosphatidylcholine (DPPC). Response of detection measured in voltage (mV) for 15 min run time. 173

Figure 6-2: Chromatogram of Span® 60 standard at (concentration 2.0 mg/mL) showing three response peaks (retention times at 3.8 min, 5.1 min, and 6.5 min). 174

Figure 6-3: Chromatogram of cholesterol standard at 1.0 mg/mL. 175

Figure 6-4: Chromatogram showing distinctive peaks for Span® 60 (retention times at 3.9 min, 5.2 min, and 6.6 min) and cholesterol (retention time at 10 min). Equimolar composition of Span® 60 and cholesterol was used (total lipid content at 2.0 mg/mL). Molecular mass of Span® 60 is 430.62 g/mol and molecular mass of cholesterol is 386.65 g/mol. 175

Figure 6-5: Linear calibration plot of Span® 60 standards (0.1 to 2.0 mg/mL) was constructed to quantify Span® 60 concentration..... 177

Figure 6-6: Linear calibration plot of cholesterol standards (0.05 to 1.0 mg/mL) was constructed to quantify cholesterol concentration. 178

List of abbreviations

% RSD	percentage of relative standard deviation
C-6	coumarin-6
CHOL	cholesterol
CHS	chitosan

CIN	cinnarizine
DLS	dynamic light scattering
DSC	differential scanning calorimetry
EE	entrapment efficiency
ELP	Cremophor® ELP
ELSD	evaporative light scattering detection
FL	fluorescence
FTIR	Fourier transform infrared
GAV	Gaviscon®
GIT	gastrointestinal tract
GRAS	generally recognized as safe
HCl	hydrochloric acid
HS15	Solutol® HS15
ICH	International Conference on Harmonisation
kcps	kilo count per second
MB	methylene blue
MeOH	methanol
MF	microfluidic
NaOH	sodium hydroxide
PBS	phosphate buffered saline
PDI	polydispersity index
pH	negative log of the hydrogen ion concentration
pKa	negative log of the ionisation constant (acid dissociation constant)
R ²	correlation coefficient
RH40	Cremophor® RH40

RPM	revolution per minute
S60	Span® 60
SD	standard deviation
SGF	simulated gastric fluid
TFA	trifluoroacetic acid
TFH	thin film hydration
Trizma	Trizma® buffer
UHPLC	ultra-high-performance liquid chromatography
UV	ultraviolet
UV-Vis	ultraviolet-visible
ZP	zeta potential

List of equations

$dC/dt = k(C_s - C)$	Equation 1.1	4
$\Delta G = \Delta H - T\Delta S$	Equation 1.2	4
$\text{pH} = \text{pK}_a + \log ([\text{salt}]/[\text{acid}])$	Equation 1.3.....	5
$\text{pH} - \text{pK}_a = \log [(S - S_0)/S_0]$ for acids	Equation 1.4.....	5
$\text{pH} - \text{pK}_a = \log [S_0/(S - S_0)]$ for bases	Equation 1.5.....	5
$S_r \equiv C_s / C_\infty \equiv S_{\text{app}} / S_0$	Equation 1.6.....	37
$\ln S_r \equiv \ln [C_s / C_\infty] = [2\gamma M] / [\rho RTr]$	Equation 1.7.....	38
$\text{LOD} = 3.3 \delta/S$	Equation 2.1	78
$\text{LOQ} = 10 \delta/S$	Equation 2.2	78

EE (%) = $\frac{\text{found drug concentration (mcgmL)}}{\text{theoretical drug concentration (mcgmL)}} \times 100 \%$	Equation 2.3	87
Drug loaded (mg) = $\text{found drug concentration (mcgmL)} \times 1000 \times \text{volume (mL)}$	Equation 2.4.....	87
% cumulative release = $\frac{\text{drug loaded at predetermined time interval}}{\text{total amount of encapsulated drug}} \times 100$ Equation 2.5	87
Adsorption (%) = $\frac{\text{total amount of mucin used} - \text{free mucin determined}}{\text{total amount of mucin used}} \times 100$	Equation 2.6	89
$d_H = kT3\pi\mu D$	Equation 3.1	103
$y = y^0 + K x^n$	Equation 5.1	154
Recovery (%) = $\frac{\text{Found concentration (mgmL)}}{\text{Theoretical concentration (mgmL)}} \times 100$	Equation 6.1	175

Chapter One: General introduction

1. Introduction

Poor drug properties such as solubility and bioavailability continue to be challenging especially with the increasing number of those poorly water-soluble drugs in the market and the development pipeline. According to Kalepu and Nekkanti (2015), about 40% of marketed drugs and nearly 90% of drug molecules in the development pipeline are consist of poorly water-soluble drugs. Limited absorption rate of poorly water-soluble drugs upon oral administration is often resulted in low bioavailability, high intra- and inter-subject variability and lack of dose proportionality. As oral route is preferred over other routes of administration especially with drugs that are indicated for chronic diseases, it is of utmost importance to translate those poorly water-soluble drugs into feasible favourable drug delivery dosage forms. To achieve this, formulation technological advances and approaches have a huge role to improve drug solubility for enhanced oral absorption and bioavailability with predictable plasma concentration profile of the drug after administration.

The process of dissolution and remained dissolved of a poorly water-soluble drug are fundamental topics to be appreciated in order to enhance its absorption upon administration via the oral route (Boyd et al., 2019). From a viewpoint of formulation development, the aims are to formulate nanocarriers in the form of niosome vesicles, to entrap poorly water-soluble drug in which its oral absorption is limited by dissolution rate, in order to enhance its dissolution and potential bioavailability. This chapter introduces the importance of solubility and dissolution process for oral drug absorption, the concepts and the theory of preparing niosomes over other delivery approaches. This research aims to formulate an oral drug delivery system in the form

of niosomes to encapsulate and deliver a poorly water-soluble drug, cinnarizine (narrow absorption window) to the stomach for absorption.

1.1. Drug solubility and dissolution

The aqueous solubility of a drug is paramount that all drugs must be dissolved for their therapeutic efficacy regardless of the route of administration. Solubility is defined as the dispersion of molecules or ions of a drug of a crystalline solid state into an aqueous solution until a dynamic equilibrium is reached under a certain experimental condition. The degree of solubility of a drug can be affected by a change in temperature, difference in particle size and the presence of polymorphism. According to the British Pharmacopoeia (2020), a description of solubility terms is shown in Table 1-1.

Table 1-1: Description of solubility terms (Part II - British Pharmacopoeia, 2020).

Solubility term	Approximate volume of solvent (mL) required to dissolve 1 g of solute
Very soluble	< 1
Freely soluble	1-10
Soluble	10-30
Sparingly soluble	30-100
Slightly soluble	100-1000
Very slightly soluble	1000-10 000
Practically insoluble	> 10 000

The process of mass transfer is known as dissolution (Aulton and Taylor, 2017). Dissolution is a heterogenous process of a solid drug where a diffusion layer is assumed to form around its surface and with time, the dissolved drug molecules diffuse to the bulk aqueous medium. Following this diffusion layer model, saturation

solubility is the driving force of dissolution rate according to the Noyes-Whitney equation (Equation 1.1).

$$\frac{dC}{dt} = A \cdot \frac{D}{h} \cdot (C_s - C) \quad \text{Equation 1.1}$$

where D is the diffusion coefficient of the drug in solution;

h is the thickness of the diffusion boundary layer of the drug;

A is the effective surface area of dissolving drug;

C_s is the saturation solubility of the drug;

C is the concentration of the bulk fluid at time t .

According to Noyes-Whitney equation, a low value of drug concentration will favour more rapid dissolution of the drug by virtue of increasing the value of term $(C_s - C)$. In the case of drugs whose absorption is dissolution-rate limited, the value of C is normally kept very low by absorption of the drug. Hence, dissolution occurs under sink conditions in which the value of $(C_s - C)$ approximates to C_s .

The dissolution process involves bond-breaking and bond-forming with water molecules to allow drug molecules to interact with the solvent, forming and maintaining a thermodynamic system with a negative Gibb's free energy change (ΔG). The change in Gibb's free energy (Equation 1.2) where dissolution occurs is defined as a balance between the enthalpy of dissolution (ΔH) and the associated entropy (ΔS) at the temperature (T) of dissolution (Jones, 2016).

$$\Delta G = \Delta H - T\Delta S \quad \text{Equation 1.2}$$

The aqueous solubilities of acidic or basic drugs are pH-dependent and can be affected by their forming salts that are exhibiting different equilibrium solubilities under

a controlled experimental condition, maintaining a thermodynamically stable system (Aulton and Taylor, 2017). Depending on the pH of the aqueous solution as the forming salt is hydrated, the aqueous solubility of a salt of a weak acidic or basic drug is shown to be more affected by the changes in pH, compared to a salt of a strong acidic or basic drug.

The aqueous solubility of these ionisable drugs will also depend on their ionisation constant (K_a). The pK_a of a drug is defined as the pH at which 50 % of the drug is in unionised state. The solubility of a weak acid or base increases with the increasing degree of ionisation depending on its pK_a and the pH of the aqueous medium (Jones, 2016). Based on the derivation of the Henderson-Hasselbalch equation (Equation 1.3), the extent of ionisation of a weak acid or base can be predicted (Equations 1.4 and 1.5) (Cairns, 2012).

$$pH = pK_a + \log \left(\frac{[salt]}{[acid]} \right) \quad \text{Equation 1.3}$$

$$pH - pK_a = \log \left[\frac{(S - S_0)}{S_0} \right] \text{ for acids} \quad \text{Equation 1.4}$$

$$pH - pK_a = \log \left[\frac{S_0}{(S - S_0)} \right] \text{ for bases} \quad \text{Equation 1.5}$$

where S refers to the solubility of the drug;

S_0 refers to the intrinsic solubility (solubility of the free form of the drug)

Intrinsic solubility of the drug in its free form provides a good estimation of solubility value at 2 pH units above pK_a for basic drugs whilst at 2 pH units below pK_a for acidic drugs (Makary, 2014). At pH values above the pK_a , the solubility of acidic drugs increases. At pH values below the pK_a , the solubility of basic drugs increases.

1.2. Drug absorption

Drug absorption is determined by the drug's physicochemical properties, formulation and route of administration (Boyd et al., 2019). Regardless of the dosage forms and the route of administration, drugs must be dissolved in solution to be absorbed. In oral administration, bioavailability is defined as the rate and extent at which an active drug reaches systemic circulation by crossing the gastrointestinal barrier. Drug molecules in solution must cross semi-permeable cell membranes before they can reach the systemic circulation. Cell membranes comprised of a bimolecular lipid matrix determine its membrane permeability characteristics. Drugs molecules may cross cell membranes by passive diffusion, facilitated passive diffusion, active transport and pinocytosis. In passive diffusion, drugs diffuse across a cell membrane from a region of high concentration (gastrointestinal fluids) to the region of low concentration (blood). Diffusion rate is directly proportional to the drug concentration gradient but also dependent on the molecule's lipid solubility, size, degree of ionization, and the area of absorptive surface. The un-ionised form (lipid soluble) usually diffuses readily across cell membranes. The proportion of un-ionised and ionised forms is determined by the environment pH and the drug's pKa.

Drugs with both hydrophilic and lipophilic parts in their structures tend to partition between aqueous and lipid compartments. Their hydrophilicity is dependent on the pH of the aqueous medium. Therefore, any pH change affects the aqueous solubility of these drugs and also their partitioning. Lipophilicity is the ratio of the drug concentration in 1-octanol to the drug concentration in water (Box and Comer, 2008). Generally, lipophilicity can be expressed as distribution coefficient, D (or usually as Log D) value, which is the ratio for all species (ionised and unionised) of a compound

at a given pH. The lipophilicity of a compound can also be expressed as partition coefficient, P (or usually as $\text{Log } P$) value of a compound is obtained over a range of pH where the compound is at unionised state.

1.2.1. Oral drug absorption from the gastrointestinal (GI) tract

Drug absorption has may be affected owing to the interactions between the drug, the formulation and the gastrointestinal physiology (Yu and Amidon, 1999). The characteristic of poorly water-soluble drugs continues to pose challenges and exhibit transformations between different states (dissolved, unionised, precipitated or crystallised) in the complex dynamic gastrointestinal environments upon oral administration of a dosage form. This presents the problem of unpredictable dissolution processes with the consequences affecting drug solubilisation and bioavailability.

Multiple complex gastrointestinal variables such as the fluid composition, fluid volume, gastric emptying rate, gastrointestinal motility and pH can influence the degree of ionisation of a drug. In particular, poorly water-soluble drugs are facing oral bioavailability issues due to poor dissolution, unpredictable absorption, inter- and intra-subject variability and lack of dose proportionality (Gurrapu et al., 2012). The dynamic gastrointestinal environments and intra- and inter-subject variability may affect the behaviour of poorly water-soluble drugs and consequently their absorption due to a limited intrinsic driving force for permeation across the gastrointestinal barrier (Boyd et al., 2019).

1.2.2. Factors affecting gastric drug absorption

The stomach has a relatively large epithelial surface, but its thick mucus layer barrier and short transit time (<4 hours) affect drug absorption (Kimura and Higaki, 2002), generally depends on the state of the stomach. Food slows gastric emptying and the rate of drug absorption. Drug absorption from the stomach is typically very slow (Prescott, 1974). Apart from the effect of gastric motility on drug absorption, the stomach lining is coated with a thick protective mucus which makes drug diffusion difficult. The degree of ionisation of the drug at the absorption site influences the diffusion rate. Factors which favour well drug absorption in the stomach include small lipophilic molecules, weakly acidic (pK_a higher than the pH of stomach acid) and in highly concentrated form (large dose). As a result, basic drugs will be more readily soluble in the stomach with the possibility of precipitation in the fed state or as the stomach contents empty into the small intestine (Boyd et al., 2019). In particular for Biopharmaceutical Classification System (BCS) class II drug that has poor aqueous solubility and high permeability, they often show poor gastrointestinal absorption due to inadequate drug solubility in GI fluids, very low aqueous solubility and oral absorption of this drug is dissolution-rate limited (Chakraborty et al., 2009).

1.2.3. Solubility and dissolution enhancement approaches

This section will present different approaches used to modify the solid-state characteristics of poorly water-soluble drugs for oral delivery of hydrophobic drugs. Numerous pharmaceutical strategies and approaches include particle size reduction, use of cyclodextrin, lipid-based systems, liposomes and micelles, followed by niosomes (Section 1.3.) as the main topic in this work.

The increase in saturation solubility of drug by solubilisation in surfactant could result in more rapid rate of dissolution and hence more absorption for higher bioavailability. Drug solubilised in aqueous nano-dispersion of nanoparticles in the forms of micelles, niosomes, liposomes, and complexes enable higher apparent drug solubility and avoidance of drug precipitation, whereas supersaturated solutions increase molecularly soluble free drug (Boyd et al., 2019; Raina et al., 2015). Despite the risk of drug precipitation, supersaturated systems such as amorphous solid dispersions and lipid-based formulations increase the drug flux across the membrane due to higher concentration and chemical potential gradient. Schultz et al. (2020) reported the use of precipitation inhibitors to prevent or avoid precipitation by decreasing the degree of supersaturation and stabilizing the systems. Drug distribution/solubilization behaviour during digestion *in vitro* of long-chain or medium-chain triglyceride lipid formulations are seen to produce a dispersed aqueous colloidal phase that supports supersaturated drug concentrations (Kaukonen et al., 2004).

1.2.3.1. Salt formation

Approaches to enhance oral bioavailability of poorly water-soluble drugs can be categorised into pre-formulation and formulation approaches. In pre-formulation approaches to improve the physicochemical properties of poorly water-soluble drugs, salt is formed where the drug molecule and counterion are attracted by ionic intermolecular forces. The solubility of the resultant salt is dependent on its counterion species influencing the crystal lattice free energy and the free energies upon hydration of the ions (Boyd et al., 2019). One of the properties of a salt is pH_{max} which is the pH value at which the maximum solubility of the drug in its salt form (ionised form) is obtained. This parameter is critical to predict the precipitation behaviour of the salt in

the gastrointestinal tract as it governs the conversion of salt form (ionised) to free form (non-ionised). The higher the pH_{max} of a basic drug or the lower for an acidic drug, the better the stability of the drug in a salt form (Boyd et al., 2019). However, the partition of the salt form through lipophilic phases may be reduced owing to their ionised state, impacts on the permeability through physiological biological barrier for absorption. Hydrochloride salts have been reported to show a reduced dissolution rate and decreased solubility in the stomach due to precipitated free acid or base of poorly water-soluble drug at the surface of the solid dosage form (Makary, 2014).

1.2.3.2. Drug nanocrystals/nanosuspensions

Several particle size reduction techniques have been used to produce drug nanocrystals to enhance dissolution rate and oral absorption of poorly water-soluble drugs owing to increased surface area (nano-sized) and amorphous state (Salazar et al., 2014; Schultz et al., 2020). Drug nanocrystals are solid crystalline drug particles with a particle size of typically less than 500 nm (Babadi et al., 2021), which mechanical energy has been applied to breakdown coarse particles into fine particles. In general, drug nanocrystals are manufactured by top-down approaches such as milling and high-pressure homogenisation (Loh et al., 2015; Müller and Peters, 1998) or bottom-up approaches through precipitation process (Salazar et al., 2014; de Waard et al., 2011). Prior to size reduction processes, pre-treatment processing techniques include spray drying and microprecipitation is often employed to generate a semi-crystalline micronized drug as the starting material, in order to overcome limitations on long milling times, high numbers of homogenisation cycles and high solvent residues (Möschwitzer and Müller, 2006). The reduction in particle size, alteration in surface area and shape, and amorphization of the drug crystals increased

both the saturation solubility and dissolution rate. Stabilisers such as surfactants and/or hydrophilic polymers are often used in order to disperse and formulate drug nanocrystals into dosage forms; preventing sedimentation, agglomeration and crystal growth (Wu et al., 2011).

1.2.3.3. Cyclodextrins (CDs)

The use of hydrophilic cyclodextrins such as beta-cyclodextrin derivatives has been extensively studied for solubilisation of poorly water-soluble drugs through the formation of inclusion complexes. Upon oral administration, enhanced rate and extent of oral bioavailability of a poorly water-soluble drug from its dissolved complexes can be obtained, where the free form of the drug is in equilibrium with the complexed form of the drug in solution (Hirayama and Uekama, 1999). In addition to the multifunctional characteristics of natural and chemically modified CDs for their self-assemblies and supramolecular architectures, various molecular conjugation with crosslinking polymers have been investigated for the development of oral delivery systems (Adeoye and Cabral-Marques, 2017). For instance, cyclodextrin-based nano-sponges are non-toxic and stable nano-systems with a high solubilising efficiency for poorly water-soluble drugs (Babadi et al., 2021).

1.2.3.4. Amorphous solid dispersion (ASD)

Amorphous solid dispersion (ASD) is a single-phase amorphous system formed consisting of a blend of poorly water-soluble drug in an amorphous carrier (Boyd et al., 2019). As dissolution limits the absorption rate of hydrophobic drugs in their crystalline-state, amorphous form of the drug can be useful. The system increases drug dissolution rate and bioavailability as a result of drug supersaturation within the system.

The physical stability of drugs in their amorphous form is generally lower than that of drugs in their crystalline form, due to the higher free-energy level of the amorphous form (Di Marzio et al., 2013). Due to this thermodynamic instability, amorphous solid transforms into its stable crystal form through crystalline mesophases exhibiting intermediate properties (Shalaev et al., 2016). Often, stabilisation of amorphous drug form can be obtained by using polymers, mesoporous silica or via co-amorphous formulations to enhance the time window of its sustained supersaturation feature (Boyd et al., 2019).

1.2.3.5. Solid lipid nanoparticles (SLNs)

Solid lipid nanoparticles are comprised of an aqueous dispersion of lipid matrix that remains in solid state at both room and body temperatures (Babadi et al., 2021). They are typically between 50 and 1000 nm in average diameter, comprised of physiological lipid components that are biocompatible and non-toxic, leading to a higher lymphatic transport and lesser first pass metabolism effect. However, SLNs have shown limited drug loading efficiency and drug leakage.

1.2.3.6. Nanostructured lipid carriers (NLCs)

Nanostructured lipid carriers are a new generation of solid lipid nanoparticles that comprised of lipid molecules are mixed by blending incompatible solid lipids with liquid lipids forming a highly ordered self-assembled lipid particles in a dispersed cubic crystalline phase (Hong et al., 2019; Müller et al., 2002). NLCs are solid in nature (also in body temperature) help minimise drug expulsion by avoiding lipid crystallisation during manufacturing process and upon storage (Ghasemiyeh and Mohammadi-Samani, 2018). Similar to liposomes but with an internal lipid crystalline structure in

addition to the internal water channels, NLCs provide a mechanism for sustained release of highly incorporated drugs (Tan et al., 2019).

1.2.3.7. Self-emulsifying systems

Self-nanoemulsifying drug delivery systems (SNEDDs) are thermodynamically stable lipid-based nano-dispersions of oil globules in an aqueous medium that are formed spontaneously and stabilised by surfactant molecules. SNEDDs as oral formulation for poorly water-soluble drugs have been studied to enhance solubility and drug release for absorption (Babadi et al., 2021). The drug release from the lipid phase in a molecular dispersion as the formulation is diluted into an aqueous phase within the gastrointestinal tract. Due to this emulsion nature, drug absorption can be more consistent and faster to reduce the variability in rate and extent of absorption (Mohsin, 2012). However, precipitation of drug might occur in the formulation or during digestion in the gastrointestinal tract, as it has been reported that drug loaded are usually at 50-90 % equilibrium solubility in the SNEDDs (Larsen et al., 2013; Siqueira et al., 2017).

1.2.3.8. Micelles

Micellar solubilisation of poorly water-soluble drug occurs above the surfactant critical micelle concentration (CMC) where surfactants self-assembled to form colloidal aggregates of heterogeneous microstructure with different polarity. Generally, micelles formed from surfactants with low CMC values (<1 mM) are more stable upon dilution in biological fluids (Lu et al., 2018). For instance, polymeric micelles have a significantly low CMC (10^{-6} - 10^{-7} M) showed a high colloidal stability due to its long hydrophobic block of the amphiphilic copolymers, avoiding aggregation or precipitation in bulk solution.

1.2.3.9. Liposomes

Liposomes are formed by spontaneous self-assembly of phospholipid molecules into lipid bilayer enclosing aqueous compartments. Many studies showed the potential on formulating liposomes in enhancing drug solubility owing to its intrinsic multipurpose structure and properties that are influenced by the phospholipid types and formulation compositions. Liposome encapsulation enhanced systemic absorption upon oral administration and a higher oral bioavailability was achieved at a higher amount of lipophilic drug encapsulated (Ong et al., 2016). Through the solubilisation of poorly water-soluble drugs, enhancement on drug absorption and bioavailability of poorly water-soluble drugs can be achieved as oral delivery system in the form of liposomes (Abed et al., 2021). However, one of the main instability issues in liposomes is the degradation of the vesicles upon in contact with gastric acids, bile salts and pancreatic lipases, leads to drug leakage causing drug degradation and precipitation of lipophilic drugs. Consequently, the gastrointestinal instability of liposomes contributed to the decrease in the total fraction of oral drug absorption (He et al., 2019).

1.3. Niosomes as drug delivery system

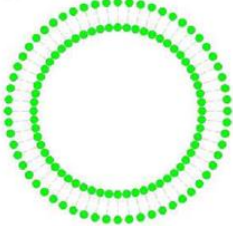
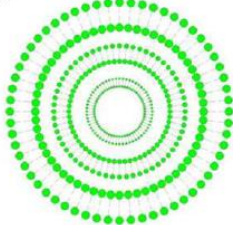
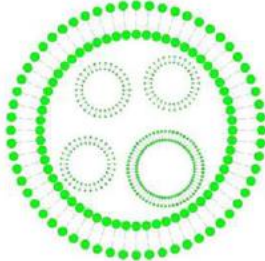
Non-ionic surfactant-based vesicles, niosomes are highly versatile and can be used for the delivery of pharmaceutical agents - enabling targeted and controlled release while shielding the encapsulated drugs from environmental degradation agents and the immune system. Depending upon the structure and composition of the bulk solution, the performance of vesicle-based drug carriers has been shown to depend on both their constituent chemistry (i.e. surface moieties) and their physical properties (i.e. size, shape).

Niosomes are non-ionic surfactant-based bilayer membrane vesicles that are formed by self-assembly upon hydration of surfactant monomers. The self-assembly of non-ionic surfactants into vesicles was first reported in cosmetic products by Handjani-Vila et al. (1979) and following that niosomes preparation and characteristics were investigated by (Baillie et al., 1985). They are consisting of single or multiple surfactant bilayers (lamellae) enclosing an aqueous core. The formation of vesicles is a result of a high interfacial tension between water and the hydrophobic region of the amphiphiles, and the steric interaction (hydrophilic repulsion) between the head groups in contact with water (Uchegbu and Florence, 1995). Typically, vesicles are categorised according to their size - small unilamellar vesicles (SUVs), large unilamellar vesicles (LUVs) and multilamellar vesicles (MLVs) (Table 1-2).

Non-ionic surfactants are surface active agents that have no charge groups in their hydrophilic head region. Therefore, they are biodegradable, biocompatible and non-immunogenic. They are amphiphilic molecules with a high interfacial activity and upon hydration forming bilayer membrane vesicles that are capable of entrapping both hydrophilic and hydrophobic drugs (Mahale et al., 2012). Non-ionic surfactants have different surface activity properties that are dependent on the balance between their hydrophilic and hydrophobic regions of their chemical structures. This is expressed empirically as hydrophile-lipophile balance (HLB) with a value from 0 to 10 which indicates lipid soluble and a value from 11 to 20 which indicates water soluble. Surfactants with a HLB value between 3 and 8 are suitable to form a bilayer membrane vesicles, are commonly referred to as water-in-oil (W/O) emulsifiers (Moghassemi and Hadjizadeh, 2014). By having no charge groups in the hydrophilic regions, non-ionic surfactants are less toxic and more resistant against pH changes in the gastrointestinal

tract and with a wider compatibility when compared to ionic surfactants. Increasing the hydrophobicity of the surfactant attributed to increasing surface activity and decreasing surface free energy (surface tension) resulted in a decrease of the vesicles size (Khoee and Yaghoobian, 2017).

Table 1-2: Niosome vesicle types, vesicle size ranges and their structures.

Vesicle types	Vesicle structure
Small unilamellar vesicle (SUV) 10 nm – 100 nm	
Large unilamellar vesicle (LUV) 100 nm – 400 nm	
Multilamellar vesicle (MLV) 200 nm – 3 μm	
Multi-vesicular vesicle (MVV) 200 nm – 3 μm	

Other than HLB value, the structure of a non-ionic surfactant has a great impact on the geometry formation of its vesicle attributed to critical packing parameters (CPP, Figure 1-1) including the hydrophobic group volume, critical hydrophobic group length and the area of the hydrophilic head group (Biswal et al., 2008). According to the CPP

value, spherical vesicles may form using surfactant with CPP value between 0.5 and 1.0. The shape and size of the amphiphile aggregation would evolve from spherical micelles ($CPP \leq 0.33$) to cylindrical micelles ($0.33 \leq CPP \leq 0.5$), bilayers ($0.5 \leq CPP \leq 1$) or inverse micelles ($CPP \geq 1$) (Marianecci et al., 2014). Larger vesicles are formed when hydrophilic portion of the molecule is decreased relative to the hydrophobic portion as increasing in alkyl chain length would result in an increase in the CPP value (Akhter et al., 2012).

Non-ionic surfactants that are commonly used in niosomes are classified in four categories: alkyl esters, alkyl amides, alkyl ethers and esters of fatty acids (Moghassemi and Hadjizadeh, 2014).

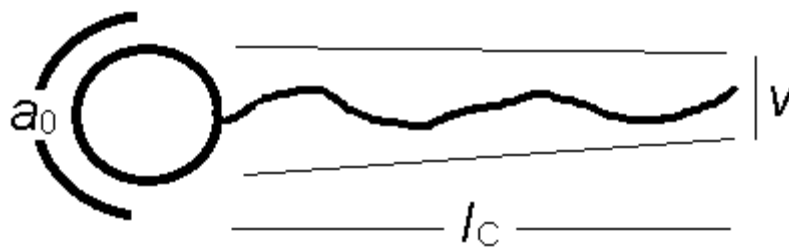


Figure 1-1: Critical Packing Parameter (CPP) of surfactant where v is lipophilic tail volume, l_c is the critical lipophilic tail length, and a_0 is the polar head surface area per molecule at the hydrocarbon-water interface.

The phase transition temperature (T_c) and the length of alkyl chain of non-ionic surfactants are also crucial factors that affect entrapment efficiency, membrane permeability, bilayer rigidity and stability. Surfactants having a saturated alkyl chain length with a higher number of carbons, have a higher gel-to-liquid T_c in which they form less leaky niosomes with lower membrane permeability and a higher entrapment efficiency. With T_c dependent on the unsaturation degree of alkyl chain, T_c impacts

on chain fluidity, membrane permeability and drug release kinetics (Khoee and Yaghoobian, 2017).

Niosomes have been studied extensively as a drug carrier for various hydrophilic and hydrophobic drugs. They have been successfully manufactured for delivery of cytotoxic agents such as paclitaxel (Bayindir and Yuksel, 2010) at a lower cost with various surfactant combinations by thin film hydration method. Niosomes are similar to liposomes that are comprised of phospholipids as drug delivery system. Unlike liposomes, niosomes have less chemical instability problems and costs, but they are associated with physical stability issues such as fusion, aggregation, sedimentation and drug leakage during storage in dispersion form (Gurrapu et al., 2012). Hence, this research investigated storage stability of the prepared niosomes.

The increase in the saturation solubility of drug by solubilisation in surfactant could result in increasing dissolution rate and hence greater absorption for higher bioavailability. The wetting effect of surfactant as a result of reduced interfacial tension may aid the penetration of gastro-intestinal fluids into the mass of conventional dosage forms and/or reduce the tendency of poorly water-soluble drug particles to aggregate in the gastro-intestinal fluids, thus increasing the effective surface area and dissolution rate for higher bioavailability. With niosomes as drug delivery system, sustained release pattern can be beneficial for drugs with low water solubility and a low therapeutic dose required (Kazi et al., 2010).

1.3.1. Niosome component: Spans

Spans are the product name marketed for sorbitan fatty acid esters, they are produced by the dehydration of sorbitol. All Span surfactants have a similar sorbitan head group with different hydrophobic alkyl chain (Hao et al., 2002). The HLB value of Span decreases with increasing the length of alkyl chain. Their gel transition temperature increases as the length of the acyl chain increases resulted in decreased leakage of drug from niosomes (Kumar and Rajeshwarrao, 2011). As the hydrophobic alkyl chain length increases, the higher the entrapment efficiency of hydrophobic drug and stability of the niosomes will be achieved. The increased drug entrapment of low solubility drugs could be related to the increased hydrophobic volume within the bilayer membrane that made of surfactant with a longer alkyl chain length.

Numerous studies have utilised Span® as the non-ionic surfactant in the preparation of niosomes via different preparation methods for encapsulation of hydrophilic and hydrophobic drugs (Table 1-3). Results were in agreement with the entrapment efficiency (%EE) reported by Uchegbu and Vyas (1998) decreasing from Span® 60 (C₁₈), Span® 40 (C₁₆), Span® 20 (C₁₂) and Span® 80 (unsaturated C₁₈). This was in an agreement with flurbiprofen proniosomes studied by Mokhtar et al. (2008). In addition, the study found that with increasing total surfactant/lipid or drug concentration used resulted in an increased %EE of the hydrophobic flurbiprofen. Sorbitan monostearate (Span® 60, Figure 1-2) with a C₁₈ chain has a gel transition temperature of 56-58 °C and a HLB value of 4.7, exhibits the highest entrapment efficiency. Therefore, Span® 60 was used as the choice of non-ionic surfactant for preparation of niosome vesicle in this research.

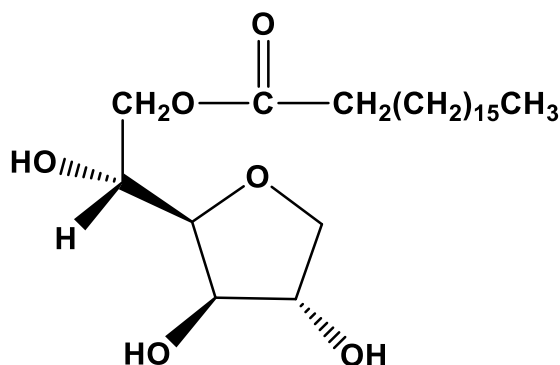


Figure 1-2: Chemical structure of sorbitan monostearate (Span® 60; $C_{24}H_{46}O_6$). Drawn by ChemDraw.

Table 1-3: Examples of Span® niosomes that have been investigated as oral drug delivery system.

Drug	Surfactant	Method of preparation	EE (%)	Reference
Celecoxib	Span® 60	Proniosome	~95	(Nasr, 2010)
Ganciclovir	Span® 40, 60	Reverse phase evaporation	~90	(Akhter et al., 2012)
Valsartan	Span® 60	Proniosome	~60-92	(Gurrapu et al., 2012)
Clarithromycin	Span®	Thin film hydration	~60-95	(Shilakari Asthana et al., 2016)
Paclitaxel	Span®, Tween®, Brij®	Thin film hydration	~12-96	(Bayindir and Yuksel, 2010)
Griseofulvin	Span®	Thin film hydration and ether injection	~40-75	(Jadon et al., 2009)
Insulin	Span®	Sonication	~17-40	(Varshosaz et al., 2003)
Cefdinir	Span® 60	Sonication	~45-70	(Bansal et al., 2013)
Candesartan	Span® 60 Pluronic P85	Thin film hydration with sonication	~36-99	(Sezgin-Bayindir et al., 2014)
Telmisartan	Span® 60	Thin film hydration	~83	(Ahad et al., 2018)

1.3.2. Niosome component: Cholesterol

The molar ratio of cholesterol (Figure 1-3) incorporated with surfactants may affect the entrapment of drugs into niosomes. Nasser (2005) investigated the effects of cholesterol concentrations and temperatures on the elasticity of the niosomal membranes composed of Span® 60, cholesterol and poly-24-oxyethylene cholesterol (Solulan® 24). The study found that increasing cholesterol content (10 to 40 mol %) increased the value of shear modulus indicating an increasing rigidity of the niosomal membrane and reached the maximum rigidity with cholesterol content of 47.5 mol% (equimolar ratio) at all temperatures. The equimolar mixture represented the critical composition as there is only one hydrogen bonding group on the cholesterol moiety to interact with oxygen functionalities on the Span® 60, resulted in an increase in membrane cohesion (see Figure 1-4). In agreement to the membrane stabilising ability of cholesterol, Marwa et al. (2013) reported that niosomes of equimolar ratio of Span® 60 and cholesterol revealed a decrease in membrane permeability by a marked reduction of the efflux of diclofenac and prolonged drug retention.

Hence, cholesterol is the most commonly used additive agent to enhance the stability of bilayer vesicles. The incorporation of cholesterol with surfactants of lower HLB values has shown to promote the gel liquid transition temperature of the vesicle (Moghassemi and Hadjizadeh, 2014). Kumar and Rajeshwarrao (2011) reported the addition of cholesterol enables more hydrophobic surfactants (lower HLB values) to form niosomes by suppressing the tendency of aggregation. Cholesterol, by increasing the orientation order of their relatively mobile hydrocarbon chains of liquid-crystalline phospholipid bilayers, decreasing bilayer permeability and reducing the

efflux of the entrapped drug. As a result of using a sufficient amount of cholesterol in the formulation system, the gel-to-liquid phase transition endotherm of bilayers can be abolished (Ali et al., 2013) and effectively prevent leakage of drug from niosomes (Hao et al., 2002). Incorporation of cholesterol into lipid bilayers modifies membrane fluidity by decreasing the movement of the mobile hydrocarbon chains of non-ionic surfactant leading to the loss of bilayer permeability.

The presence of cholesterol also appeared to transform the kinetics of drug release from the liposomes from a zero-order for formulations with no cholesterol content as a stabiliser to a first-order release when increasing cholesterol content from 11 to 33 % total molar (Ali et al., 2010). These drug release profile models suggested a more fluidised membrane to a more condensed membrane with increasing less permeable cholesterol. The increased drug loading could be related to the increased hydrophobic volume and/or hydrophobic bonding offered by the longer alkyl chain lipids, as shown by studies by (Manosroi et al., 2003; Mohammed et al., 2004). The study indicated that both molecular weight and lipophilicity of drug contribute to drug loading efficiency within bilayer. Cholesterol helps to increase the orientation order of bilayer membrane and form a more condensed and theoretically less permeable vesicle membrane. Higher retention rate of hydrophobic drug with the increase of cholesterol content in the formulation as the cholesterol stabilizes vesicle membrane and reduce the leakage of the hydrophobic drug. Therefore, an equimolar ratio of surfactant (Span® 60) and cholesterol was used in this research to prepare niosome vesicles of having less permeable bilayer membrane structure.

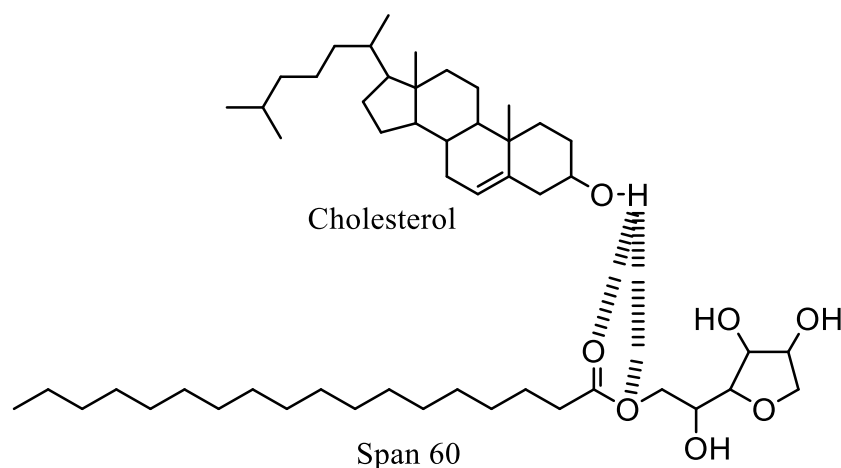


Figure 1-3: Chemical structures of Span® 60 and cholesterol showing the hydrogen bonding interaction between the two molecules drawn by ChemDraw. [Adapted from Nasser, 2005]

1.3.3. Niosome component: Co-surfactants

Co-surfactants are additive agents to enhance the characteristics of the niosome vesicles. Hydrophilic co-surfactants are commonly used in the literature working as emulsifiers, solubilising and wetting agents as they have a higher HLB value from 12 to 16 and a higher molecular weight of over 1000 Da. Berthelsen et al. (2015) reported that solubilisation effect of different types of polyoxyethylated non-ionic surfactant was drug dependent.

Cremophor® ELP (purified polyoxyl 35 castor oil) is a synthesised product by reaction between hydrogenated castor oil (glycerol triricinoleate) and ethylene oxide. It is recommended for parenteral use and also suitable for oral and other dosage forms due to the fact that it has controlled free acid and potassium content with low moisture level in which the hydrolysis of drug can be prevented. In vitro studies by Berthelsen et al. (2015) revealed the highest bioavailability of fenofibrate, hydrophobic drug from

formulation with Cremophor® ELP, indicating its solubilisation effect to increase drug absorption upon oral administration.

Cremophor® RH40 (hydrogenated polyoxyl 40 castor oil) is chemically very stable but combining with strong bases or acids should be avoided to prevent saponification of its ester components. However, it has demonstrated high solubilisation capacity of poorly water-soluble drugs at different concentrations. Increasing the amount of Cremophor® RH40 increased the solubilisation of drugs.

Solutol® HS15 (polyoxyl 15 hydroxystearate) is a polyoxyethylated non-ionic surfactant that consists of ethoxylated hydroxystearic acid and ethylene oxide. It is highly polydisperse and widely used in numerous preparations of self-emulsifying system, microemulsion and solid lipid nanoparticles. Solutol® HS15 is known to inhibit P-glycoprotein, which is an ATP-dependent pump that is responsible for reducing drug intestinal absorption by efflux transportation. The addition of this agent has shown to enhance paclitaxel aqueous solubility and permeability across Caco-2 monolayer cell without inducing cytotoxicity (Alani et al., 2010).

1.4. Niosomes manufacturing methods

Conventional bulk methods have been studied and used in the preparation of niosome vesicles e.g. thin film hydration, reversed phase evaporation, ethanol injection and heating methods. The spontaneous association of non-ionic surfactants into closed bilayers requires energy input in the form of heat or mechanical shaking (Ag Seleci et al., 2016).

1.4.1. Reverse phase evaporation method

Large unilamellar vesicles are formed generally by reverse phase evaporation method (Figure 1-4) and followed by an extrusion process which are reported to be favourable for encapsulating water-soluble drugs (Junyaprasert et al., 2008). Surfactants and additives are dissolved in organic solvent where the aqueous phase is added and the mixture is sonicated to form emulsion prior to removal of organic solvent using rotary evaporator under reduced pressure (Moghassemi et al., 2017). Compared with thin film hydration method, this method prepares vesicles with a higher internal aqueous loading in which it is beneficial for hydrophilic drug encapsulation. In addition, incomplete evaporation process of organic solvent might interrupt the stability of vesicles.

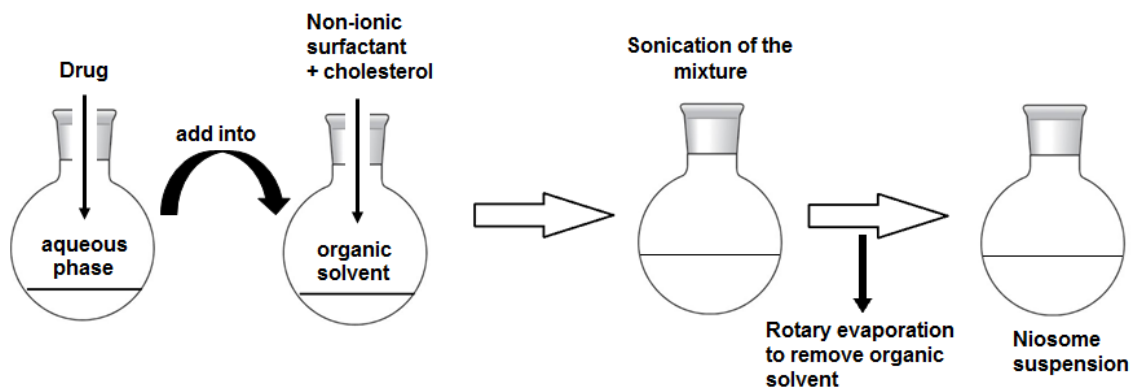


Figure 1-4: Schematic illustration for niosome preparation by reverse phase evaporation method.

1.4.2. Heating method

Without using any organic solvent, heating method (Figure 1-5) produces large particles with high polydispersity in which various components are hydrated in aqueous phase at room temperature followed by heating at 140 °C with continuous stirring and before being subjected to extrusion (Obeid, Khadra, et al., 2017). A size reduction method following preparation of niosome suspension is required due to

insufficient control on chemical and mechanical parameters during preparation process by heating method.

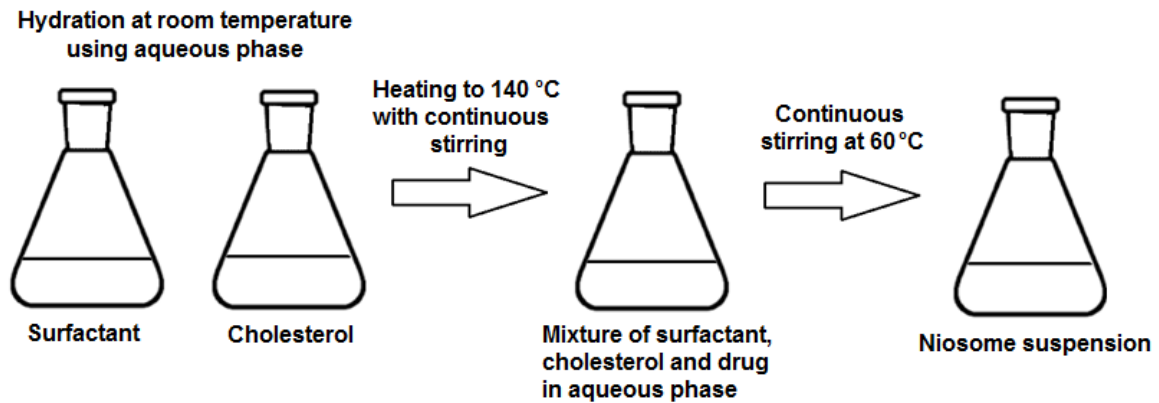


Figure 1-5: Schematic illustration of niosome preparation by heating method.

1.4.3. Ether injection method

In ether injection method (Figure 1-6), surfactant molecules and additives are dissolved in organic solvent prior to injection slowly through a needle into aqueous phase at 60 °C that containing the drug for encapsulation. At the same time of evaporating the organic solvent using a rotary evaporator, large unilamellar vesicles were formed (Marwa et al., 2013).

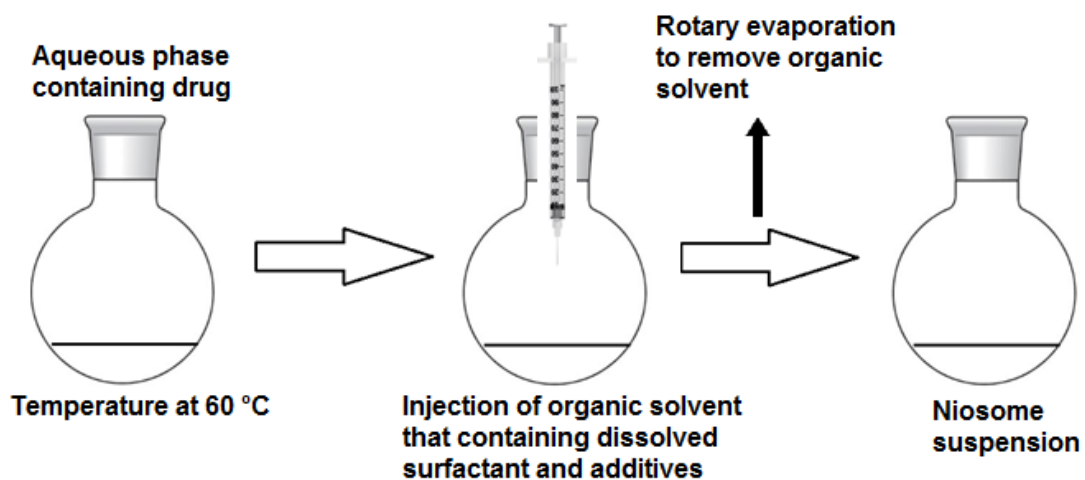


Figure 1-6: Schematic illustration for niosome preparation by ether injection method.

1.4.4. Thin film hydration method

The thin film hydration method was reported by (Azmin et al., 1985; Baillie et al., 1985). In thin film hydration (TFH), surfactants and additives are dissolved in organic solvent in a round-bottomed flask. The thin film formed on the inside wall of the flask after removing the organic solvent under reduced pressure using the rotary evaporator. The thin film is then hydrated with an aqueous solution above the phase transition temperature (T_c) of the surfactant for forming multilamellar vesicles.

Guinedi et al. (2005) reported a higher encapsulation efficiency was achieved in multilamellar vesicles prepared by thin film hydration method in comparison with reverse phase evaporation method, showing the ability of loading more hydrophobic drug. Similar results were shown in the study comparing niosomes prepared by thin film hydration and ether injection methods (Ravalika and Sailaja, 2017). Therefore, thin film hydration method was used in this research.

Firstly, non-ionic surfactants and additives e.g. cholesterol, charge-inducing agent and co-surfactant are dissolved in organic solvent in a round-bottomed flask (Figure 1-7). Under reduced pressure, the formation of thin film on the inside wall of the flask occurs after removal of the organic solvent by using the rotary evaporator. The dried thin film is then hydrated with an aqueous solution containing drug at a temperature above the phase transition temperature (T_c) of the surfactant used, to forming multilamellar vesicles using a water bath shaker or rotary evaporator. These vesicles are subjected to size reduction step e.g. sonication, extrusion and homogenisation, for generating homogenous mono-disperse vesicles. Sonication induces cavitation multilamellar vesicles into small unilamellar vesicles.

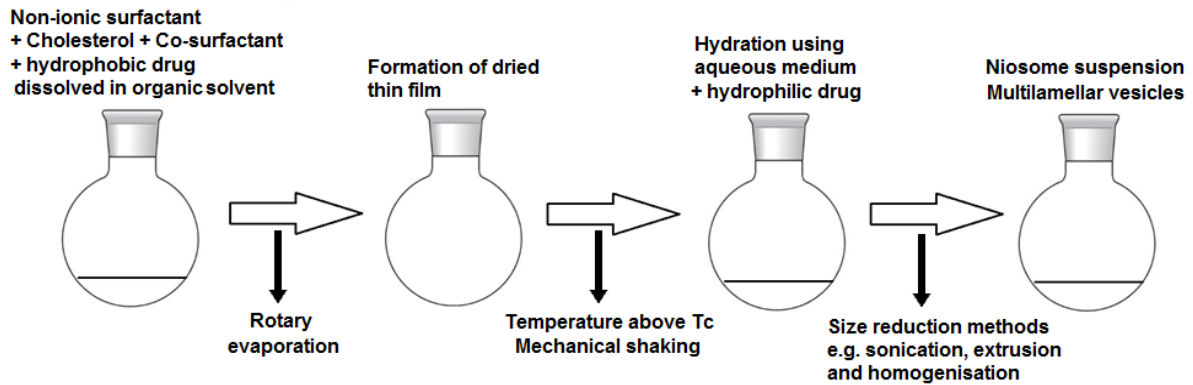


Figure 1-7: Schematic diagram for niosome preparation using thin film hydration method.

1.4.5. Microfluidic method

Advanced technology approaches such as microfluidic has been explored to control preparation process and overcome the lack of consistency using traditional methods. Conventional methods typically show limited control over the morphological characteristics of vesicles (He et al., 2013). Sections 1.5. and 2.2.2. will discuss more about the microfluidic method used in this research project on the theory and experimental aspects.

1.5. Microfluidic method

Microfluidic or lab-on-a-chip (LOC) is an advanced technology that is based on a device with micro-channels to control the flow behaviour of small volume of fluids within the micro-channels (Capretto et al., 2013). This microfluidic-based approach is similar to the ethanol injection method where the surfactant/lipid molecules are dissolved in an alcohol solution, prior to be mixed with an aqueous solution in a microfluidic device with a micromixer. The microchannels in the microfluidic device enable laminar flow of two miscible fluids into the interfacial and mixing regions where the two fluids are mixed rapidly in order to maintain a homogenous environment. From

the merging point of two fluids, the microfluidic platforms (or mixers) that enable mixing processes include hydrodynamic flow focusing (HFF), microfluidic micro-mixer and staggered herringbone micro-mixer (SHM) (Damiati et al., 2018) (see Figure 1-8).

In formulation development, microfluidic platforms provide high-throughput, reproducible, and low-cost methods for producing, screening and optimising nanocarriers (Ahadian et al., 2020). Microfluidic technology enables an efficient and a low-cost production of various micro- and nanoparticles that are composed of various materials and therapeutic agents, using small amount of materials and solvents, as compared to conventional bulk mixing methods (Ahadian et al., 2020).

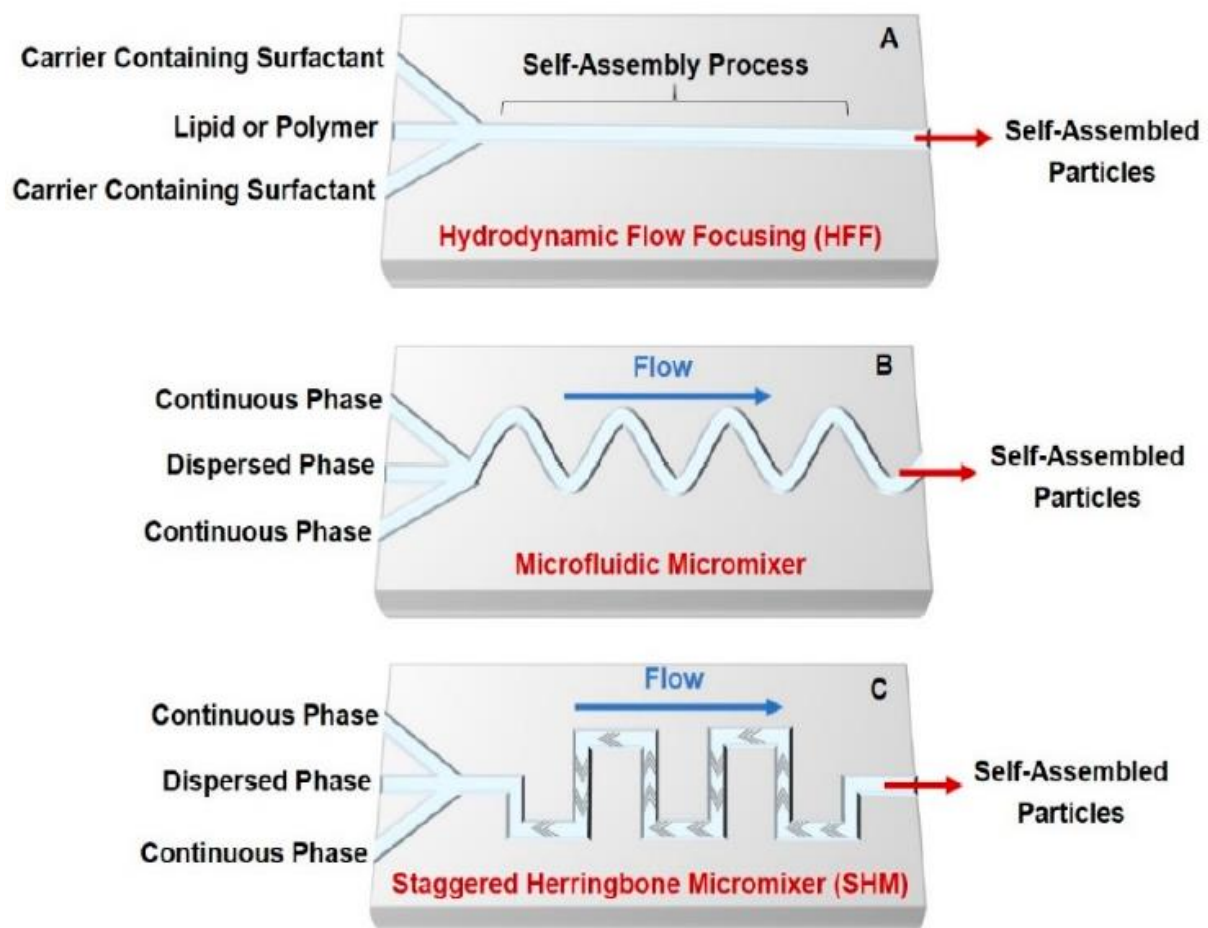


Figure 1-8: Schematic diagrams of microfluidic platforms: (A) a hydrodynamic flow focusing; (B) a microfluidic micro-mixer; and (C) staggered herringbone micro-mixer. Figure adapted from Damiati et al., (2018).

1.5.1. NanoAssemblr® Benchtop system

NanoAssemblr® Benchtop system (Precision NanoSystems Inc., Vancouver, Canada) was employed as the microfluidic method for the production of microfluidic-based niosomes in this research project. The system is comprised of an instrument (Figure 2-7) with a controlled syringe pump platform; a microfluidic cartridge (Figure 2-8) consisted of two inlets and a single outlet and; a heating block for controlling temperatures of the system.

The microchannels of the microfluidic cartridge (dimension of 200 μm in width and 79 μm in height) allow laminar flow of two independent miscible fluids toward the staggered herringbone micromixer (SHM) region with dimension of 50 μm in width and 31 μm in height, at 45 ° angle with asymmetry index of 2:1 (Dimov et al., 2017; Xu et al., 2016) (see Figure 2-8 in Chapter 2).

1.5.1.1. System parameters

The physical characteristics of mass and fluid transfer are fundamental in microfluidic system and the mixing process occurs in the microfluidic cartridge is primarily determined by two system (or process) parameters. Firstly, the rate of mixing (total flow rate, TFR) and secondly, the ratio of aqueous and organic solvent streams (flow rate ratio, FRR). Both independent process parameters can have impact on niosome characteristics.

Total flow rate (TFR) is the total mixing speed (mixing rate) in mL/min at which the two fluid stream inlets are being pumped through the cartridge. Flow rate ratio (FRR) is

the volumetric ratio (mixing ratio) of the aqueous and organic phases being mixed through the microfluidic cartridge.

1.5.1.2. Staggered Herringbone Micromixer (SHM)

The microfluidic cartridge used in the preparation of microfluidic-based niosomes in this research project has a staggered herringbone micro-mixer (SHM) structure within its mixing region. The microfluidic staggered herringbone micromixer (SHM) works through a controlled nanoprecipitation process where the dissolved surfactant/lipid molecules spontaneously self-assemble into closed vesicles when the water-miscible organic solvent is mixed with aqueous solution (Garg et al., 2016).

Microfluidic technology as a bottom-up manufacturing technique enables chaotic advection mixing of the two miscible fluids where the transverse diffusion of solvents and colloids across the diffusive boundary area to trigger the assembly of amphiphiles into vesicles (He et al., 2013). The herringbone patterns provide an exponential increase in surface area of the distance travelled between the two fluids, resulting in higher diffusional mixing than the hydrodynamic flow focusing (HFF) technique at equivalent flow rate ratios and this correspondingly has enhanced the ability of producing nanoparticulate system of defined size distribution (Zhigaltsev et al., 2012). In addition, flow rate ratios of 30 or higher were reported when using hydrodynamic flow focusing technique to achieve particle size 50 nm that resulting in substantial material dilutions, compared to low flow rate ratios used in microfluidic SHM system (Belliveau et al., 2012). With the incorporation of the herringbone pattern, this enhances the rapid and reproducible generation of self-assembled vesicles at a low

shear stress. As a result, microfluidics is capable of producing reproducible and homogeneous nanocarriers for drug delivery system.

The design of SHM is based on the patterns of grooves on the floor of the mixing region where they generate transverse flow to induce steady chaotic flow to facilitate mixing process (Stroock, 2002). In addition, the SHM feature increases the surface of exchange between reactants in order to facilitate diffusive mixing as a result of chaotic advection greatly increases the efficiency of the mass-transfer rate (Ottino, 1990). SHM feature introduces a non-turbulent advection mixing in the micro-channel by inducing the fluids to a steady twisting flow profile that can be achieved by the series of repeating herringbone patterns.

Fluid flow for mixing in microchannel

Microfluidic technology advances the fluid dynamic characteristics to ensure a controlled homogeneous microfluidic environment. The laminar flow condition in microfluidic microchannel creates a well-defined and predictable interfacial region between two miscible fluids, which can be used for rapid mixing and patterning based on the feature of the microfluidic device.

Considering that the microfluidic device characteristic dimension is very small, fluid rheological behaviour and flow speed are crucial to maintain laminar flow conditions. The fluid flow profiles can be predicted by Reynolds number that shows the magnitude of inertial to viscous forces ratio (Michelon et al., 2017). Reynolds number (Re) is a ratio that categorises laminar flows (low Re values) from the turbulent flows (high Re values), as follows: $Re = Ul/\nu$ where U is the average flow speed, l is the cross-

sectional dimension, and, ν is the apparent kinematic viscosity of a fluid (Stroock, 2002).

At a low Re value, the mixing between two converging fluids is at a low flow rate and is diffusive-dominated without the advection contributions of turbulence and no hydrodynamic instabilities (Xu et al., 2016). In addition, Maeki et al. (2015) reported that the mixing of two solutions is found to be difficult at high Re values. This is in agreement with a suitable range of Reynolds number that was presented by Stroock et al. (2002) at $0 < Re < 100$, for creating transverse flows to induce steady chaotic mixing in the mixer that was based on SHM design. The chaotic (non-turbulent) mixing of the microfluidic approach differs from turbulent mixing where collisions are used to speed up the mixing process which is highly dependent on both geometry and speed profiles.

Flow speed for mixing in microchannel: rapid mixing

Microfluidic technology provides a platform to enable a rapid mixing process to occur in order to suppress the mass transfer of dissolved molecules that could lead to larger and heterogeneous lipid aggregation, promoting the formation of homogeneous monodispersed nanoparticles (Zhigaltsev et al., 2012). The use of a microfluidic cartridge with SHM feature enables rapid component mixing at a molecular level under focused hydrodynamic flow to prevent suboptimal mixing and heterogeneous nanoprecipitation of components (Obeid, Gebril, et al., 2017). In a single step process, microfluidic mixing technique is less harsh than sonication and is more robust than ethanol injection method, producing controlled vesicles with desirable size within seconds (Zhigaltsev et al., 2012).

It is estimated that the time required for diffusive mixing across the channel, t_m , decreases with flow speed, U , as follows: $t_m \sim \lambda / [U \ln (U/D)]$ where λ and l are characteristic mixing lengths determined by the geometry of the device and D is the molecular diffusivity (Chen et al., 2012; Stroock, 2002). Michelon et al. (2017) reported average flow speed is inversely proportional to the residence time inside of microfluidic device. At constant hydrodynamic fluid flow conditions, the transverse diffusion of two streams can be quantitatively described by the mixing time (He et al., 2013). The groove patterns on the floor of the microchannel in the staggered herringbone micromixer (SHM) generates a three-dimensional twisting flow that greatly increases the rate of mixing between two fluid streams (Xu et al., 2016).

In conclusion, SHM enables homogenous and rapid mixing between carrier materials and drug at a molecular level to form nanoparticles in the form of niosome vesicles. With the incorporation of the herringbone pattern enhances the rapid and reproducible generation of self-assembled vesicles at a low shear stress. As a result, microfluidic technique is capable of producing reproducible and homogeneous nanocarriers for drug delivery system.

Focused hydrodynamic flow: identical mixing conditions

Correia et al. (2017) reported that microfluidic systems step up in the area of drug delivery with promising features that allow the production of controlled particle size and good stability of the final liposome product characteristics, by applying different flow rate ratios (FRR) and total flow rate (TFR) during preparation. In the microchannels of the microfluidic cartridge, the organic and aqueous phases are isolated by two separated fluid inlet streams in laminar flow manner to prevent cross-

contamination and this leads to advection mixing which is highly consistent and repeatable. As opposed to turbulent flow, laminar flow ensures continuous flow at a steady state with each unit volume flowing through the micromixer region is under identical mixing conditions.

This focused hydrodynamic flow mixing conditions enables a controlled nanoprecipitation process to occur through the microfluidic platform via computerised syringe pumps. Hence, microfluidic method can be used to rationally optimise nanoparticle size for desired applications in drug delivery. The nano-sized of the vesicles can be precisely controlled by tuning the hydrodynamic flow conditions (e.g. flow rates of the fluids and diffusion coefficient of components) in the preparation process (He et al., 2013).

Theory of vesicle formation

According to Lasic (1988), lipids dissolved in an organic solvent were transformed into immediate structures called bilayer phospholipid fragments (BPFs). The diffusive mixing between water and organic solvent within the microchannel causes instabilities at the edges of BPFs, inducing bending and closing of the thermodynamically semi-stable BPFs, transforming into closed vesicles (Maeki et al., 2015). In a hydrodynamic flow focusing device, the changes in flow rate ratio can affect the organic solvent concentrations that are dependent on the variable stream widths of the focused solvent stream (Huang et al., 2010). As the flow rate ratio increases, the stream width of the organic solvent at the central region decreases while at the same time increases the organic solvent concentration. The higher lipid-ethanol concentrations can stabilise the structure of BPFs by causing more fragments to link with each other

forming larger liposomes. On the contrary, under a high flow rate, the ethanol content in the thin solvent stream is diluted rapidly owing to its smaller concentration gradient, therefore limiting the time of BPFs formation and forming smaller liposomes (Huang et al., 2010).

Solvent dilution rate (dilution of organic solvent initiates precipitation)

Maeki et al., (2017) proposed formation mechanism of lipid nanoparticles based on fluid dynamics by estimating the critical ethanol concentration through the dilution rate, the lipid concentration and the properties of lipids used. The study performed measurement of fluid dynamics in the microfluidic devices (with and without micromixer) using a laser scanning confocal microscope to capture fluorescence images for evaluation on mixing performance.

During ethanol dilution, the planar fragments grow by fusion (Chen et al., 2012; Stroock, 2002). At low ethanol concentrations, the destabilised fragments bend to form closed nanoparticles. When ethanol is diluted rapidly to low concentrations, the planar fragments have little time to grow before closing into vesicles, resulting in smaller particles (Maeki et al., 2017). At low flow rates where the mixing is slow, pockets of high ethanol concentration develop, favouring stabilisation and growth of intermediate fragments that lead to larger lipid nanoparticles.

Change in solvent polarity: flow rate ratio

When dissolved lipid molecules containing low-polarity organic solvent is mixed with water or buffer (high polarity), the change in polarity initiates the spontaneous self-assembly of the lipid molecules into vesicles. Upon reaching a critical polarity as the

polarity of the lipid solution increases with the rapid advective mixing of the two miscible fluids, a controlled precipitation process occurs resulting in the formation of lipid nanoparticles (Belliveau et al., 2012). Generally, the change in polarity of the mixed fluids is dependent on the flow rate ratio (FRR). At a higher FRR with increased volume of the aqueous phase, a faster change in the magnitude of polarity upon mixing can be achieved to increase the driving force for self-assembly of lipid molecules. Typically, higher FRRs lead to greater polarity changes and producing smaller liposomes. Similarly, a significant reduction in niosome sizes was reported with increased FRRs found to be TFR dependent (Obeid, Gebril, et al., 2017).

Formation of drug nanoparticulate system: Supersaturation

The addition of aqueous phase decreases the solvent potency to dissolve solute, resulting in a supersaturation state system (Martínez Rivas et al., 2017). Supersaturation as a function of the mixing ratios of solvent to aqueous phase, this can influence the final nanoparticle properties in which a higher supersaturation leads to a smaller particle size (D'Addio and Prud'homme, 2011).

Supersaturation ratio, S_r , is defined as the ratio of the particle solubility at the interface, C_s , to the bulk solubility, C_∞ .

$$S_r \equiv C_s / C_\infty \equiv S_{app} / S_o \quad \text{Equation 1.6}$$

Where S_{app} is the apparent solubility of the nanoparticle;

S_o is the equilibrium solubility.

Using Kelvin's equation (Equation 1.7), solubility at the nanoparticle interface in terms of the local supersaturation at the particle surface, S_r .

$$\ln S_r \equiv \ln [C_s / C_\infty] = [2\gamma M] / [\rho R T r] \quad \text{Equation 1.7}$$

Where γ is the surface tension (interfacial free energy);

M is the molecular mass of the solute;

ρ is the density;

R is the gas constant;

T is the absolute temperature;

r is the particle radius.

Formation of drug nanoparticle system: Nanoprecipitation and nucleation

Precipitation occurs when the solution is supersaturated (D'Addio and Prud'homme, 2011). Nanoprecipitation process occurs when the fully dissolved lipid molecules in water-miscible organic solvent is mixed with water. The polarity of the resulting solution increases and the solute concentration increases above saturation limit, which causes the lipid molecules to self-assemble into vesicles. Starting from a multi-component, single phase system, the precipitation occurs at the onset of supersaturation in order to reduce the system free energy (Capretto et al., 2013).

In a study by Kastner et al. (2014), the mathematical predictive modelling identified an increased dilution at higher FRR has contributed to a decreased diffusional mixing rate within the employed SHM for liposome manufacturing, which impacted on liposome size, polydispersity and efficiency. Moreover, the study found a lower rate of liposome formation and incomplete nucleation as a result of decreasing diffusional mixing rate and lipid concentration in the final liposome suspension. Nucleation phase is more dependent on the supersaturation level in comparison to the growth phase. Therefore,

a high supersaturation level is favourable to nucleation over the growth process to equilibrium concentration.

In order to produce monodisperse formulation, it is important to maintain a controlled microfluidic environment in terms of mixing rate, concentration and temperature. Throughout the production process, temperature can be controlled to achieve a better heat transfer owing to large surface areas due to small volumes of fluid being used.

1.6. Encapsulation efficiency, drug loading and drug release

Drug entrapment into vesicles as nanocarriers can contribute a significant improvement of the drug bioavailability in order to enhance therapeutic efficiency and reduce undesirable toxicity. It is one of the properties of nanocarriers that govern their fate in the process of drug absorption (Roger et al., 2010). In niosomes, they are self-assembled surfactant/lipid bilayer structure that encapsulates hydrophilic drugs into its aqueous core and compartments; while hydrophobic drugs are embedded within the bilayer membrane (Moghassemi and Hadjizadeh, 2014). Niosome encapsulation efficiency is commonly reported between 10-40 % and could reach approximately 75-90 % regardless of the aqueous solubility of the drug molecules (Dan, 2017) (Table 1-3). One important factor influencing the encapsulation efficiency of niosomes is gel-liquid phase transition temperature (T_c) of the non-ionic surfactant types used within the niosome formulation. Generally, a longer alkyl chain length leads to a higher phase transition temperature and higher encapsulation efficiency. Additionally, the degree of unsaturation in the alkyl chain changes the chain flexibility and niosome permeability can influence encapsulation efficiency and drug release (Khoee and Yaghoobian, 2017). Another factor influencing the niosome encapsulation efficiency is the

cholesterol level used within the niosome formulation composition (refer to Section 1.3.2.) for its membrane-stabilising property to improve the stability and EE of the vesicular formulations.

Drug loading is the encapsulation process where the drug entraps into a vesicle. Generally, drug can be entrapped via passive loading where the drug is firstly dissolved for simultaneous entrapment during the vesicle manufacturing process. This direct entrapment is widely used for hydrophobic drug loading into niosomes where the organic solvent to be removed completely in the conventional bulk manufacturing methods. Consequently, a purification process is required following the manufacturing process to remove unloaded drugs, often by using dialysis, centrifugation or gel filtration. Remote loading using transmembrane pH or ion gradient that favours the drug influx to the vesicles where it remains entrapped after the loading process (Moghassemi and Hadjizadeh, 2014).

Drug loading is based on the principle of passive loading within vesicles prepared using microfluidic, where both drug and lipids are co-dispersed in the water miscible fluid (Joshi et al., 2016). Using microfluidics, the highly efficient mixing can be seen in the incorporation of poorly water-soluble propofol within the membrane bilayers simultaneously as the vesicles form (Kastner et al., 2015). Furthermore, the drug loading during manufacturing process of nanoparticulate system did not show to alter vesicle size or distribution. However, the amount of lipophilic drug encapsulation was found to be affected by the process parameters used in microfluidic process (total flow rate and flow rate ratio) manufacturing methods.

From niosomes prepared by thin film hydration method with sonication, the in vitro release rate of poorly water-soluble drug (candesartan) was found to be sustained release compared to free drug solution (Sezgin-Bayindir, Antep and Yuksel, 2014). Similar retarded release results revealed for hydrophobic drug entrapped niosomes in simulated gastric fluid (Shehata, Abdallah and Ibrahim, 2015). For microfluidic-based niosomes encapsulating curcumin as hydrophobic drug model, the study reported a biphasic drug release pattern with an initial burst followed by constant release independent of different EE (Obeid et al., 2019). A study by Ali et al. (2010) reported that the drug release kinetics are mostly dominated by the lipid formulation composition and physicochemical properties of the vesicles manufactured regardless of manufacturing methods, following a first-order release kinetics. In contrast, manufacturing method was found to affect the amount of hydrophobic drug loading into the vesicles and that it demonstrated a zero-order release kinetics (Kastner et al., 2015).

1.7. Gastric physiology (stomach)

The primary function of stomach is to mix and grind up food into smaller size to pass through the pylorus sphincter, with the other three distinct muscular regions: fundus, body, and antrum (Peppas, Thomas and McGinty, 2009) (Figure 1-9). The muscle layers in the fundus region relax upon food entry and contract to force food towards the body and antrum regions. As the physiology of stomach such as low pH, motility and gastric emptying, provides barrier to drug delivery, very little absorption process occurs in the stomach (Pinto, 2010). In order to retain dosage forms in the stomach, variable formulation strategies employed to prolong gastric residence time such as

lower density (achieved via high porosity and/or swelling), floating (raft-forming), and bioadhesion (use of mucoadhesive polymers) (Sigurdsson, Kirch and Lehr, 2013).

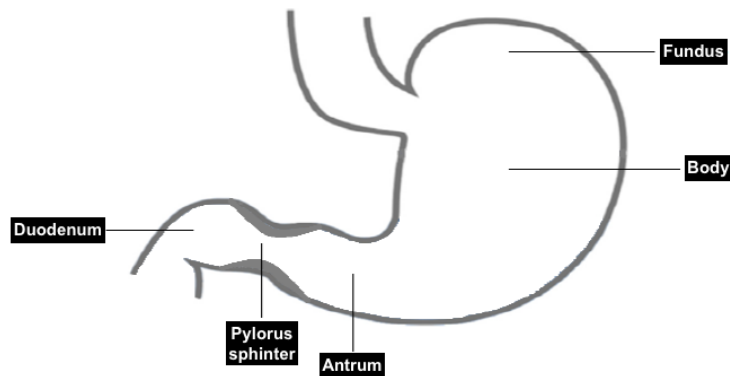


Figure 1-9: The stomach (adapted from Wilson and Washington, 1989).

1.7.1. Gastric mucus layer as physiological barrier

The stomach has a two-layered mucus system: attached inner layer acts as a diffusion barrier for hydrochloric acid, and loosely unattached outer layer (Johansson et al., 2013). Foveolar cells or surface mucus cells that are lining over the gastric region are primarily responsible for mucus secretion (Authimoolam and Dziubla, 2016). Mucus layer is comprised of a heterogeneous aqueous mixture of gel-forming mucin glycoprotein molecules that are located at the interface between mucosal surfaces and the external environment (Sigurdsson et al., 2013).

1.7.2. Mucus composition and structure

The main components of the mucus layer include water (up to 95% by weight), mucins (no more than 5% by weight), inorganic salts, carbohydrates and lipids (Peppas and Huang, 2004). The main structural component of the mucus layer is the mucin, providing a dense network of size-dependent mesh-like architecture matrix owing to their intermolecular cross-linking between mucin molecules (Murgia et al., 2018).

Mucins are crucial for maintaining the structure of mucus hydrogel layer with their conformations hindering proteolytic degradation and the reduction of intermolecular disulphide bonds which could lead to loss of gel formation. Therefore, fundamental understanding of mucin structure and intermolecular interactions is essential to gaining an insight into the viscoelastic gelation (aggregation/association) characteristics of gastric mucus layer.

Mucin glycoproteins are responsible for the characteristic viscoelastic and gel-forming properties of mucus that are essential for its protective barrier function on mucosa surfaces. Mucin networks are viscoelastic lubricious layers that formed from a continuous deposition of the mucin glycoprotein chains (self-association). Mucin networks can be visualized as multilayers of mucin glycoproteins that consisting of two distinctive zones – loosely adherent outer layers with an expanded free volume that are prone to easy removal (via disulphide intermolecular bonding); and dense, more intact mucosal adherent inner layer where hydrophobic domains of the longer mucin chains firmly anchored to the epithelial surface (Authimoolam and Dziubla, 2016). Despite mucin's importance, it is often considered a barrier that affects drug permeability and therapeutic bioavailability.

Mucin

In general, different mucin species among others can be described by different mass, different protein sequence and different level and quality of glycosylation for their physiological roles within different environments in which they are expressed. Once secreted by epithelial cells, mucin forms a mucus barrier layer not only to cover and

protect the epithelial surfaces against extracellular environment, but also to filter and select substances for binding and uptake by the epithelial cells.

Mucins can be divided into two classes: the classical gel-forming secretory mucins and the membrane-bound mucins. Membrane-bound mucins differ from secretory mucins as they contain a hydrophobic membrane-spanning domain that favours anchoring the molecules in the plasma membrane and also lack of intermolecular associations through disulphide bonding (Sigurdsson, Kirch and Lehr, 2013).

A monomer of mucin has a high molecular weight of 640kDa, with protein contributing to only 20% of its molecular weight. A mucin macromolecule is a block co-polymer that is characterised by highly branched oligosaccharide chains that are attached to the asparagine, threonine and serine side chains (*O*-glycosidically and *N*-glycosidically linked) of a polypeptide backbone (glycosylated hydrophilic blocks); and unbranched polypeptide backbone (non-glycosylated hydrophobic blocks). The highly branched oligosaccharide chains that constitute 75% of the length of polypeptide backbone contributed to the polymer's water holding capacity and therefore the hydrogel is resistant to proteolysis and essentially maintained its 3-dimensional structured barrier network (Peppas and Huang, 2004). Each branched oligosaccharide chain consists of 5 to 20 monosaccharide residues with terminal groups are often fucose, sialic acid, sulphate esters of galactose and *N*-acetylglucosamine (Murgia et al., 2018). Therefore, mucins are negatively-charged macromolecules due to these monosaccharide residues on the terminal ends of the branched oligosaccharide chains (Strous and Dekker, 1992).

Non-glycosylated regions of a polypeptide backbone chain are the sites where two or more polypeptide chains are linked via disulphide bridges between the cysteine residues to form the gel polymer network. Segregated domains of mucins form gel-like mucus layer through non-specific intermolecular interactions include hydrogen bonding, hydrophobic interactions and physical entanglements; and through disulphide linkages between cysteine residues in the non-glycosylated polypeptide backbone. At low pH, the conformation of a mucin macromolecule becomes extended to shield non-glycosylated polypeptide hydrophobic blocks from its surrounding aqueous environment (MacAdam, 1993).

pH-dependent solution-gel transition and viscosity of mucins

Highly acidic environment in the stomach causes the aggregation of mucin fibres that increase its viscoelasticity (Celli et al., 2007). The thickest mucus layer that present in human GIT can be found in the stomach and colon. Mucins are constantly secreted and then washed off in a cyclic manner, where they determine the thickness of mucus with gastric mucosal clearance time of 1-4 hours (Murgia et al., 2018).

Gastric mucin glycoprotein molecules have a pH-dependent solution-gel transition, which is crucial to act as protective barrier by forming the gastric mucus layer (Celli et al., 2005). For the maintenance of a cohesive gel layer over the gastric epithelial surface, the mucus will stay neutral below a pH value of 2 and negatively charged above pH 2. By having ionic constant (pK_a) of less than 3 in both sialic acid and sulphate esters, they will be fully ionised at all pH except the lowest pH, therefore the mucin molecules behave as negatively-charged polyelectrolytes (MacAdam, 1993). This contributes to the viscous property of the mucus gel layer due to the electrostatic

repulsion between the adjacent oligosaccharide chains (MacAdam, 1993) and the macromolecular structure is more expanded with a higher sialic acid content. The capacity of mucins to protect epithelial surfaces depends largely on their high content of oligosaccharides and their ability to form a protective gel (Strous and Dekker, 1992).

Mucus network's structure and rheology can be highly interdependent and impacted by localized pH and ionic concentration. For instance, Hong et al. (2005) have demonstrated that porcine gastric mucus undergoes pH-dependent physical state changes from solution (pH6) to gel (pH2) with transition at pH4 with glycoprotein chains showing an extended conformation as opposed to the random coil state in which this re-orientated chains favours the hydrophobic complexation between glycoprotein chains causing gelation to occur.

Macro- and micro-rheology of mucus

On a macroscale level, mucus represents a significant barrier to the absorption of some compounds when compared to an unstirred layer of equal thickness, while other compounds diffuse freely through the water network of the mucus hydrogel. This is because on a microscale level, mucus behaves as a low viscosity fluid that has different viscous and elastic properties than the bulk fluid (macroscale non-Newtonian) (Lai et al., 2009). Therefore bulk-fluid macro-rheological properties alone are not suitable to describe the barrier properties of the mucus against drug transport (Sigurdsson et al., 2013).

Mucus turnover and clearance

In stomach, mucins must be highly resistant to its extremely low pH to maintain an intact mucus layer to withstand the action of hydrolytic enzymes and shear forces (Strous and Dekker, 1992). Fast mucus turnover by mucociliary clearance where adhered mucin fibres are washed off as mucin layer replaces itself constantly. This rapid elimination hinders the diffusion of nanoparticles through the mucus layer (Murgia et al., 2018).

Diffusion across mucus layer

Gel-forming mucin glycoprotein molecules interacts with its surrounding and a mesh like structure has a feature of size filtering property with an average pore size between 10-500 nm (Grießinger et al., 2015; Lock et al., 2018). Unlike particle diffusion in water, which is non-restrictive and unchangeable with time, particles will undergo varying degrees of hindrance during their diffusion through a polymeric gel matrix such as mucus. Here the mucin fibres are undergoing continuous association and disassociation and the network as a whole undergoes elastic behaviour (Grießinger et al., 2015). At absorption site, the drug and drug carriers must overcome mucus turnover, clearance and binding interactions to penetrate the epithelium (Lock et al., 2018).

1.8. Mucoadhesion

There are several mucoadhesive biopolymers showing promising potential properties to improve the chemical and physical stability of the final formulation as well as showing a sustained release pattern (Essa et al., 2021). These mucoadhesive biopolymers such as alginate, chitosan and dextran derivatives, have been reported

to enhance vesicular systems via several approaches. Mucoadhesion improves drug absorption by prolonging the residence time of the drug carriers at absorption site, hence, increasing bioavailability of the drug (Takeuchi et al., 2001).

Shaikh et al. (2011) describes four main theories of mucoadhesion i.e. wetting, electrostatic, diffusion, and adsorption covering the two phases mechanism of mucoadhesion – contact phase followed by consolidation phase to enable a sufficient adhesion onto the mucosa membrane.

Wetting theory is related to spontaneous spreading of liquid formulation systems onto mucus surface, and involves surface tension and interfacial energies (Beri, Sood and Gupta, 2013). The theory calculates the contact angle as well as the thermodynamic work of adhesion. The wetting will be incomplete if the contact angle is greater than zero, indicates lower mucoadhesion.

Electrostatic theory is based on the transfer of electrons occurs across the adhering surfaces in contact due to differences in their established electrical double layer at the interface. Attractive forces maintain the adhesion between the two layers. For example, electrostatic interaction between cationic polymer and the anionic sulfonic and sialic acid residues within the mucus matrix (Han, Shin and Ha, 2012).

Diffusion theory is where the polymeric chains from the bioadhesive interpenetrate into mucin chains, reaching an equilibrium penetration depth within the mucus gel matrix to create a semi-permanent adhesive bond. The diffusion process is affected by the

polymeric chain lengths, and their mobility and availability. The interpenetration into each other depends on the diffusion coefficient and the time period of contact.

Adsorption theory is the attachment of adhesives based on the hydrogen bonding, hydrophobic bonding and van der Waals' forces, following the initial contact between two surfaces.

1.9. Analysis of non-ionic surfactant-based drug delivery system

In addition to the assay of the active pharmaceutical ingredient, one of the critical quality attributes of nanoparticle products is the concentration of lipid component in the formulation (Fan, Marioli and Zhang, 2021). For quantification, the analysis of lipid component within a formulation composition has been investigated by liquid chromatography for separation and then detection using several detectors such as diode array ultraviolet, refractive index, evaporative light scattering detector, and charged aerosol detector. Detection of the lipid component within the formulation composition used in the nanoparticulate formulation has been challenging as most lipids lack of a detectable ultraviolet (UV) chromophore (Brouwers et al., 1998). Due to this, several studies investigated the lipid quantification analysis employing mass detector i.e. evaporative light scattering detector to achieve quantitative detection and validation of lipids with a lower volatility than the mobile phase (Roces et al., 2016; Zhong, Ji and Zhang, 2010).

Similarly, non-ionic surfactant such as sorbitan ester surfactants are lacking UV chromophore, makes UV detection difficult as they do not absorb in the UV region. In addition, the composition complexity of sorbitan ester surfactants is due to the

distribution of the degree of esterification of the polyol, producing very complicated mixtures. Due to the fact that the evaporative light scattering detector provides a linear detection response for surfactants independent of molecular weight (Bear, 1988), high-performance liquid chromatography coupled with this detection technique was used in this research to demonstrate the recovery of niosome component and formulation.

1.10. Posed research questions

The main challenge to be addressed in this research is how the niosome manufacturing can affect the encapsulation and improve the solubility of poorly water-soluble drug using cinnarizine as the hydrophobic model drug, for targeted delivery to its narrow absorption site in the stomach.

Can the conventional thin film hydration and microfluidic as niosome manufacturing methods help to effectively encapsulate hydrophobic and hydrophilic drugs?

Can the niosome manufacturing methods and different niosome formulation compositions affect their characteristics?

Can the microfluidic as advanced niosome manufacturing method able to effectively minimise the variability and produce homogeneous niosomes?

Can mucoadhesive biopolymers such as chitosan and alginate, help to prolong the residence time of niosomes in the gastrointestinal mucosa to effectively enhance the absorption of poorly water-soluble drug?

1.11. Aim and objectives

The overall aim of this research project is to encapsulate poorly water-soluble drug (cinnarizine) within niosomes as nanoparticulate drug delivery system for targeted delivery to the stomach (narrow absorption site for cinnarizine). Studying the characteristics of niosome formulations manufactured by thin film hydration and microfluidic methods, to provide a better understanding of the effect of manufacturing methods and process parameters for formulation development and performance.

Overall objectives are to:

- Prepare niosomes entrapping cinnarizine as a model poorly water-soluble drug and methylene blue as a model of hydrophilic drug.
- Compare and evaluate characteristics of niosomes manufactured by thin film hydration and microfluidic methods.
- Investigate the manufacturing process and parameters affecting niosome characteristics.
- Investigate the effect of niosome formulation composition incorporating different co-surfactants on niosome characteristics.
- Investigate and explore the method for quantification of formulation composition recovery study using high-performance liquid chromatography with evaporative light scattering detection (HPLC-ELSD) technique.
- Investigate and explore the determination of mucoadhesion interactions (viscosity and zeta potential) of mucoadhesive biopolymers and niosome formulations.

1.12. Novelty of the research

With the aim to deliver hydrophobic drug (cinnarizine) orally into the stomach (narrow absorption site), the use and the manufacturing of niosome formulation to encapsulate the drug have been of utmost importance in this research. To the best of our knowledge, no study has demonstrated a direct comparison between thin film hydration and microfluidic methods for niosomes encapsulating hydrophilic and hydrophobic drugs. In addition to different niosome formulation parameters (formulation composition and concentration), this research also highlighted the manufacturing parameters for both methods in the preparation of niosomes encapsulation hydrophilic and hydrophobic drugs independently. Accordingly, the results generated and presented in this research will be beneficial in the understanding of the characteristics of niosomes as a nanoparticulate drug delivery system to be effectively manufactured.

1.13. Thesis structure

This thesis consists of eight chapters:

- Chapter One (the current chapter) provides a general introduction and overview on drug solubility issues and the various approaches used in the solubility enhancement with a focus on niosomes as oral drug delivery system. Methods of manufacturing niosomes are also discussed in this chapter with a focus on the conventional thin film hydration and the advanced microfluidic methods. The mucoadhesion strategy to enhance retention of the nanoparticulate system in the gastrointestinal tract is also discussed in this chapter.

- Chapter Two demonstrates the materials and experimental methods used throughout this research project, including descriptions and explanation of the theory and operational parameters.
- Chapter Three shows the use of methylene blue as a coloured hydrophilic drug for encapsulation into niosomes, for optimisation of niosome manufacturing process parameters and evaluation on niosome characteristics. Both conventional thin film hydration and microfluidic methods were discussed in this chapter. This chapter paves the way for the next chapter that involves a hydrophobic model drug, cinnarizine.
- Chapter Four evaluates the effect of the incorporation of cinnarizine as poorly water-soluble drug into niosomes following the optimisation of hydrophilic drug encapsulation into niosomes in Chapter Three. Both conventional thin film hydration and microfluidic methods were discussed in this chapter.
- Chapter Five presents the effectiveness of using mucoadhesive biopolymers (chitosan and alginate) for mucoadhesive niosomes to study the retention of encapsulated hydrophobic drug (coumarin-6) on the gastric mucosa, through fluorescence measurement and quantitation.
- Chapter Six explores the recovery of niosome formulation component (Span® 60 and cholesterol) using high-performance liquid chromatography technique with evaporative light scattering detection (HPLC-ELSD).

- Chapter Seven concludes the overall key findings of this research work and potential future works evolved from this research.
- Chapter Eight shows references

Chapter Two: Materials and Methods

2. Materials and methods

2.1. Materials

2.1.1. Model drugs

Model drugs used include pure cinnarizine (C5270), methylene blue 1.5 % (3978) and coumarin-6 (442631). They were all obtained from Sigma-Aldrich, UK.

Methylene blue (MB) was used as a model hydrophilic drug in this research project. It is a cationic heteroaromatic compound that is commonly commercialised as a chloride salt to be used as a photoactive phenothiazine dye. MB produces an intense blue colour in its aqueous solution.

Cinnarizine (CIN) was used as a model of poorly water-soluble drug. The weakly basic drug is a piperazine derivative with two tertiary amine groups. It is classified as a Class II drug in the Biopharmaceutical Classification System (BCS) owing to its low solubility and high permeability properties.

Coumarin-6 (C-6) was used as a hydrophobic fluorescent model drug. It is a member of 7-aminocoumarin.

Table 2-1: Physicochemical properties of cinnarizine (CIN), methylene blue (MB) and coumarin-6 (C-6).

Compound	Chemical formula	CAS number	Molecular weight	Log P	pKa	Melting point (°C)
CIN	C ₂₆ H ₂₈ N ₂	298-57-7	368.51	6.14	1.95 7.80	118-122
MB	C ₁₆ H ₁₈ CIN ₃ S	61-73-4	319.85	--	3.14	100-110
C-6	C ₂₀ H ₁₈ N ₂ O ₂ S	38215-36-0	350.43	5.42 (Steele et al, 2011)	2.98	208-210

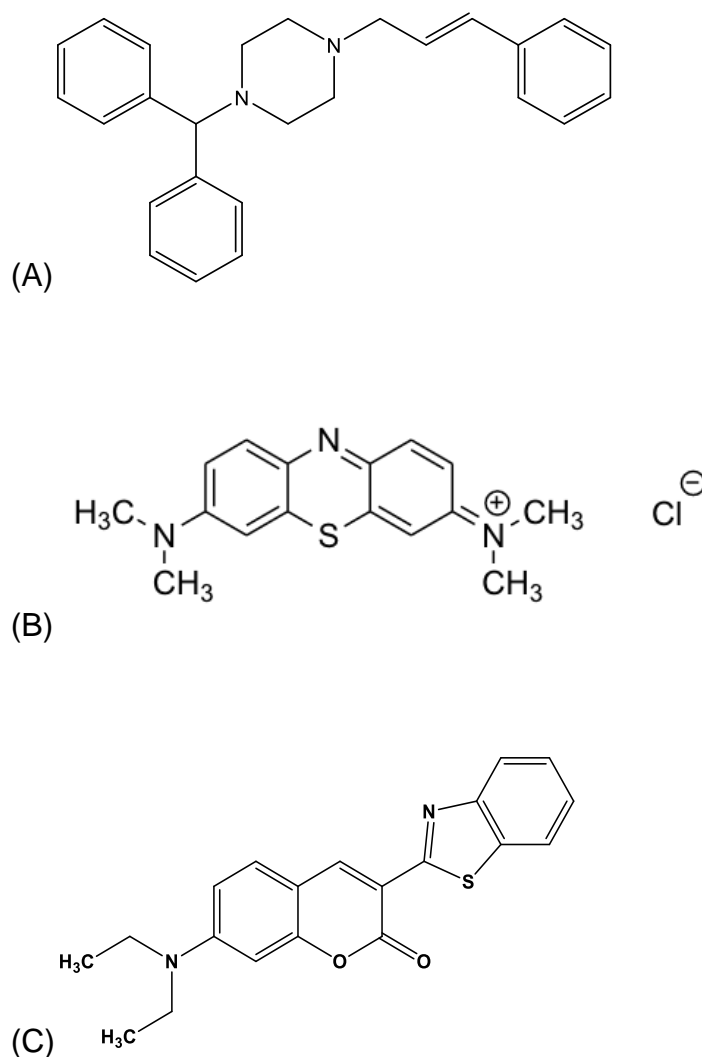


Figure 2-1: Chemdraw chemical structures of (A) cinnarizine, (B) methylene blue, and (C) coumarin-6. All drawn by ChemDraw.

2.1.2. Non-ionic surfactant and co-surfactants

Non-ionic surfactant sorbitan monostearate (Span® 60) was obtained from Sigma-Aldrich, UK. Co-surfactants used include Cremophor® ELP, Cremophor® RH40 and Solutol® HS15 were obtained from BASF, Germany. Non-ionic surfactant propylene glycol monolaurate (Lauroglycol™ 90) was obtained from Gattefossé, France.

Co-surfactants are additive agents to enhance the characteristics of the niosome vesicles. Hydrophilic co-surfactants are commonly used in the literature as emulsifiers, solubilising and wetting agents as they have a higher HLB value from 12 to 16 and higher molecular weight of over 1000Da.

2.1.2.1. Non-ionic surfactant: Span® 60 (S60)

Span® 60 (sorbitan monostearate) is an ester product produced by the dehydration of sorbitol and reaction with stearic acid (a saturated C18 long-chain fatty acid).

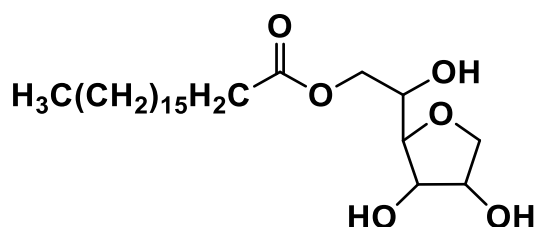


Figure 2-2: Chemdraw chemical structure of Span® 60.

Table 2-2: Physicochemical properties of Span® 60.

Chemical formula	CAS number	Molecular weight	HLB	Transition temperature
C ₂₄ H ₄₆ O ₆	1338-41-6	430.63	4.7	56-58 °C

2.1.2.2. Co-surfactant: Cremophor® ELP (ELP)

Cremophor® ELP is a purified polyoxyl-35-castor oil (polyethylene glycol 35 castor oil). It is a synthetic product that comprised of hydrogenated castor oil with ethylene oxide in a molar ratio of 1: 35. It is recommended for parenteral use and also suitable for oral and other dosage forms due to the fact that it has controlled free acid and potassium content with low moisture level in which the hydrolysis of drug can be prevented. In vitro studies by (Berthelsen et al., 2015) revealed that the highest bioavailability of fenofibrate (hydrophobic model drug) obtained from formulation

composed of Cremophor® ELP, indicating its solubilisation effect for increased absorption upon oral administration.

2.1.2.3. Co-surfactant: Cremophor® RH40 (RH40)

Cremophor® RH40 is a hydrogenated polyoxyl 40 castor oil. It has been shown to solubilise poorly soluble drug (fenofibrate) in an aqueous micellar formulation for increased absorption upon oral administration (Berthelsen et al., 2015).

2.1.2.4. Co-surfactant: Solutol® HS15 (HS15)

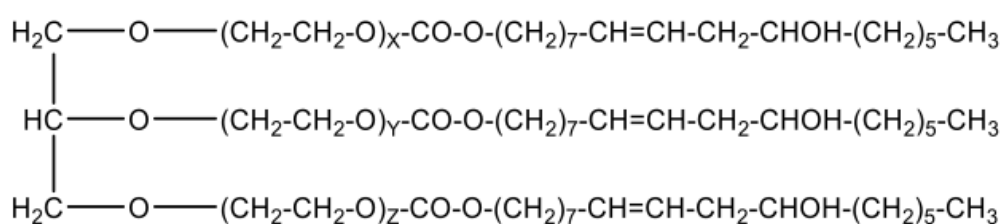
Solutol® HS15 (polyoxyl 15 hydroxystearate) is a polyoxyethylated non-ionic surfactant that consists of ethoxylated hydroxystearic acid and ethylene oxide. It has been widely used in numerous preparations such as self-emulsifying system, microemulsion and solid lipid nanoparticles. Solutol® HS15 is known to inhibit P-glycoprotein, which is an ATP-dependent pump that is responsible for reducing drug intestinal absorption by efflux transportation. Addition of this agent has shown to enhance paclitaxel aqueous solubility and permeability across Caco-2 monolayer cell without inducing cytotoxicity (Alani et al., 2010).

2.1.2.5. Co-surfactant: Lauroglycol® 90 (L90)

Lauroglycol® 90 is a non-ionic water-insoluble surfactant that is mainly comprised of monoesters and a small fraction of diesters of propylene glycol monolaurate. It is used as co-surfactant in oral formulations to solubilise poorly soluble drugs and enhance bioavailability.

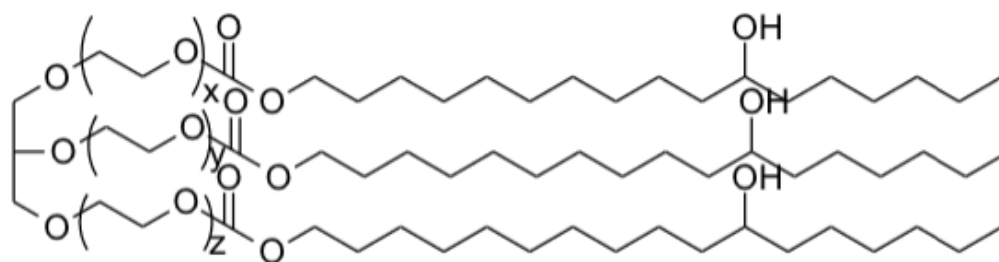
Table 2-3: Physicochemical properties of co-surfactants.

Co-surfactant	CAS number	Molecular weight	HLB	pH
Cremophor® ELP	61791-12-6	1630	12-14	5-7
Cremophor® RH40	61788-85-0	2625	15	5-7
Solutol® HS15	70142-34-6	1069	16	5-7
Lauroglycol® 90	27194-74-7	258.4	3	5-7



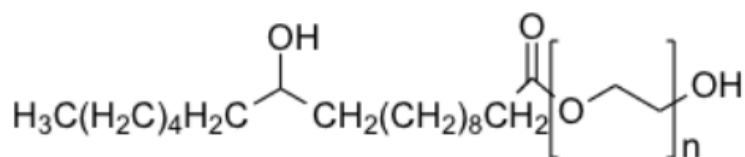
$$(X + Y + Z \sim 35)$$

(A)

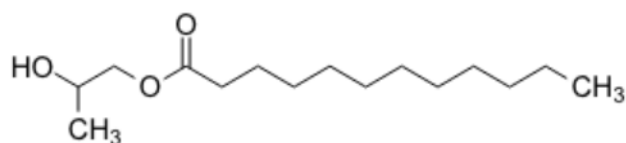


$$x + y + z = 40$$

(B)



(C)



(D)

Figure 2-3: Chemdraw chemical structures of (A) Cremophor® ELP; (B) Cremophor® RH40; (C) Solutol® HS15; and (D) Lauroglycol® 90 (C₁₅H₃₀O₃).

2.1.3. Lipids

Lipids used include cholesterol (C8667), glycerol monostearate (M2015) and dipamitoylphosphatidylcholine (P0763) were all obtained from Sigma-Aldrich, UK.

2.1.3.1. Cholesterol (CHO)

Cholesterol is the most commonly used additive agent as a membrane stabilizer in bilayered vesicles. The incorporation of cholesterol has shown to promote the gel-liquid transition temperature of niosome vesicles (Moghassemi and Hadjizadeh, 2014). With increasing less permeable cholesterol, a more condensed membrane (less fluidised membrane) was shown through drug release profile models by Ali et al. (2010).

2.1.3.2. Glycerol monostearate (GMS)

Glycerol monostearate is a glycerol ester of stearic acid consists of a saturated C18 long-chain fatty acid.

2.1.3.3. Dipamitoylphosphatidylcholine (DPPC)

DPPC is an amphipathic phospholipid that consists of two hydrophobic tails (C₁₆ palmitic acid) attached to a hydrophilic head group (phosphatidylcholine).

Table 2-4: Physicochemical properties of lipids.

Lipids	Chemical formula	CAS number	Molecular weight	Log P	Melting point (°C)
Cholesterol	C ₂₇ H ₄₆ O	57-88-5	386.65	7	147-149
GMS	C ₂₁ H ₄₂ O ₄	123-94-4	358.56	5.97	68-72
DPPC	C ₄₀ H ₈₀ NO ₈ P	2644-64-6	734.04	12	41

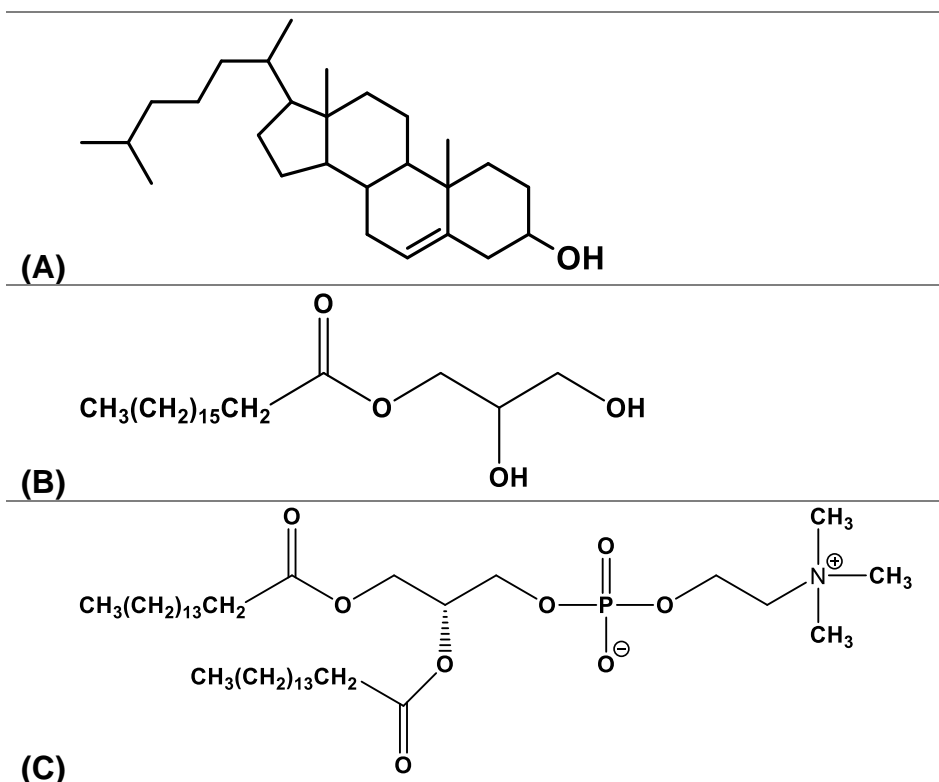


Figure 2-4: Chemdraw chemical structures of (A) cholesterol ;(B) glycerol monostearate (GMS); and (C) dipalmitoylphosphatidylcholine (DPPC).

2.1.4. Polymers for mucoadhesion study

Polymers used include chitosan highly viscous (48165) and chitosan low molecular weight (448869) were obtained from Sigma-Aldrich, UK; Gaviscon® Advance oral suspension was obtained from market.

2.1.4.1. Chitosan

Chitosan polymer was used in this research project to coat niosome due to its mucoadhesive, biodegradable and non-toxic properties. Chitosan is a natural cationic polysaccharide that is soluble in an acidic medium with a mucoadhesive property that has been shown to enhance the solubility of nanoparticles in aqueous solutions for targeted drug delivery (Sonia and Sharma, 2011). It is a linear polymer of N-acetylglucosamine and D-glucosamine units that is obtained by the alkaline deacetylation of

chitin, which is a long chain polymer of N-acetylglucosamine (derivative of glucose). It has a pKa value of about 6.5 which makes it insoluble in water. The solubility of chitosan increases with increasing the degree of deacetylation (DD), since the number of free amine group increases which are available to form complexes with polyanions. Chitosan exhibits polymorphism with different DD and average molecular weight (MW) dependent on the reaction conditions during its manufacturing process (Sonia and Sharma, 2011).

2.1.4.2. Alginate-based system: Gaviscon® Advance suspension

Alginate-based system, Gaviscon® Advance oral suspension (floating liquid alginate preparation) consists of a mixture of alginate which forms insoluble alginic acid (Figure 2-5) gel and a carbonate component. Upon administration, the suspension reacts with gastric acid and releases carbon dioxide bubbles that contribute to the buoyancy capability of the viscous gel floating on the gastric content (Singh and Kim, 2000).

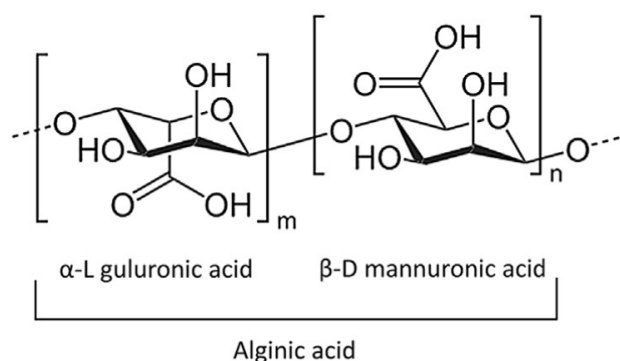


Figure 2-5: Alginic acid structure from Liang et al. (2015).

2.1.4.3. Mucoadhesion study

Period acid (P7875), Schiff (S5133), sodium metabisulfite (71932), acetic acid and mucin from porcine stomach Type II (2378) were obtained from Sigma-Aldrich, UK.

Simulated gastric fluid (SGF) 0.1 M HCl for dissolution and mucoadhesion studies was prepared from hydrochloric acid 37 % (Sigma-Aldrich, UK). Freshly excised porcine stomach tissue was obtained from (Green Marshall Abattoir, Bishop Auckland, UK).

2.1.5. Reagents, buffers and solvents

Methanol, trifluoroacetic acid and formic acid were obtained from Thermo Fisher, UK. Ethanol, chloroform and isopropanol were obtained from Sigma-Aldrich, UK. All solvents were of HPLC grade.

Buffer preparation salts include Trizma® hydrochloride (T3253), Trizma® base (10315), the composition of phosphate-buffered saline (sodium chloride, potassium chloride, disodium phosphate and potassium phosphate) were obtained from Sigma-Aldrich, UK. Mannitol powder (M9546) and sodium hydroxide pellets were obtained from Sigma-Aldrich, UK. All materials and chemicals were of analytical grade and used as received.

The PBS buffer contained 0.42 g/L sodium hydroxide, 6.19 g/L sodium chloride and 3.95 g/L monobasic sodium phosphate monohydrate in purified water. The pH was adjusted to 7.4 by either 1 M hydrochloric acid or sodium hydroxide.

Ultrapure water (18.2 MΩ-cm) used in all experiments was obtained from Triple Red Laboratory Technology with Nanopure™ Barnstead™ D3750 filter (0.2 µm).

2.1.5.1. Reagent for electron microscopy

Negative stain reagent (2% w/v sodium silicotungstate, Sigma Aldrich, UK) used was electron microscopy grade.

2.1.5.2. Purification and drug release

Sephadex® G50 (G50150, Sigma Aldrich, UK) for gel filtration chromatography was obtained from Sigma-Aldrich, UK. Dialysis membrane (MWCO 3500 Da) was used in drug release study.

2.2. Methods

2.2.1. Manufacturing of niosomes: Thin film hydration method (TFH)

In this research project, thin film hydration method was used as the conventional bulk method for preparation of all thin film-based niosomes. Firstly, non-ionic surfactants and additives e.g. cholesterol, and co-surfactant were weighed (see Table 2-5) and then dissolved in chloroform in a round-bottomed flask (Figure 2-6). Under reduced pressure (325 ± 10 mbar), the formation of thin film on the inside wall of the flask occurs after removal of the organic solvent by using the rotary evaporator for about 5 minutes. The thin film obtained was left to dry completely and cooled at room temperature (23 ± 2 °C) to ensure a complete loss of chloroform overnight. Subsequently, the dried thin film was hydrated with an aqueous buffer solution containing drug at 60 °C (temperature above the phase transition temperature (T_c) of Span® 60), to form multilamellar vesicles using an orbital shaking water bath or rotary evaporator at 100 revolutions per minute (rpm). All niosome suspensions prepared and purified were stored in a refrigerator for characterisation studies.

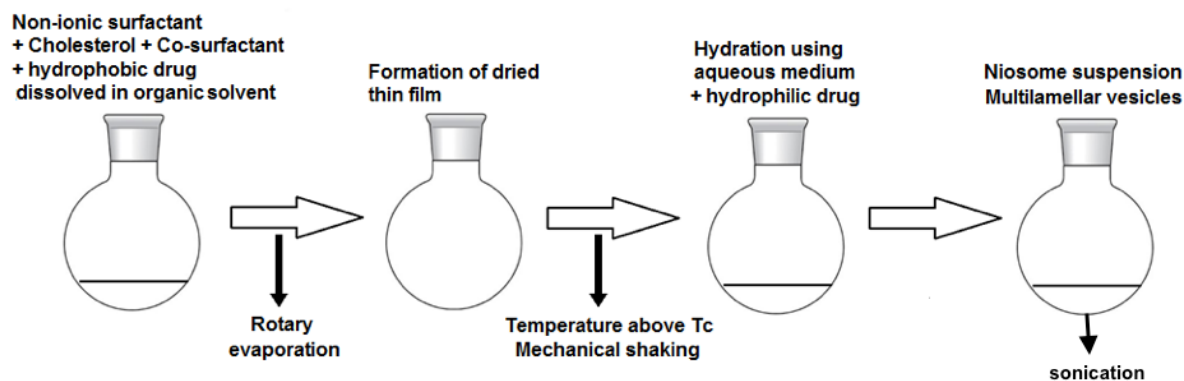


Figure 2-6: Process overview of thin film hydration method for niosome preparation.

Table 2-5: Compositions of niosomal formulations (total surfactant/lipid content of 200mg and drug content of 0.5 mg/mL).

Formulation component Composition (mg)	% Molar ratio	Total excipient content (mg)
Span® 60: cholesterol 105.4: 94.6	50: 50	200
Span® 60: cholesterol: Cremophor® ELP 73.0: 65.6: 61.4	45: 45: 10	200
Span® 60: cholesterol: Cremophor® RH40 61.6: 55.2: 83.2	45: 45: 10	200
Span® 60: cholesterol: Solutol® HS15 81.8: 73.2: 45.0	45: 45: 10	200

Probe sonication

Probe sonication technique was used to reduce the size of niosome vesicles manufactured by thin film hydration method. Probe sonication (130-Watt Ultrasonic Processor, Cole Parmer, UK) applied with amplitude set at 40 % for two cycles of two minutes with a minute rest in between; samples were placed in an ice bath throughout the whole process to prevent overheating. This was then followed by centrifugation (Mistral 1000 centrifuge, MSE, UK) at 5000 rpm for 5 minutes to remove any impurities.

2.2.2. Manufacturing of niosomes: Microfluidic method (MF)

2.2.2.1. Microfluidic NanoAssemblr™ Benchtop system

NanoAssemblr® Benchtop system (Precision NanoSystems Inc., Vancouver, Canada) was employed as the microfluidic method for the preparation of niosomes in this research project. The system is comprised of an instrument with a controlled syringe pump platform, a microfluidic cartridge consisting of two inlets and a single outlet and a heating block for controlling temperatures. The microfluidic cartridge is a cyclic olefin copolymer-based micromixer device that is compatible with the use of water-miscible solvents such as ethanol, methanol and isopropanol.



Figure 2-7: NanoAssemblr® Benchtop instrumental system (image was taken in our laboratory, Fleming 107, University of Sunderland).

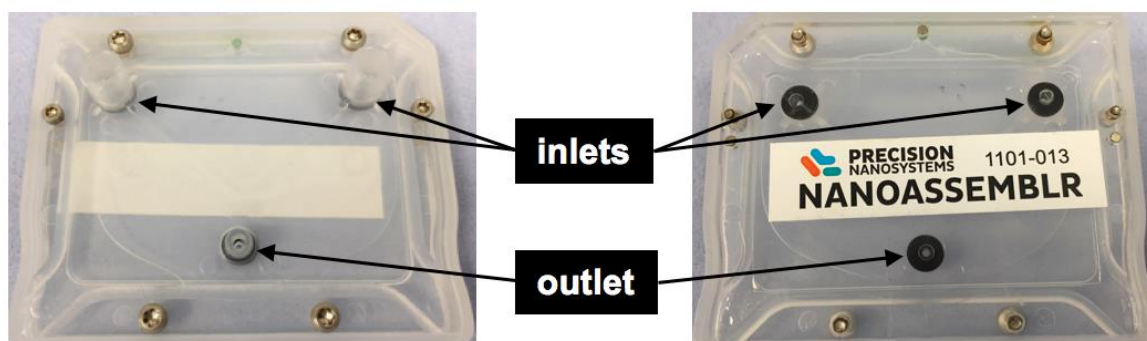


Figure 2-8: NanoAssemblr® microfluidic cartridge back (left) and front (right).

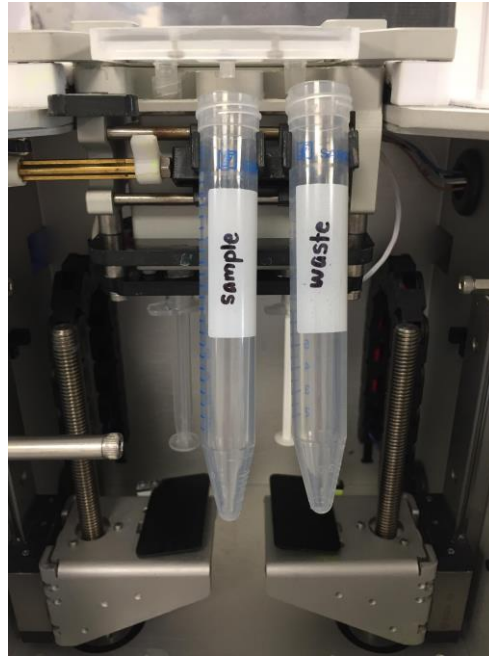


Figure 2-9: Inner view of the Benchtop instrument showing the syringe pump system and the outlets (sample and waste collection).

2.2.2.2. Microfluidic: Experimental method

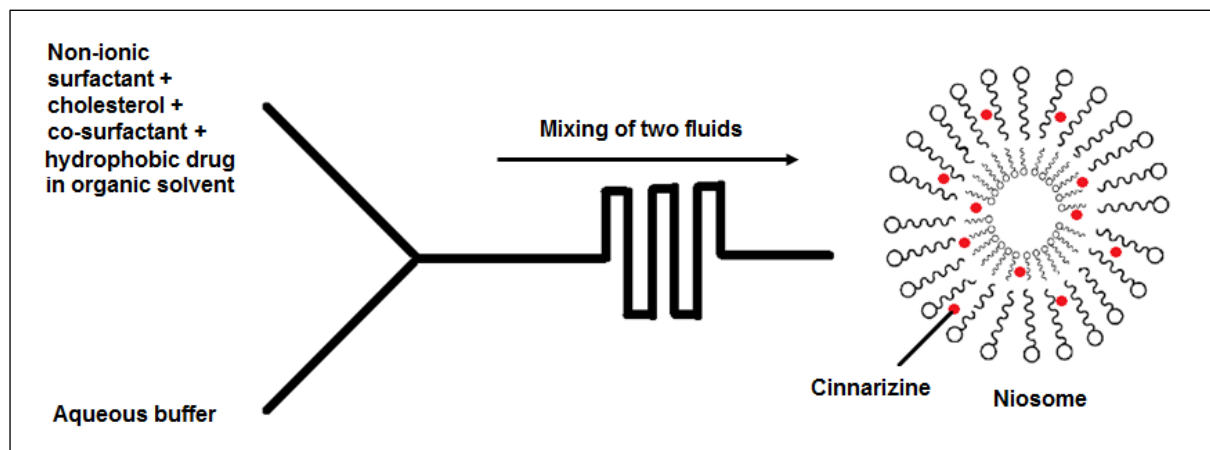


Figure 2-10: Schematic diagram for the mechanism of action of NanoAssemblr™ microfluidic cartridge in the niosome preparation to encapsulate cinnarizine. Mixing of two fluids occurs at the staggered herringbone micromixer (SHM) feature. Niosome encapsulation of methylene blue prepared from the mixing between MB-containing aqueous buffer and dissolved excipients-containing organic solvent.

In all experiments, all excipient ingredients (non-ionic surfactant, cholesterol and co-surfactant) were firstly dissolved in ethanol to be used as the organic phase (refer to

Table 2-5 for formulation compositions). The mixture was sonicated and warmed in a water bath at 60 °C to ensure all the excipient ingredients were dissolved to a clear solution prior to use in the microfluidic system. For the aqueous phase, phosphate-buffered saline (PBS, pH 7.4) and Trizma® buffer (pH 7.4) were used for cinnarizine and methylene blue, respectively. According to individual concentrations as stated in Table 2-5, the poorly water-soluble cinnarizine was dissolved in the ethanol (organic phase) together with excipient ingredients; whereas the hydrophilic methylene blue was dissolved in the buffer (aqueous phase). All solutions were warmed in a water bath at 60 °C and sonicated to ensure even mixing, prior to withdrawal for use in the microfluidic system, using appropriate disposable syringes of polypropylene/polyethylene Luer-Lock™ tip (Becton, Dickinson and Company, Wokingham, UK) fitting to the inlets of the microfluidic cartridge (Figures 2-8 and 2-9): 1 mL syringe for ethanol lipid solution and 3 mL syringe for aqueous buffer solution.

Table 2-6: General experimental details on system and formulation parameters.

Formulation component and composition	Span® 60: cholesterol: co-surfactant (45: 45: 10 mol%)
	Span® 60: cholesterol: dicetyl phosphate (50: 40: 10 mol%)
Organic phase	Ethanol
Aqueous phase	Phosphate buffered saline (PBS) pH 7.4
	Trizma® buffer pH 7.4
	0.1M hydrochloric acid solution (HCl) pH 1.2
Operating temperature	60 °C
Total output volume	2 mL
Start and end waste volume	0.4 mL

Table 2-7: Experimental details and formulation compositions (component concentrations) in determining the effect of total flow rate (mixing speed).

Formulation component and composition	Span® 60: cholesterol: co-surfactant (45: 45: 10 mol%)
Final lipid concentration	20 mg/mL
Final drug concentration	0.5 mg/mL
Flow rate ratio (aqueous: ethanol)	4: 1
<u>Variable:</u> Total flow rate (mL/min)	2, 4, 6, 8, 10, 12

Table 2-8: Experimental details and formulation compositions (component concentrations) in determining the effect of flow rate ratio (aqueous: organic).

Formulation component and composition	Span® 60: cholesterol: co-surfactant (45: 45: 10 mol%)
Final excipient concentration	20 mg/mL
Final drug concentration	0.5 mg/mL
Total flow rate	12 mL/min
<u>Variable:</u> Flow rate ratio (aqueous: organic)	1: 1 3: 2 3: 1 4: 1 9: 1

2.2.2.3. Microfluidic: Staggered Herringbone Micromixer (SHM)

In this research project, the microfluidic cartridge used in all the preparation of microfluidic-based niosomes has the feature of a staggered herringbone micromixer (SHM). Microfluidic staggered herringbone micromixer (SHM) works through a controlled nanoprecipitation process where the dissolved lipid and surfactant molecules spontaneously self-assemble into closed vesicles when the water-miscible organic solvent is mixed with aqueous solution. The design of SHM is based on the

patterns of grooves on the floor of the microchannel mixing section where they generate transverse flow to induce a steady chaotic mixing (Stroock, 2002). The repeating herringbone structure of SHM generates a three-dimensional twisting fluid flow that greatly increases the mixing rate between the two fluid streams (Xu et al., 2016) by providing an exponential increase in surface area of the distance travelled to generate a higher diffusional mixing (Zhigaltsev et al., 2012). This rapid non-turbulent, advective mixing of the two miscible fluids correspondingly increases the polarity of the lipid solution and hence, the precipitation and formation of lipid nanoparticles at a critical polarity (Belliveau et al., 2012).

2.2.2.4. Microfluidic process parameters

The rate of mixing (total flow rate, TFR) and the ratio of aqueous and organic solvent stream (flow rate ratio, FRR) are the primary process parameters that impact on niosome characteristics.

Total flow rate (TFR) is the total mixing speed (mixing rate) in mL/min at which the two fluid stream inlets are being pumped through the cartridge. Flow rate ratio (FRR) is the volumetric ratio of the aqueous and organic phases being mixed through the microfluidic cartridge.

Defined characteristics: Process parameters

- Total flow rate (mixing rate)
- Flow rate ratio

Defined characteristics (Size and polydispersity index): Formulation parameters

- Excipient (lipid/surfactant) concentration (mg/mL)
- Chemical composition/formulation, drug/component ratio/concentrations

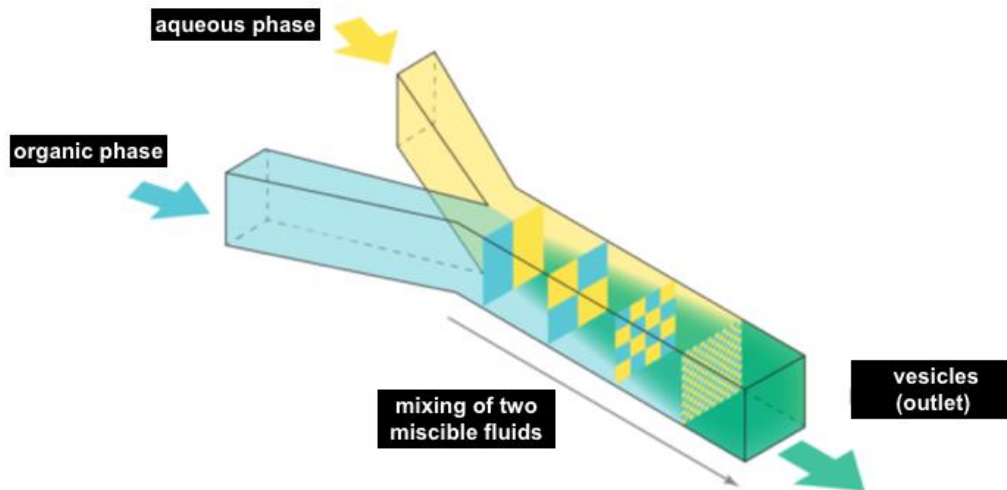
Mixing mechanism

Figure 2-11: Diagram depicting two fluids mixing in a NanoAssemblr™ microfluidic cartridge (adapted from Precision Nanosystems Inc.).

Two miscible fluids are computerised controlled and pumped independently into each inlet of the NanoAssemblr™ microfluidic cartridge under a laminar flow and at a low shear stress (Figure 2-11). The microscopic structures in the microchannel are causing the two fluid streams to mingle in a controlled, reproducible, and non-turbulent manner. The intermingling of the fluids increases as they move through the micromixer, effectively increasing the surface area and the interface between the two fluids across which diffusion can take place by reducing the diffusion distance. The diffusional mixing occurs through an advection process that is reproducible at determined process parameters (TFR and FRR). The fluid output from the outlet of the cartridge is completely mixed containing vesicles.

2.3. Calibrations

Calibration determines the relationship between the known analyte concentrations and their analytical responses e.g. absorbance, peak area, peak height, etc. A calibration curve can be obtained by plotting the responses and fitting them to a best fit linear equation in the method of least squares. By having the best-fit equation, an unknown analyte concentration of a sample can be calculated using its obtained response signal.

2.3.1. Calibration plot: Cinnarizine

Preparation of cinnarizine standards for calibration

Cinnarizine pure powder (100 mg) was weighed and dissolved in 500 mL of 0.1 M hydrochloric acid. The stock solution was sonicated for 10 minutes until the drug completely dissolved. Serial dilution of stock solution to produce drug concentration of 20 µg/mL and a range of concentration from 1 to 20 µg/mL (1, 2, 3, 4, 5, 8, 10, 15 and 20 µg/mL).

2.3.1.1. Cinnarizine calibration using ultraviolet (UV) spectrophotometry

The cinnarizine solution was measured at wavelengths between 245 to 256 nm with a bandwidth of 1.0 nm by using a UV-Vis single beam spectrophotometer (Model M501, Spectronic Camspec Ltd. Cambridge, UK) to determine the wavelength with highest absorbance peak for cinnarizine. The wavelength of maximum absorbance (λ_{\max}) obtained at 255 nm and was used in the measurement of cinnarizine absorbance in order to construct a calibration curve. Based on the calibration plot, an equation was generated to calculate the unknown drug concentration in relative to absorbance measured.

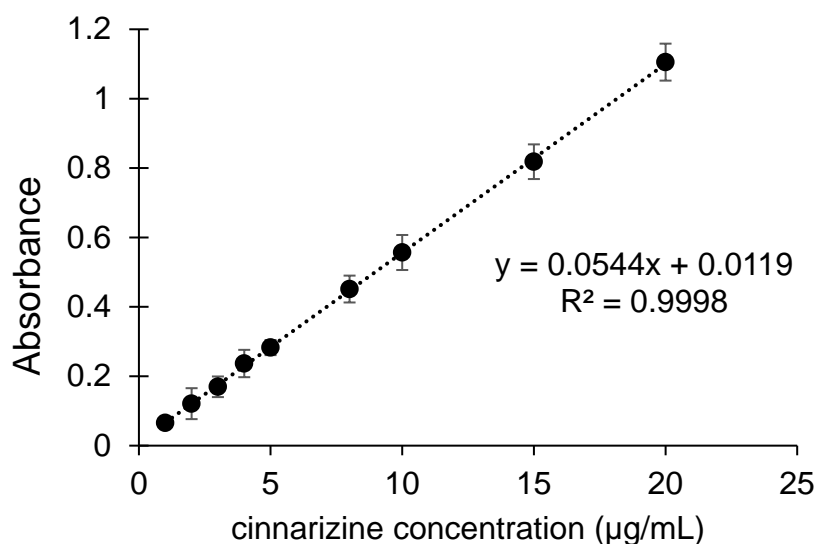


Figure 2-12: Calibration plot for cinnarizine measured using UV spectrophotometry.

2.3.1.2. Cinnarizine calibration using reversed-phase high-performance liquid chromatography (HPLC)

A reversed phase ultra-high-performance liquid chromatography (RP-UHPLC) system (Agilent technologies, Germany) with spectrophotometric (ultraviolet) detection was used for cinnarizine quantification based on previous method with modification (Abdel-Hamid et al., 2012). The column used was Agilent Zorbax Eclipse Plus C18 (50 mm, 2.1 mm, 1.8 µm) and the column temperature was maintained at 30 °C. Flow rate at 0.3 mL/min and injection volume used was 10 µL. The detection wavelength was 255 nm. Gradient elution (Figure 2-13) was used consisting of mobile phase A (0.1 % v/v formic acid in water) and mobile phase B (0.1 % v/v formic acid in methanol) according to Figure 2-13. Analysis time was set at 5 min and elution peaks obtained showed well separation with a flat baseline. All samples were prepared in methanol and subjected to be filtered using 0.2 µm syringe filter prior to measurements. Agilent ChemStation software was used to process and quantitate all the responses measured. All the experiments were performed in triplicates. The mean and standard deviation of peak

responses were calculated for each concentration. Calibration curve was constructed by plotting the peak responses versus the known drug concentration standards.

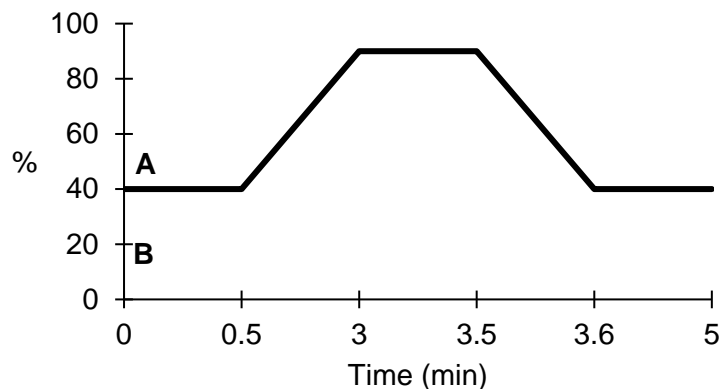


Figure 2-13: Gradient elution.

2.3.1.2.1. High-performance liquid chromatography (HPLC) method validation

The HPLC method for cinnarizine assay was validated according to the International Conference of Harmonization (ICH) guideline Q₂ (R₁) for linearity, specificity, sensitivity, precision, and accuracy. These validation characteristic parameters are for the purpose of evaluation on the analyte identification, testing for impurities and assay (quantitation of analyte). Using the gradient elution method described in Section 2.2.1.3., the elution peak of cinnarizine can be seen at 2.2 minutes and quantified spectrophotometrically (255 nm).

Linearity/working range is the linear relationship between a range of known standard analyte concentrations and their responses (peak area) detected, also known as the calibration plot. The standard calibration curve was generated based on the known standard analyte concentrations from 0.01 to 10 µg/mL. This was to include the standard concentrations between the range of 50-150% of the expected working range.

Three replicates of standard concentrations were injected into the HPLC system in triplicate (n=9). The average of obtained peak areas and standard deviation were plotted against the known drug standard concentrations. All responses obtained show good consistency. Linearity was obtained using the range of known standard concentrations used and the level of correlation coefficient (R^2) was generated. Calibration curves showed a good linear fit with a correlation coefficient (R^2) approaching 0.9998 (Figure 2-14).

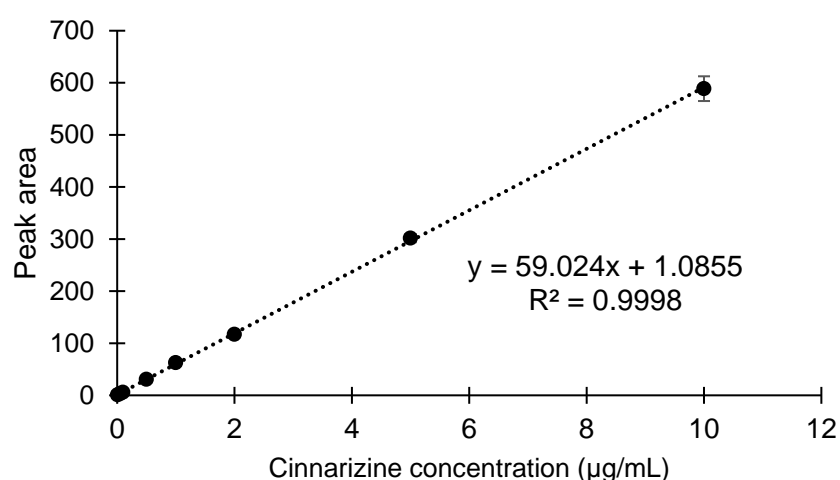


Figure 2-14: Calibration plot of cinnarizine (0.01 to 10 µg/mL) measured using HPLC - linearity assessment of the method. The known cinnarizine concentrations were 0.01, 0.05, 0.1, 0.5, 1, 2, 5 and 10 µg/mL. Calibration curve was plotted starting from 0.01 µg/mL.

Specificity of the analytical method refers to its ability to differentiate and quantitate the analyte in a mixture that contains formulation components and potential degradants. To assess specificity, no-drug niosome formulation and drug-containing niosome formulation were dispersed in methanol before injected into the HPLC system. Figure 2-15 shows the responses obtained on formulation samples that comprised of the same formulation excipients without and with cinnarizine. In (B), the peak of the analyte can be clearly seen as well detected in the drug-containing sample.

Analyte was shown to be separated from the mixture with its response peak observed at about same retention time in different formulations comprised of different components. Additionally, this retention time of drug-containing sample is of the same to those of standard drug concentrations.

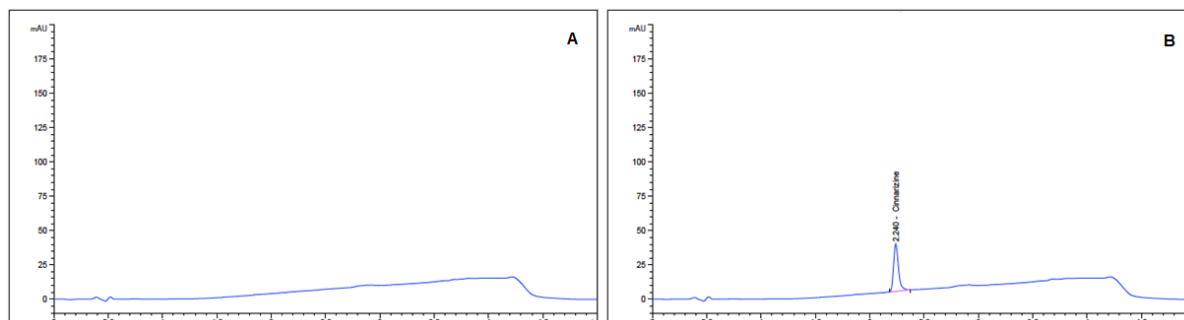


Figure 2-15: (A) drug-free formulation (baseline); (B) cinnarizine-containing formulation.

Sensitivity was assessed based on the limit of detection (LOD) and the limit of quantitation (LOQ). Both limit values were determined based the standard deviation of the response (δ) and the slope (S) obtained from the calibration curves generated during the linearity assessment. A signal-to-noise ratio of 3.3 was considered for LOD, whereas, a signal-to-ratio of 10 was considered for LOQ (Equation 2.1 and 2.2). This was to determine the lowest concentration used to obtain a sharp and symmetrical peak that resolves within 10 % of the chromatogram baseline. The estimated values for limit of detection and limit of quantification were 0.026 $\mu\text{g/mL}$ and 0.077 $\mu\text{g/mL}$, respectively.

$$LOD = 3.3 \delta/S \quad \text{Equation 2.1}$$

$$LOQ = 10 \delta/S \quad \text{Equation 2.2}$$

Where δ is the standard deviation of intercepts of calibration curves;

S is the slope of linearity plot.

Precision

Intraday precision (repeatability) and interday (intermediate) of the method was determined for cinnarizine from 0.01 to 10 µg/mL. This was to determine how closely measurement values are to each other under the same experimental conditions over a short interval of time and over different days. For each cinnarizine standard concentration, three replicates were analysed (measured peak areas) to construct a calibration curve (Figure 2-14). The linearity assessment results show high consistency (correlation coefficients > 0.9970) in all the calibration curves (Figure 2-16) for both intraday and interday, demonstrating a reproducible method.

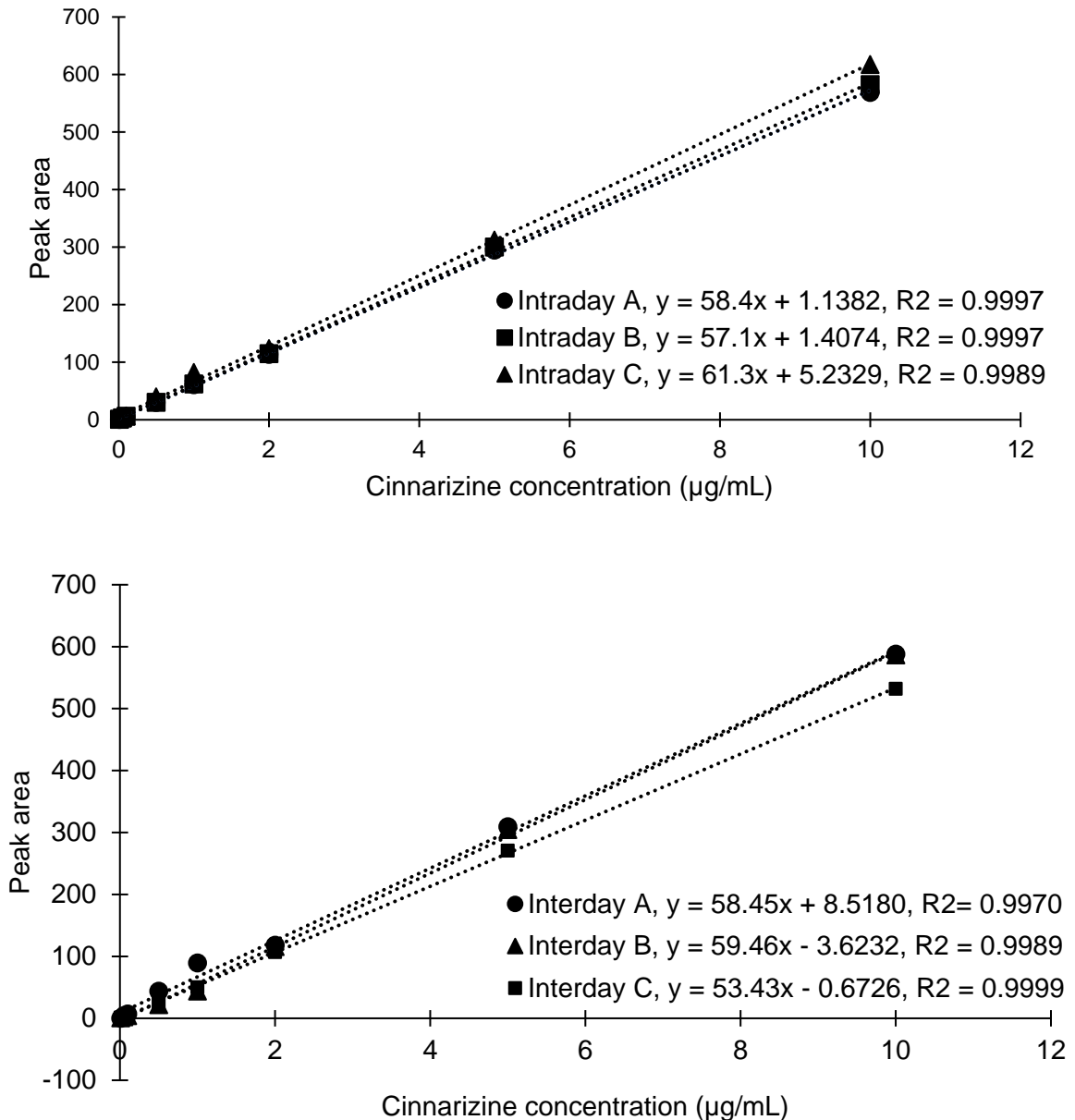


Figure 2-16: Cinnarizine quantification – method precision assessment (top) intraday and (below) interday linearity plots with linear regression coefficients.

Accuracy expresses the closeness of agreement between the value which is accepted as a conventional true value (known) and the value found (measured). In this study, accuracy of the assay (blank) was tested by quantifying spiked standards prepared. Three batches of cinnarizine concentrations at 0.05, 0.1 and 0.5 µg/mL were injected into the system in triplicate (n = 9). The relative standard deviation (% RSD) and the recovery of cinnarizine were calculated for each standard concentration. The %

RSD and the extent of percent recovery for each cinnarizine concentration level were within the acceptable limit of $\leq 5\%$ and 90-110% respectively.

Table 2-9: Evaluation of %RSD and recovery during the assessment of accuracy.

Known standard concentration ($\mu\text{g/mL}$)	Peak area (mAU.s)	Found concentration ($\mu\text{g/mL}$)	Average known standard concentration ($\mu\text{g/mL}$)	Standard deviation	Average found concentration ($\mu\text{g/mL}$)	Relative standard deviation (%)	Percentage recovery (%)
0.05	3.94	0.0484	0.05	0.00282	0.0504	5.60	100.79
0.05	3.99	0.0492					
0.05	4.25	0.0536					
0.1	6.82	0.0972	0.10	0.00127	0.0972	1.31	97.21
0.1	6.90	0.0985					
0.1	6.75	0.0960					
0.5	30.39	0.4965	0.50	0.01566	0.5026	3.12	100.52
0.5	30.06	0.4909					
0.5	31.80	0.5204					

2.3.2. Calibration plot: Methylene blue

Preparation of methylene blue standards for calibration using ultraviolet (UV) spectrophotometry. Dilutions of methylene blue have been prepared in a 1:1 mixture of Trizma buffer (pH 7.4) and isopropanol (0.2, 0.4, 0.6, 1.0, 1.2 and 1.4 $\mu\text{g/mL}$). The absorbance of the drug was taken at 665 nm using the UV-Vis single beam spectrophotometer (Model M501, Spectronic Camspec Ltd. Cambridge, UK). Calibration curve for methylene blue was generated and showed in Figure 2-17.

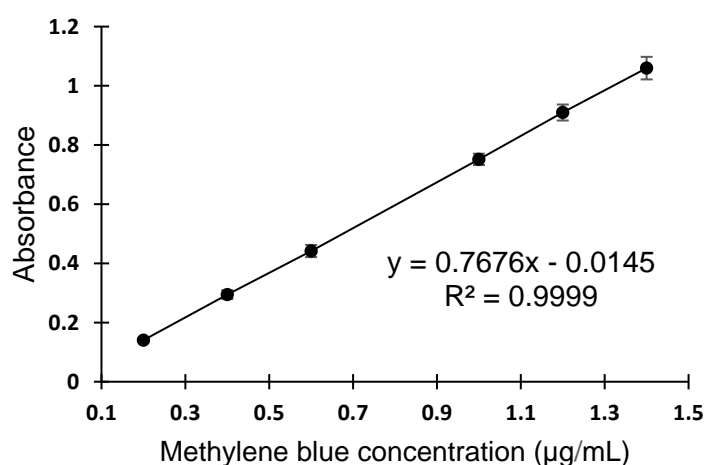


Figure 2-17: Methylene blue calibration curve.

2.3.3. Calibration plot: Mucin

Preparation of mucin dispersion for calibration

A 1 mg/mL of stock mucin dispersion was prepared by adding mucin (from porcine stomach Type II, bound sialic acid $\leq 1.2\%$, Sigma M2378) into deionised water and placed in an ultrasonic bath (Model FRM100, Hilsonic, Bromborough, UK) for 30 min (Sogias, Williams and Khutoryanskiy, 2008). The mucin dispersion was then centrifuged for 5 min at 1000 rpm to remove any insoluble glycoprotein fractions. The supernatant was collected and diluted to produce standard solutions (25, 50, 75, 100 and 150 $\mu\text{g/mL}$). All mucin dispersions were freshly prepared for each experiment. All measurements were made from three independent batches. Highest absorbance obtained at 555 nm by using xMark microplate spectrophotometer for mucin standards.

2.3.3.1. Mucin calibration using colorimetric method

A colorimetric method was used for mucin calibration (mucin standard solutions - see 2.2.3.1.) based on the Periodic acid and Schiff (PAS) reaction method from Alam, Paget and Elkordy (2016). (Mantle and Allen, 1978).

Period acid reagent: 10 μL of 50% Periodic acid (5mg) was added to 7mL of 7 % acetic acid.

Schiff reagent: 0.1g of sodium metabisulfate was added to every 6mL of Schiff reagent and incubated at 37°C to ensure the reagent remained in colourless.

Process overview: Periodic acid reagent (0.2mL) was added to 2 mL sample and incubated at 37 °C for 2 hours followed by addition of 0.2mL of Schiff reagent and then

kept at room temperature for 30 minutes before measurement using a UV spectrophotometer or microplate reader.

Measurements:

The ultraviolet (UV) absorbance of mucin was taken at 555 nm using a UV-Vis single beam scanning spectrophotometer (Model M501, Spectronic Camspec, Leeds, UK).

A calibration curve for mucin solution was generated and shown in Figure 2-18.

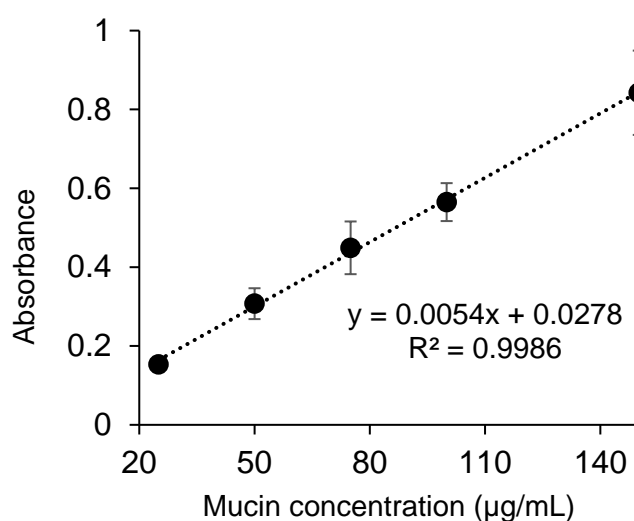


Figure 2-18: Calibration curve of mucin.

2.3.4. Calibration plot: Coumarin-6

Preparation of coumarin-6 standards for calibration

Standard solutions (0.5, 1.25, 2.5, 5.0 and 10.0 µg/mL) were prepared from dilutions of the working solution (10 µg/mL) using methanol as diluent. Methanol was used as blank (without coumarin-6).

2.3.4.1. Coumarin-6 calibration using reversed-phase high-performance liquid chromatography (HPLC)

A reversed phase mode HPLC with fluorescence detection (excitation wavelength at 440 nm; emission wavelength at 460 nm) was used to detect and quantify coumarin-6 (Agilent Chemstation). The column used was ACE UltraCore SuperC18 (100 mm x 4.6 mm x 2.5 μm ; 95 \AA) and maintained at 35 $^{\circ}\text{C}$ column temperature. Gradient elution used (Table 2-10) was comprised of mobile phase A (0.1% TFA in water) and mobile phase B (0.1% TFA in methanol). Flow rate was (1 mL/min) with injection volume used was 10 μL . All experiments were performed in three independent batches. Calibration curve for fluorescent coumarin-6 was generated and showed in Figure 2-19.

Table 2-10: Gradient elution.

Time (min)	%A	%B
0	70	30
5	0	100
7	0	100
9	70	30
10	70	30

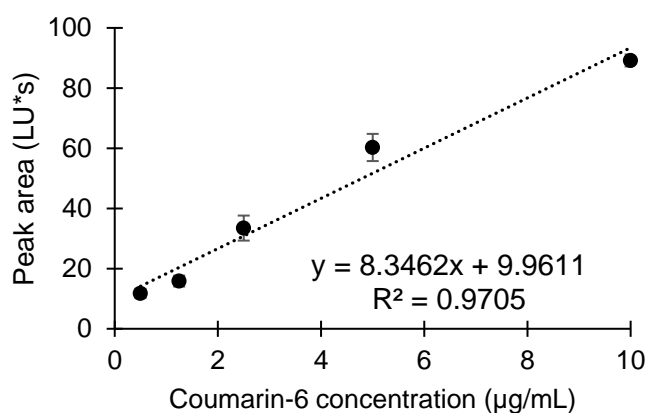


Figure 2-19: Calibration curve of coumarin-6 standard solutions.

2.4. Purification of niosomes: Gel chromatography filtration

Purification of manufactured niosome suspensions was performed to remove the untrapped drug, using gel chromatography filtration in all experiments. This dynamic gel column filtration technique is based on size exclusion chromatography for the separation of analytes based on their sizes. The gel column employs porous beads with a defined pore size distribution as the stationary phase. Smaller beads with a smaller range of pore sizes permit higher resolution by having a lower flow rate through the column for a slower separation. Niosomes are nano-sized vesicles ranging from several nanometres up to microns. For this reason, Sephadex® G50 column (lower and upper sizes are 1.5 and 30 kDa) was employed in this research project. The gel columns were prepared by loading swollen beads into a 25 mL graduated burette column and allowed to equilibrate overnight before use.

A 0.5 mL of each individual niosome suspension prepared was eluted down a Sephadex® G50 column. Aqueous mobile phases i.e. phosphate buffered saline and Trizma® buffer were used for the elution process with respect to the buffer solution used in the manufacture of niosomes encapsulating cinnarizine and methylene blue respectively. As vesicles (drug-loaded and non-drug-loaded) are larger in size than free non-entrapped drug and/or excipient compounds, they enter few pores in the gel and therefore vesicles move quicker down the column and are eluted sooner. The total volume of the first fraction collected from the gel column for each eluted niosome suspension was taken into the account for dilution factor. Empty niosomes (no drug) of corresponding formulations were used to assess the efficiency of gel chromatography filtration as the purification method.

Purified niosomes were assessed for their encapsulation efficiency and drug loading into niosomes (Section 2.4.1.), followed by the in vitro drug release study (Section 2.7.6.). Characterisation of purified niosomes was performed for their morphological properties (Sections 2.7.1. and 2.7.2.) and vesicle size distributions (Section 2.7.3.).

2.4.1. Determination of encapsulation efficiency (EE) and drug loading into niosomes (for actual and expected loading)

Encapsulation efficiency was calculated as the percentage of entrapped drug content after excluding free drug (non-entrapped drug). Found drug concentrations were calculated based on the respective known drug concentration calibration curves obtained in Section 2.3. Theoretical drug concentrations were calculated based on the initial amount of drug used in the manufacturing of niosomes. By using both found and theoretical drug concentrations, encapsulation efficiencies (%) of niosomes were determined (Equation 2.3).

Drug loading into niosomes was quantified using purified niosomes (Section 2.4.) was determined by solvent extraction method where the niosome formulation was disrupted by dispersing in methanol at a ratio of 1:1, and then subjected to bath sonication prior to HPLC analysis as described in Section 2.3.1. for cinnarizine and Section 2.3.4. for coumarin-6.

Purified niosomal formulations loaded with methylene blue were disrupted with isopropanol at a ratio of 1:1. Each drug absorbance was taken at 665 nm using a UV-Vis single beam scanning spectrophotometer (Model M501, Spectronic Camspec,

Leeds, UK) to calculate found drug concentration based on the methylene blue calibration plot generated in Section 2.3.2.

$$EE (\%) = \frac{\text{found drug concentration } \left(\frac{\text{mcg}}{\text{mL}}\right)}{\text{theoretical drug concentration } \left(\frac{\text{mcg}}{\text{mL}}\right)} \times 100 \% \quad \text{Equation 2.3}$$

$$\text{Drug loaded (mg)} = \frac{\text{found drug concentration } \left(\frac{\text{mcg}}{\text{mL}}\right)}{1000} \times \text{volume (mL)} \quad \text{Equation 2.4}$$

Calculated total amount of drug loaded into niosome vesicles (Equation 2.4) was used in the in vitro drug release study (Section 2.6.6.) expressed in % cumulative release (Section 4.3.6.) in relation to the initial amount of drug encapsulated based on found drug concentration (Equation 2.5).

$$\% \text{ cumulative release} = \frac{\text{drug loaded at predetermined time interval}}{\text{total amount of encapsulated drug}} \times 100 \quad \text{Equation 2.5}$$

2.4.2. Freeze-drying of purified niosomes

Purified niosome pellets obtained from centrifugation (15000 rpm for 20 minutes at 4 °C) were re-dispersed with 5 mL deionised water (TFH-based niosomes) and 5 % mannitol (MF-based niosomes), and then kept in ultra-low freezer (-80 °C) for 2 hours prior to freeze-drying process using a freeze dryer (Christ Advance Alpha 2-4 LSCplus, Germany) for 24-48 h. The vacuum was set to 0.035 mbar with an ice condenser was at -81 °C and shelf temperature at 10 °C.

Freeze-dried samples were investigated for molecular interactions between drug-excipients and their compatibilities by using Fourier-transform infrared spectroscopy (Section 2.7.4.) and differential scanning calorimetry (Section 2.7.5.).

2.5. Preparation of mucoadhesive niosomes

Equal volumes of purified niosome suspension (after gel chromatography) and mucoadhesive polymer solution were mixed using magnetic stirring at ambient temperature for 15 minutes. Mucoadhesive polymer suspensions used were 0.6% w/v low molecular weight chitosan in 1% v/v glacial acetic acid; 1.25% w/v highly viscous chitosan in 2.5% v/v glacial acetic acid; and alginate (Gaviscon® suspension).

2.5.1. Mucin adsorption study

Adsorption of mucin (porcine gastric mucin, Type II) on the polymer-coated niosomes was measured to evaluate the mucoadhesive properties of niosomes. Determination of free mucin after mucin interaction/adsorption on the mucoadhesive polymer coated niosomes. Mucin concentration (1mg/2mL) was prepared and mixed with equal volume of coated and uncoated niosome suspensions.

Following centrifugation process at 18000 rpm at 4 °C (Rinaldi et al., 2020), the amount of free mucin was determined by using the Periodic-Acid Schiff colorimetric method (Section 2.3.3.1.) in order to assess the amount of mucin adsorbed on the niosomes, based on the difference between the total mucin used and free mucin determined (Equation 2.6).

$$\text{Adsorption (\%)} = \frac{\text{total amount of mucin used} - \text{free mucin determined}}{\text{total amount of mucin used}} \times 100 \quad \text{Equation 2.6}$$

2.5.2. Period Acid Schiff (PAS) mechanism

Schiff's reagent is a colourless reagent that comprised of 1 % pararosaniline and 4 % sodium metabisulfite in a 0.25 mol/L hydrochloride acid. The cationic triphenylmethane dye reacts with three molecules of sulphur dioxide (released from sodium metabisulfite) to prevent oxidation and remain in colourless solution until a reaction with aldehyde to occur.

Firstly, periodic acid was added resulting in oxidation of the 1,2-glycols (of mucin molecules) into aldehydes (oxidised groups of mucin molecules). In the second step, the addition of Schiff's reagent causes the aldehydes to react to form a magenta colour (Figure 2-20).

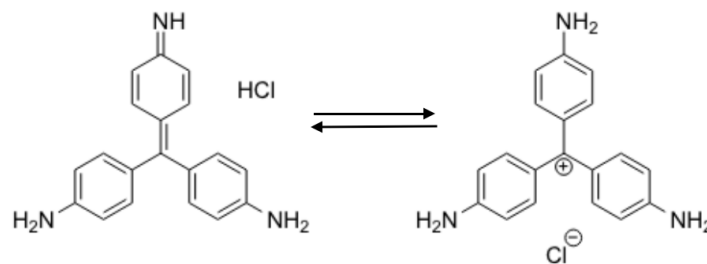


Figure 2-20: Pararosaniline hydrochloride (colourless on the left and magenta colour on the right).

2.5.3. Viscosity measurement of mucoadhesive biopolymers

Rheological properties of the freshly prepared biopolymer solutions were measured by using Brookfield Ametek Digital Viscometer DV-II+Pro (Model LV, Brookfield

Viscometer Ltd., Essex, UK). All biopolymer dispersions were sonicated prior to measurements.

Spindle #4LV cylindrical spindle used in the study has a defined spindle geometry that facilitates mathematical analysis to calculate shear stress, shear rate and viscosity (Rheocalc V3.3 Build 49-1: Rheometer). Selection of spindle and speed were based on the measurement results made between 10-100 on the instrument % torque scale. A 500mL of individual polymer solution was used and the speed (RPM) of the spindle was adjusted accordingly (Table 2-11). Triplicate measurements on temperature pre-determined polymer solutions were performed and kept at a temperature of 25 ± 0.5 °C using a water bath.

Table 2-11: polymer solutions used in viscosity measurement study with parameters used.

Polymer solution	Spindle	Speed (RPM)
0.6 % CS HV	LV61	1-9
1.25 % CS LMW	LV61	20-160
GAV	LV64	20-200
Water (control)	LV61	150-200

The flow curves were plotted between shear stress (N/m^2 or dyne/cm^2) and shear rate (s^{-1}) for each polymer. Consistency index (k), yield stress (N/m^2) and flow behaviour index (n) were investigated from the linear fitting confidence of the flow curves to describe a suitable mathematical analysis model. The consistency index (k) is an indication of the viscous nature of the system. The value of flow behaviour index (n) is a measure of departure from Newtonian flow: < 1.0 shear-thinning (pseudo-elastic) and > 1.0 shear-thickening (dilatant). Plastic viscosity and yield stress were

investigated from the linear fitting of flow curves. Multiple data points measurement was performed for comprehensive analysis of flow behaviour.

2.5.4. Mucoadhesion study using mucoadhesive niosomes entrapped with coumarin-6

Freshly excised porcine stomach was obtained and cut into 2 x 2 cm specimen square slices. All mucosa squares were immersed in simulated gastric fluid to ensure full hydration. A 100 μ L of niosome formulation was spread onto each tissue specimen and placed in each glass tube containing 5 mL of SGF at pH 1.2. All glass tubes were placed in a shaker incubator (Stuart SI500 orbital incubator, Cole-Parmer, Staffordshire, UK) at shaking rate (50 rpm) and temperature at 37 °C. At predetermined time intervals (0.5, 1, 1.5, 3, 4.5 and 6 hour), each tissue specimen was taken out from the glass tube and then rinsed with 10 mL of PBS to remove any non-adsorbed niosomes. Subsequently, the native mucus gel was scraped gently from the surface of the porcine gastric mucosa specimen and transferred carefully into 5 mL of 5 M NaOH solution (pH 12) for 12 h to dissolve mucus or any traces of specimen. After 12 h, an equal volume of methanol was added to each sample to dissolve the coating polymer and disrupt the vesicles. Centrifugation of the samples was carried out at 6000 rpm for 10 minutes to extract coumarin-6 containing supernatant to be filtered using a 0.2 μ m syringe filter for fluorescence measurement by using HPLC (Section 2.3.4.). Each SGF was kept after the removal of tissue specimen and then filtered using a 0.2 μ m syringe filter prior to HPLC measurement. Untreated mucosa sheet was used as a negative control. Quantification of coumarin-6 (in supernatant and SGF) was determined by using a calibration curve of coumarin-6 (Section 2.3.4.).

2.6. Microfluidic-based niosome component recovery

2.6.1. After preparation (Span® 60/cholesterol recovery) and after purification (niosome recovery)

Without purification, a freshly prepared MF-based empty niosome formulation (see Table 2-5) obtained directly from microfluidic cartridge was diluted and dispersed into their components, to quantify Span® 60/cholesterol. Whereas, a freshly prepared MF-based niosome formulation (see Table 2-5) was firstly purified to obtain formed niosome vesicles to separate/remove any traces of unformulated free components by using a Sephadex® G50 gel chromatography, to quantify niosome recovery.

Dilution and dispersion using methanol: chloroform (4: 1 v/v) to disrupt the self-assembled vesicles in a bath sonicator for 5 minutes. Subsequently, a filtration process was carried out using syringe filter (0.2 µm) prior to HPLC measurement to remove any unwanted aggregate components that may interfere in the sample analysis (Section 2.5.3.).

2.6.2. Preparation of niosome component standards for calibration using high performance liquid chromatography with evaporative light scattering detection (HPLC-ELSD)

Based on the method from Rocés et al. (2016) and Forbes et al. (2019) with modification, the standard samples of Span® 60, cholesterol, glyceryl monostearate (GMO) and dipalmitoylphosphatidylcholine (DPPC) were analysed independently and as a mixture of known concentrations by HPLC-ELSD in order to establish detectability and to explore separation conditions. Mixtures of niosome component (Span® 60 and cholesterol; Span® 60, cholesterol and Cremophor® ELP) were prepared at a total

concentration of 2 mg/mL. Each individual and combined mixture of lipid components (DPPC and GMO) were prepared at concentration of 1 mg/mL.

Standard solutions of Span® 60 and cholesterol were prepared individually as they were the two core formulation components used in the preparation of niosome vesicles in this study. Concentrations for S60 standard solutions were 0.1, 0.5, 1.0, 1.5 and 2.0 mg/mL. Concentrations for cholesterol standard solutions were 0.05, 0.1, 0.2, 0.5 and 1.0 mg/mL.

2.6.3. Niosome component calibration using high performance liquid chromatography with evaporative light scattering detection (HPLC-ELSD)

Method and operational parameters:

A reversed-phase mode HPLC with evaporative light scattering detection (ELSD) was used to detect and separate niosome component with quantification estimation. The column used was Phenomenex Luna C18 (2) (5 µm x 4.6 mm x 150 mm, pore size 100 Å) at a column temperature of 35 °C. The flow rate was set at 2 mL/min. Gradient elution was used consists of mobile phase A (0.1 % v/v trifluoroacetic acid in water) and mobile phase B (0.1 % v/v trifluoroacetic acid in methanol) according to Table 2-12. Analysis time was set at 15 min and elution peaks obtained shown well separation with a flat baseline. All samples were prepared in methanol and subjected to be filtered using 0.2 µm syringe filter prior to measurements. Agilent ChemStation software was used to process and quantitate all the responses measured. All the experiments were performed in three independent batches.

According to the HPLC-ELSD method setting in Roces et al. (2016), injection volume used was 30 μL in a partial loop-fill injection mode, 100 μL loop volume and 15 μL tubing volume. Evaporator carrier gas (nitrogen) inlet pressure was set at 3.5 psi (volumetric flow rate at 1.5 standard litres per minute, Parker Balston nitrogen generator). ELSD evaporator temperature was set at 52 $^{\circ}\text{C}$. ELSD instrumental controls include the lamp, gas valve, noise filter to optimise signal-to-noise ratio and peak shape, and detector gain at 10 (PMT range 1 to 12).

Table 2-12: Gradient elution.

Time (min)	Mobile phase A	Mobile phase B	Flow rate (mL/min)
0	15	85	2.0
10	0	100	2.0
11	0	100	2.0
12	15	85	2.0
15	15	85	2.0

2.7. Characterisation of niosomes

2.7.1. Niosomes morphology: optical microscopy

Freshly prepared niosome suspensions were observed under light microscope with magnification lens of x40 using MicroCam Olympus BH-2/LB with AxioCam MRc (Carl ZEISS, Jena, Germany). The formations of niosomes were confirmed by observation under optical light microscope and real-time images were taken.

2.7.2. Niosomes morphology: transmission electron microscopy (TEM)

Freshly prepared niosomes were imaged by TEM (Hitachi H7000 transmission microscope, Japan) using negative staining technique. Diluted aqueous solution of 2% (w/v) sodium silico-tungstate was used as a negative stain agent. One droplet of each niosomal suspension was applied onto a copper-coated with formvar carbon grid (400 mesh) (Agar Scientific Ltd, Essex, UK) to allow adsorption of vesicles and the excess sample was blotted away with a filter paper prior to application of the negative stain and then drying under ambient condition for 2 minutes. Imaging was carried out at an accelerating voltage of 75 kV and equipped with a camera to capture images.

2.7.3. Particle size, distribution and zeta potential measurements

An aliquot from each of the freshly prepared niosome suspensions was used for measurement of particle size, polydispersity index (PDI) and zeta potential (ZP) in 1/20 dilution with deionised water, using Malvern Zetasizer Nano ZSP (red badge version 7.11, Cambridge, UK). Measurements including the hydrodynamic sizes of thin-film-based niosomes before and after probe sonication process.

Measurement angle of 173° backscatter was used for angle of measurement detection. Hydrodynamic size and PDI were measured by using dynamic light scattering (DLS), and the zeta potential was determined by using laser Doppler electrophoresis technique, measurements using the M3-PALS method in disposable folded capillary cells. The particle size is expressed as z-average which is the vesicle diameter based on the intensity of scattered light and derived by an auto-correlation function. The PDI value is a measure of the dispersion of the size distribution and an indication of the heterogeneity of the preparation. A PDI value has a range between 0 (narrow

distribution) to 1 (wide distribution). Three measurements were taken for each sample. All measurements were carried out at room temperature.

2.7.4. Fourier-transform infrared (FTIR) spectroscopy

The infrared spectra of individual material and freeze-dried niosome samples were taken using a Shimadzu IRAffinity-1S spectrophotometer (Shimadzu UK Ltd, Buckinghamshire, UK). Identification of compound was performed by comparing the full scan spectra obtained with the spectra from literature. The spectra were recorded using 12 scans in the wavelength range ($4000 - 550 \text{ cm}^{-1}$) with resolution of 4 cm^{-1} to study their possible interactions using the Shimadzu LabSolution-IR software. The changes in the structural assemblies can be detected by analysing the frequency and the width changes of the vibrational modes. Under the same conditions, the infrared spectrum of the cinnarizine pure drug was also taken for identification of its principle functional groups.

2.7.5. Differential scanning calorimetry (DSC)

Differential scanning calorimetry (DSC) is a thermal analysis technique that measures the heat difference between a sample and a reference at the same changing temperatures. It is used commonly to determine crystallinity and melting point that can be utilised to differentiate different polymorphs. The crystallinity of encapsulated drug in freeze-dried niosome samples was analysed.

A standard mode DSC conditioning was performed at $75 \text{ }^\circ\text{C}$ for 120 minutes hold time without refrigerated cooling system (RCS) (DSC Q1000 TA Instruments, Ghent, Belgium) with an empty cell chamber and equipped with nitrogen gas (BOC Gas, UK).

Afterwards, temperature calibration was carried out using pure indium with the RCS. All freeze-dried niosome samples (see 2.6.2.) weighed between 2 to 8 mg using Mettler MT5 balance (Mettler Toledo, Leicester, UK) were placed within standard aluminium hermetic pans and lids for DSC runs. DSC measurements were performed at a heating rate of 10°C/min from 25-300°C. Nitrogen gas flow rate was 50 mL/min with the RCS turned on. Thermal Analysis 2000 software was used to perform analysis of the obtained DSC thermograms.

2.7.6. *In vitro* drug release study

In vitro dissolution studies were performed on the niosome suspension which were thin-film hydration-based and optimised microfluidic-based, using the dialysis method. Five millilitres of each purified sample and samples suspended with coating polymers was transferred into pre-soaked Visking tubing (MWCO 3500 Da) and each put into a beaker filled with 100 mL of simulated gastric fluid (SGF) that was placed in an orbital shaking water bath at 37 °C and operating at 50 rpm.

Aliquots (1 mL) were taken at pre-determined time points (5, 10, 15, 30, 45, 90 min) and were replaced with an equal volume of fresh media (1 mL) to maintain a constant volume. Samples (no need centrifuge as diffusion across semi-permeable membrane) diluted with methanol for HPLC analysis. Found drug concentrations were calculated based on the obtained drug concentration from HPLC analysis and with dilution factors. Three independent batches of samples for each formulation was analysed.

2.8. Statistical analysis

Statistical analysis was performed using SPSS v25 software package for Mac (SPSS Inc, USA). The statistical method used was Analysis of Variance (ANOVA). Univariate analysis of variance (Levene test) – samples with equal variances (homogeneity of variance). Tukey's multiple comparison test and t-test for paired comparisons in post hoc assessment. Significance was acknowledged when the P value is less than 0.05. P value is the probability of finding the observed results when the hypothesis of the research question is true. All results were reported as the average \pm standard deviation based on three independent batches unless stated otherwise.

Chapter Three:

3. Manufacturing of niosomes containing methylene blue as a model hydrophilic drug

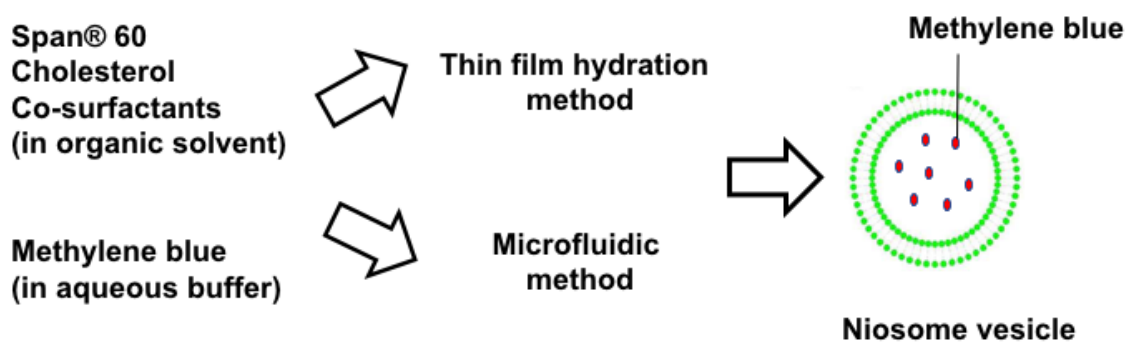


Figure 3-1: Graphical abstract for manufacturing of niosomes containing methylene blue as a model hydrophilic drug.

3.1. Overview

One of the advantages of niosomes is their ability to encapsulate both hydrophilic and hydrophobic small drug molecules due to the structural nature of a niosome vesicle. Hydrophilic drugs are often dissolved in the aqueous phase during preparation and then entrapped in the inner aqueous compartments within the formed vesicles, where encapsulation efficiencies are generally very low (Xu et al., 2012). Passive drug loading techniques including direct hydration, present challenges encapsulating hydrophilic molecules inside vesicles due to large amount of external bulk aqueous medium. Generally, hydrophilic drugs are more likely to be efficiently released out of a carrier (vesicle) because the compounds trapped within the aqueous core would be released into the aqueous external space (Nguyen et al., 2015).

Various preparation methods and processes have been studied to improve the drug loading efficiency, such as reverse phase evaporation, dehydration-rehydration of preformed empty vesicles, pH-induced transmembrane drug transport and freeze-thaw cycling. Moreover, compositional formulation factors such as surfactant type and cholesterol content, affect membrane fluidity and physical stability of vesicles for drug encapsulation efficiency and drug release (Jadon et al., 2009). It is worth noting that highly water-soluble drugs including small molecule drugs and macromolecule peptide drugs, often show limited or incomplete drug absorption into the body upon oral administration due to low intestinal permeability (Amidon et al., 1995). Niosomes as an alternative to liposomes showed a great potential in drug delivery with high encapsulation for improved bioavailability and prolonged release profiles for hydrophilic tenofovir (Kamboj et al., 2014), cephalexin (Ghafelehbashhi et al., 2019) and colchicine (Hao et al., 2002). Studies reported that large unilamellar vesicles with

a large aqueous core enabled more hydrophilic drug loading (Attia et al., 2007; Yoshioka et al., 1994).

Amongst all methods being used for niosome manufacturing, the conventional thin film hydration method is the most common method for producing multilamellar vesicles (MLVs). Following the manufacture of MLVs, size reduction methods such as sonication, size extrusion and high shear mixing, are generally used as a top-down approach for limiting vesicle size. Using acoustic energy, sonication technique introduces pressure waves in the liquid which causes the formation of microscopic bubbles (cavities) and creates a phenomenon known as cavitation (Essa, 2010). The process breaks up large, multilamellar vesicles into smaller vesicles depending on the sonication time applied and intensity of the pressure (Cho et al., 2013). It has shown to be less intensive than extrusion as a simple processing technique for reducing vesicle size without affecting their physical properties for diffusion and permeability of the bilayer (Lapinski et al., 2007). With sonication technique, the acoustic energy can be generated from either a water bath or a probe tip sonicator, which means the size distributions can be less reproducible from batch-to-batch preparations (Mozafari, 2010). Moreover, the heat generated during the sonication process of using a probe sonicator where it has been in direct contact with the vesicle suspension, suggested facilitated the solubility of vesicle components and the formation of small unilamellar vesicles (SUVs).

A highly controlled, reproducible microfluidic method has been shown as a bottom-up approach for the manufacturing of vesicles as a resultant output of a rapid molecular-level mixing and nanoprecipitation process (Belliveau et al., 2012; Zhigaltsev et al.,

2012). The use of microfluidic method has been reported in the manufacturing of various nanoparticles (niosomes, liposomes, polymeric or lipid nanoparticles), showing high potential for the production of homogenous nanoparticles of interest for nanomedicine development (Chen et al., 2012; Forbes et al., 2019; He et al., 2013; Hong, Dong and Boyd, 2019; Lo et al., 2010) due to the highly controlled process parameters of using microfluidic method.

For a hydrodynamically stable niosome dispersion, it is important to study the manufactured niosome characteristics such as vesicle size, vesicle forming and drug retention capability, which are highly dependent on their drug-lipid content and the nature of membrane compositions as well as manufacturing methods and process parameters (Mahale et al., 2012). Additionally, niosome characteristics can hugely influence drug loading and release, and consequently affect formulation performance (Abdelkader et al., 2014; Essa, 2010; Taymouri et al., 2016).

For particle characterisation, light scattering techniques are most common for detection of micro- and nanoparticles owing to their non-destructive yet versatile nature and a relatively short analysis time. Dynamic light scattering (DLS) is also known as photon correlation spectroscopy (PCS), determines the hydrodynamic diameter of particle size distribution in dispersions, sizing generally from a few nanometres up to one micrometre range. The interpretation of measurement data is based on the time-dependent intensity scattering fluctuation of a particle in dispersion with high sensitivity. The Zetasizer system incorporates patented Non-invasive Backscatter (NIBS) optics technology which allows a larger number of particles and eliminates number fluctuations, generating a stable detection signal. In the collision

between moving particles under the Brownian motion, the suspended particles of different sizes scatter a light beam and then the scattered light intensities were monitored by a detector. As a result, a correlation curve is generated from the detected signals linking the diffusion of the particles to the scatter light fluctuations over time. This generated curve can be analysed to provide size and distribution data directly from the highly automated Zetasizer system.

The diffusion constant (D) is determined in order to derive the hydrodynamic diameter (d_H) of a measured particle. The diffusion of the particles is essentially controlled by the viscosity of the suspending media (μ), the absolute temperature (T) and the Boltzmann constant (k) as based on the Stokes-Einstein relationship (Equation 3.1). Therefore, hydrodynamic diameter is determined by the measurements determining the translational diffusion coefficient of the measured particle by correlating to a hypothetical sphere (Chu and Liu, 2000). The measurement temperature needs to be stable and the sample without requiring agitation, to ensure particles are in constant random movement, where they diffuse at a speed related to their size (smaller particles diffuse faster than larger particles) is essential for accurate size measurement.

$$d_H = \frac{kT}{3\pi\mu D} \quad \text{Equation 3.1}$$

At the same time of using DLS technique for particle size determination, the heterogeneity of the particle dispersion is determined as the polydispersity index (PDI). The PDI value is typically ranging up to a maximum value of 1, giving an indication of a very heterogeneous sample having a wide particle size distribution.

3.2. Aims and Objectives

This chapter focuses on the manufacture of niosome formulations containing water-soluble drug, methylene blue (MB) by two methods - conventional thin film hydration and microfluidic method with the aim to optimise niosome manufacturing process parameters in order to pave the way for cinnarizine (poorly water-soluble drug) in the next chapter. Methylene blue was used as model drug for encapsulation in this chapter due to the fact that it is a coloured compound to facilitate the process optimisation study on niosome manufacturing. In this work, hydrophilic co-surfactants were incorporated in niosome formulation to help stabilise the vesicle bilayer, in comparison to lipophilic co-surfactant, Lauroglycol® 90, to study its effect on niosome vesicles encapsulating hydrophilic methylene blue molecules. To achieve this purpose, the main objectives were to:

- Investigate the effect of thin film hydration process and formulation parameters on niosome characteristics.
- Investigate the effect of sonication on physicochemical properties of methylene blue entrapped niosomes.
- Investigate the effect of surfactant/lipid concentration and methylene blue concentration for the characteristics of the sonicated niosomes.
- Compare and evaluate the effect of niosome manufacturing methods on encapsulating methylene blue into niosomes.
- Study the influence of manufacturing method of niosome encapsulating water-soluble drug on other niosome characteristics.

3.3. Results and Discussion

3.3.1. Effect of thin film hydration process and formulation parameters on niosome characteristics

Physical process variables such as the final surfactant/lipid concentration produced as a result of different hydration volumes used in the bulk method preparation process affect the properties of niosomes. At a constant methylene blue concentration and at constant sonication process parameter applied, niosome characteristics were influenced by the total surfactant/lipid content in the formulation. In Table 3-1, without sonication, niosome vesicle sizes decreased with increasing final total surfactant/lipid concentration from 10 to 40 mg/mL. Following the sonication process, vesicle size had reduced greatly in the lowest final total surfactant/lipid concentration (10 mg/mL), with the least size reduction in the highest final total surfactant/lipid concentration (40 mg/mL). Generally, size distributions decreased slightly after sonication yet still showing similar size distributions in all formulations.

The encapsulation of drug into vesicles usually increases niosome vesicle size due to possible interaction of drug with surfactant head groups, thereby increasing their charge and creating repulsions forming larger vesicles (Essa, 2010). This is not the case as smaller vesicles formed at a high final surfactant/lipid concentration of 40 mg/mL where it showed the highest encapsulation efficiency of 40 % before sonication (Table 3-1). Through sonication, reduction in vesicle size has contributed to the decrease in encapsulation efficiencies of methylene blue in all Span® 60: cholesterol: Cremophor® ELP formulations. The decrease of the encapsulated drug was expected due to the leakage of methylene blue into external bulk aqueous buffer owing to its hydrophilicity nature during the sonication process. Among all sonicated formulations, it was found that the highest encapsulation efficiencies were obtained in the

formulation with final surfactant/lipid concentration of 20 mg/mL. Interestingly, Span® 60: cholesterol: Lauroglycol® 90 niosome formulation showed an increase in encapsulation efficiency from 10% before sonication to 27% after sonication despite a significant reduction in vesicle size. This might be explained as large multilamellar vesicles self-assemble into smaller vesicles, more internal aqueous cores created for higher hydrophilic drug loading. In addition, the vesicle bilayer membrane might be more rigid and less fluid as a result of the incorporation of lipophilic Lauroglycol® 90 (HLB value of 3) instead of hydrophilic co-surfactant Cremophor® ELP (HLB value of 12-14). Consequently, leakage of encapsulated hydrophilic drug from inside the vesicles will be minimal.

Table 3-1: Effect of hydration volumes on niosome characteristics for before and after sonication process. Final concentration of MB expected was 0.5 mg/mL.

Span 60: Cholesterol: Cremophor® ELP (hydration time 60 minutes; 60 °C)						
Final surfactant/lipid concentration (mg/mL)	Size (nm)		PDI		EE %	
	Before sonication	After sonication	Before sonication	After sonication	Before sonication	After sonication
10 ^a	804.0 ±	272.9 ±	0.56 ±	0.39 ±	22.1 ±	14.3 ±
	294.8 *	105.1 *	0.28	0.24	12.7	1.3
20 ^b	757.7 ±	301.1 ±	0.49 ±	0.46 ±	38.3 ±	18.7 ±
	155.3	12.3	0.17	0.12	10.1 *	3.5 *
40 ^c	615.7 ±	362.2 ±	0.71 ±	0.45 ±	40.1 ±	11.6 ±
	126.8	138.3	0.25	0.17	7.9 *	4.5 *
Span 60: Cholesterol: Lauroglycol® 90 (hydration time 60 minutes; 60 °C)						
20 ^b	1463.4 ±	256.9 ±	0.46 ±	0.34 ±	10.5 ±	27.1 ±
	62.4 *	51.9 *	0.06	0.13	2.4	1.4

Data are expressed as mean ± standard deviation from triplicate experiments (n=3).

^a, ^b, ^c Hydration volumes used were 20 mL (^a), 10 mL (^b) and 5 mL (^c) respectively.

*significantly different ($p < 0.05$).

In Table 3-2, niosome characteristics for different hydration time of the formed thin film as a physical process variable were shown. At the above phase transition temperature, a longer hydration time (60 minutes) resulted in the formation of smaller vesicles with higher encapsulation efficiencies. Similarly, reduced vesicle size and narrower distributions were produced for both short and long hydration time (15 min and 60 min) after samples underwent sonication process, however, the encapsulation efficiencies were higher for niosomes with 60 min hydration. Following hydration process, sonication has significantly reduced vesicle size and consequently decreased encapsulation efficiency as discussed previously. As the cavitation bubbles created

by sonication, the efficiency of reducing the vesicle size reduces with time (Essa, 2010). Overall, it is noteworthy to highlight that the encapsulation of hydrophilic drug is more influenced by the length of hydration of the thin film in which the vesicles form under agitation and at temperature above the transition temperature (Yeo, Chaw and Elkordy, 2019).

Table 3-2: Effect of hydration times on niosome characteristics for before and after sonication process. Final concentration of MB expected was 0.5 mg/mL.

Span® 60: Cholesterol: Cremophor® ELP (final surfactant/lipid concentration 20 mg/mL; 60 °C) Hydration volume used was 10 mL						
Hydration time (minutes)	Size (nm)		PDI		EE %	
	Before sonication	After sonication	Before sonication	After sonication	Before sonication	After sonication
15	975.2 ±	301.1 ±	0.53 ±	0.46 ±	21.3 ±	13.8 ±
	124.2 *	79.4 *	0.12	0.06	7.7	1.3
60	757.7 ±	301.1 ±	0.49 ±	0.46 ±	38.3 ±	18.7 ±
	155.3 *	12.3 *	0.17	0.12	10.1	3.5

Data are expressed as mean ± standard deviation from triplicate experiments (n=3).

*significantly different ($p < 0.05$).

Another factor affecting the niosome characteristics was the amount of loading drug as one of the compositional formulation variables. In Table 3-3, vesicle size and distributions did not show a significant difference regardless of different methylene blue (MB) concentrations used, with and without sonication process, at a constant final surfactant/lipid concentration. However, the highest encapsulation efficiency (81%) was obtained from the formulation at the lowest final MB concentration (0.01 mg/mL). It is noticeable that encapsulation efficiencies decreased with increasing final MB concentrations and after sonication process. At higher MB concentrations, the direct

hydration process where the same amount of total surfactant/lipid components self-assembled to form vesicles was not efficiently and sufficiently enough to encapsulate the hydrophilic drug molecules that had been dissolved in the bulk aqueous buffer and they largely remained in the external medium.

Table 3-3: Effect of methylene blue concentrations on niosome characteristics for before and after sonication process. The final concentration of MB expected was 0.5 mg/mL.

Span® 60: Cholesterol: Cremophor® ELP (final surfactant/lipid concentration 20 mg/mL; hydration time 60 minutes; 60 °C)						
Final MB concentration (mg/mL)	Size (nm)		PDI		EE % *	
	Before sonication	After sonication	Before sonication	After sonication	Before sonication	After sonication
0.01	443.5 ±	214.8 ±	0.953 ±	0.437 ±	81.2 ±	45.7 ±
	30.7	1.4	0.04	0.01	3.6	2.3
0.02	468.3 ±	205.3 ±	0.914 ±	0.506 ±	57.4 ±	22.1 ±
	41.8	1.3	0.04	0.09	1.2	3.9
0.10	379.6 ±	241.0 ±	0.726 ±	0.623 ±	41.1 ±	22.5 ±
	5.4	3.3	0.13	0.02	4.9	2.3

Data are expressed as mean ± standard deviation from triplicate experiments (n=3).

*significantly different ($p < 0.05$).

3.3.2. Influence of manufacturing methods and formulation compositions on niosome characteristics

In Table 3-4, niosome characteristics on size distributions and encapsulation efficiencies were shown and compared for thin film hydration and microfluidic methods on manufacturing niosomes entrapping methylene blue (MB). There were significant differences in the vesicle size and distributions between the two manufacturing methods for both formulations in which microfluidic-based produced smaller and more homogeneous niosomes. It is worth noting that hardly any of the methylene blue

molecules were encapsulated in the S60: Cho: L90 microfluidic-based niosomes, while there was not much difference in the encapsulation efficiencies of S60: Cho: ELP niosomes manufactured by both methods. This suggested that the rapid mixing of microfluidic method might hinder the direct loading of the hydrophilic drug molecules into the vesicles during their rapid formation process (Stroock, 2002). In contrast, thin film hydration method allows sufficient time during the hydration process for direct loading of the hydrophilic MB molecules into the niosomes as its components self-assemble and form vesicles.

Table 3-4: Effect of manufacturing methods and formulation compositions on niosome characteristics. (All post-G50 measurements. TFH after sonication measurements. All final surfactant/lipid concentration at 20mg/mL. Final concentration of MB expected was 0.5 mg/mL.

Formulation	Size (nm) *		PDI *		EE %	
	TFH	MF	TFH	MF	TFH	MF
S60: Cho: ELP	301.1 ±	161.8 ±	0.46 ±	0.25 ±	18.7 ±	14.9 ±
	12.3	1.4	0.12	0.01	3.5	1.0
S60: Cho: L90	1412.3 ±	124.1 ±	0.40 ±	0.10 ±	13.3 ±	0.2 ±
	18.5	0.9	0.06	0.01	2.1	0.0

Data are expressed as mean ± standard deviation from triplicate experiments (n=3). TFH as thin film hydration; MF as microfluidic. *significantly different (p < 0.05).

In Table 3-5, increasing final surfactant/lipid concentration in the S60: Cho: ELP formulation had slightly increased the vesicle size for both manufacturing methods. All TFH-based samples showed polydispersity index of 0.5 or less, whereas all MF-based niosomes showed higher homogeneity with a polydispersity index of less than 0.3. In TFH-based niosomes, the highest encapsulation efficiencies were achieved in the formulation with final surfactant/lipid concentration of 20 mg/mL. For microfluidic-based niosomes, increasing encapsulation efficiencies were observed with increasing

final total surfactant/lipid concentration. At low surfactant/lipid concentration (10 mg/mL), there was a significant difference ($p < 0.05$) in encapsulation efficiencies between TFH and MF methods. In this case, other than insufficient time for direct loading of hydrophilic MB molecules in the microfluidic method due to rapid process of mixing, the total surfactant/lipid content could be a limiting factor impacting the encapsulation efficiency. At a constant MB concentration (initial concentration at 0.5 mg/mL), not a significant higher encapsulation efficiency was shown in MF-based niosomes with higher total surfactant/lipid concentration, suggesting the rapid mixing process of microfluidic manufacturing could be the limiting factor for direct loading of hydrophilic drug, despite the highly reproducible and homogeneous vesicle formation.

Table 3-5: Effect of manufacturing methods and different final surfactant/lipid concentrations on niosome characteristics. Final concentration of MB expected was 0.5 mg/mL. (All post-G50 measurements. TFH after sonication measurements.)

Span® 60: Cholesterol: Cremophor® ELP						
Final surfactant/lipid concentration (mg/mL)	Size (nm)		PDI		EE%	
	TFH	MF	TFH	MF	TFH	MF
10	272.9 ±	88.9 ±	0.39 ±	0.26 ±	14.3 ±	4.5 ±
	105.1	0.3	0.24	0.01	1.3 *	2.3 *
20	301.1 ±	112.6 ±	0.46 ±	0.24 ±	18.7 ±	14.9 ±
	12.3	1.0	0.12	0.01	3.5	1.0
40	362.2 ±	130.3 ±	0.45 ±	0.26 ±	11.6 ±	19.5 ±
	138.3	1.8	0.17	0.01	4.5	1.9

Data are expressed as mean ± standard deviation from three independent experiments (n=3). Thin film hydration (TFH); Microfluidic (MF).

*significantly different ($p < 0.05$).

3.3.3. Effect of storage on niosome size

Figure 3-2 showed the size measurements taken for over a storage period of four weeks at room temperature (23 ± 2 °C) and at fridge temperature (4 ± 2 °C) to evaluate the formulation physical stability of TFH-based niosomes without sonication (Span® 60: cholesterol: Cremophor® ELP formulation). The changes in vesicle sizes might give an indication of formulation physical stability upon storage at different temperatures. Overall, the difference in storage temperatures had no significant impact on the vesicle size regardless of the total surfactant/lipid concentrations. All formulations showed an increase in vesicle size over the storage period. Non-sonicated niosomes of 10mg/mL surfactant/lipid concentration stored at room temperature and non-sonicated niosomes of 20mg/mL surfactant/lipid concentration stored at fridge temperature had the least changes in vesicle size. At room temperature, niosomes of both 20mg/mL and 40mg/mL showed ≈ 1.2 -fold increase in vesicle size. Interestingly, at refrigerated temperature, niosomes of 10mg/mL surfactant/lipid concentration showed ≈ 1.5 -fold increase in vesicle size, and niosomes of 40mg/mL surfactant/lipid concentration showed ≈ 1.4 -fold increase in vesicle size. These results revealed stable formulations comprised of lower total surfactant/lipid concentration of 20mg/mL and below for both room temperature and refrigerated temperature.

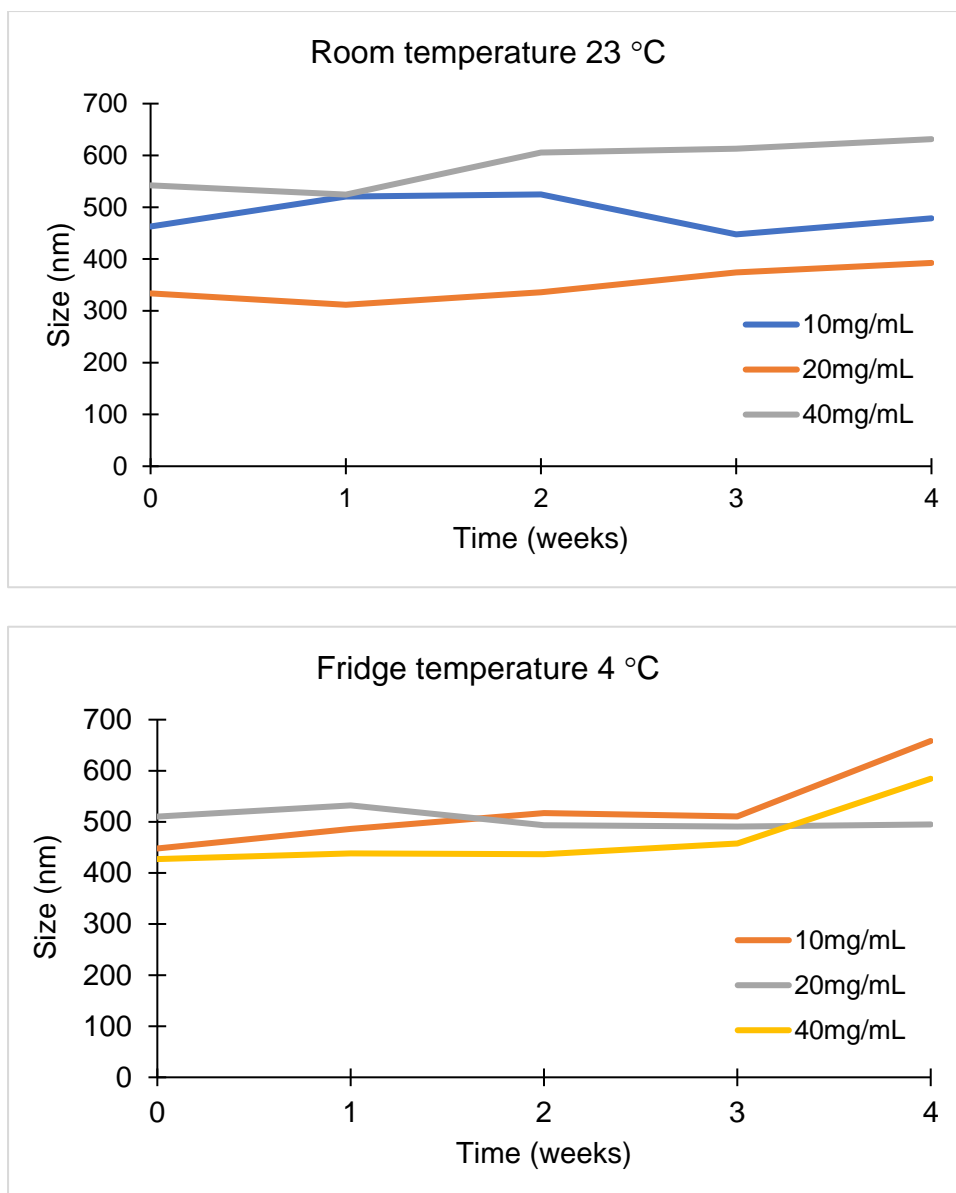


Figure 3-2: Graphs showing average vesicle sizes of Span® 60: cholesterol: Cremophor® ELP niosomes of different total surfactant/lipid concentrations prepared by thin film hydration method without sonication, stored at room temperature (top) and at fridge temperature (bottom). Initial concentration of MB used was 0.5 mg/mL. Different independent batches of niosomes prepared for room temperature and refrigerated storage.

Comparing TFH-based niosomes with sonication to no sonication involved in the preparation process, vesicle size measurements upon storage period were taken to confirm the irreversibility of sonication process as a size reduction technique. The average vesicle sizes for all Span® 60: cholesterol: Cremophor® ELP niosomes had

increased over storage period, with or without the involvement of sonication (Figure 3-3). Non-sonicated niosomes with lower total surfactant/lipid concentrations (10 and 20 mg/mL) had a higher increase in vesicle size than higher surfactant/lipid concentration (40 mg/mL). Interestingly, this was the opposite for sonicated niosomes in which then higher surfactant/lipid concentrations (20 and 40 mg/mL) had a larger increase in the vesicle size. This could be explained that the introduction of external pressures through sonication prompted a reduction in vesicle size during the preparation process, subsequently when the external pressures were removed, tiny unstable vesicles formed may fuse together to form larger vesicles (Lasic, 1988). Moreover, given that more surfactant/lipid molecules will be available at higher total surfactant/lipid concentrations, they tend to form fragments or vesicles to achieve a thermodynamically stable state.

In contrast, both sonicated and non-sonicated Span® 60: cholesterol: Lauroglycol® 90 niosomes had no significant change in vesicle size over the storage period. As the resultant niosomes comprised of stearyl chain (C₁₈) of Span® 60 and also the lauryl chain (C₁₂) of Lauroglycol® 90, this suggested that the incorporation of Lauroglycol® 90 within the niosome formulation had increased the bilayer membrane rigidity and became less fluid, owing to its hydrophobic nature. Consequently, the niosome vesicles were subjected to less physical instabilities and preserved its size over storage period.

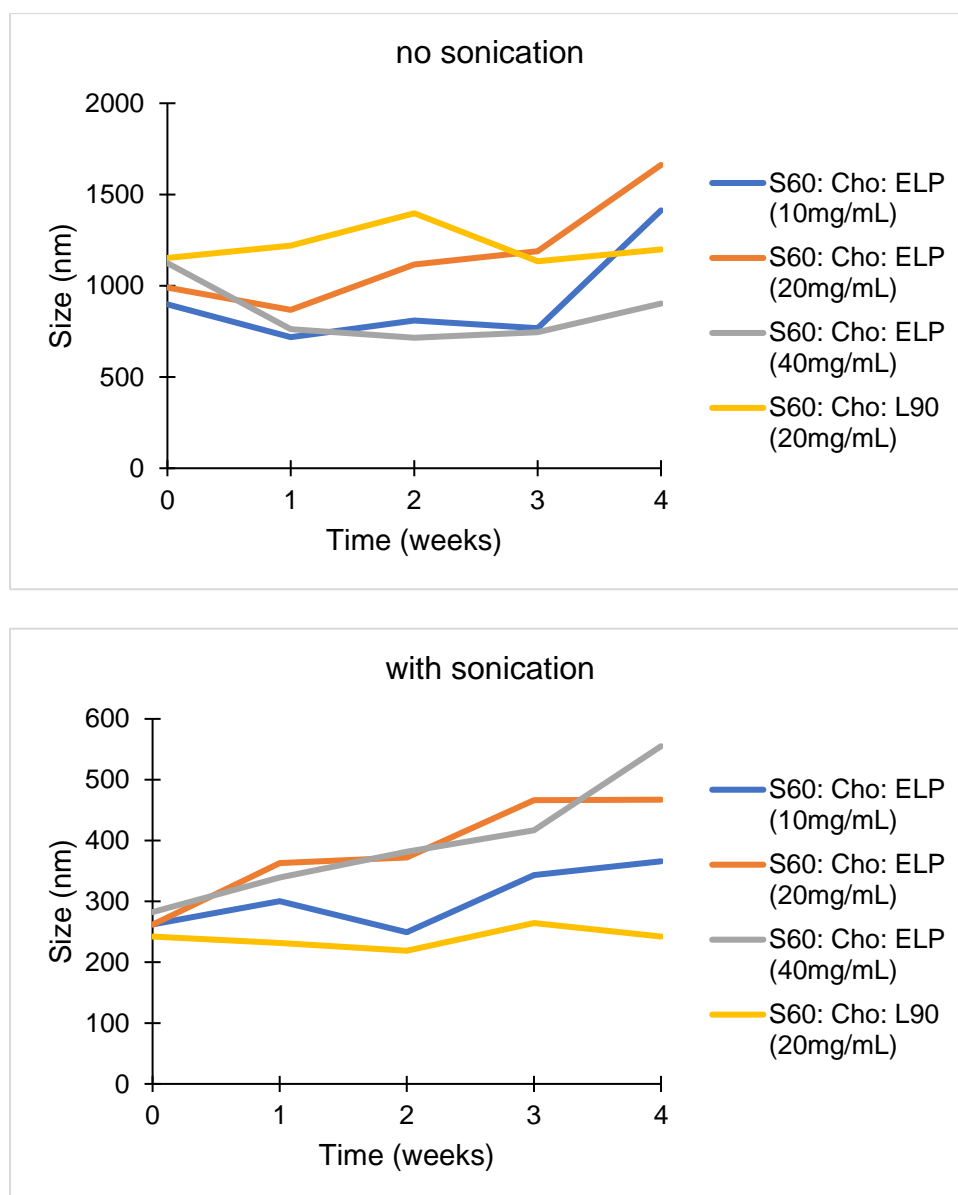


Figure 3-3: Graphs showing average vesicle sizes of thin-film hydration niosomes without sonication (top) and with sonication (bottom). Error bars were omitted for the clarity of the plot. Both niosome suspensions were stored at fridge temperature 4°C. Non-sonicated niosomes were prepared independently from the niosome batches prepared shown in Figure 3-1. Initial concentration of MB used was 0.5 mg/mL.

The vesicle size for microfluidic-based niosomes showed a gradual increase in all the formulations of increasing total surfactant/lipid concentrations (Figure 3-4). With no significant increase in vesicle size observed in niosomes composed of different total surfactant/lipid concentrations, it is suggested that the controlled rapid mixing process of microfluidic method enables production of niosomes of desirable vesicle size and

better membrane integrity against physical instabilities and allows for a prolonged shelf-life in refrigerated condition.

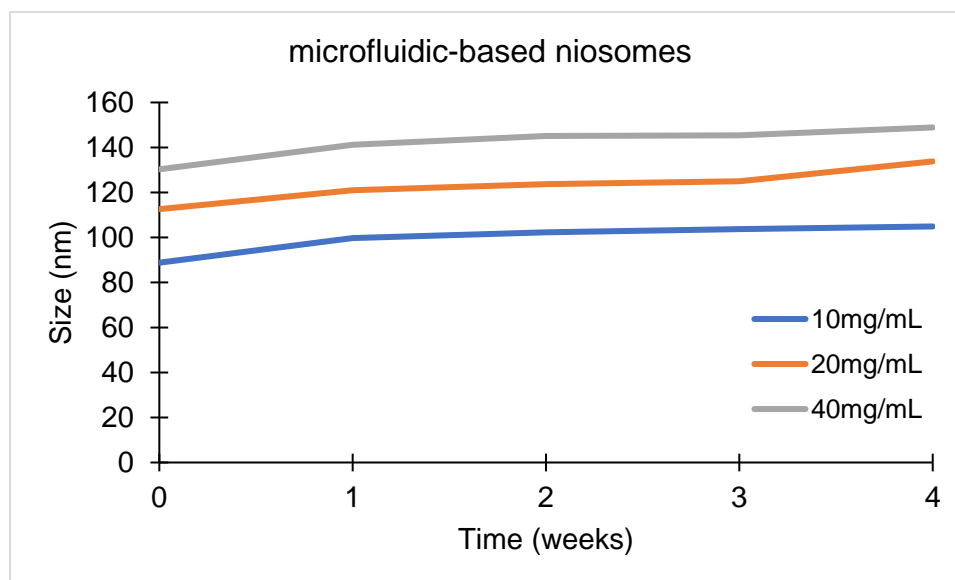


Figure 3-4: Graph showing particle size of microfluidic-based niosomes were stored at fridge temperature 4°C. Formulations of Span® 60: cholesterol: Cremophor® ELP at different total surfactant/lipid concentrations.

3.4. Conclusion

Overall, this chapter demonstrated the influence of process and formulation variables on niosome characteristics, using thin film hydration and microfluidic methods, through evaluation on niosome characteristics such as size and its distribution, and encapsulation efficiency. Conventional niosome manufacturing process often involve a size reduction process to achieve desirable vesicle size, while advanced microfluidic method allows controlled manufacturing of vesicles of limit size (Belliveau et al., 2012). The use of sonication and its effect on formulation variables such as total surfactant/lipid concentration and methylene blue concentration, offers insights on niosome formulation optimisation for encapsulating hydrophilic drug molecules within

niosome vesicles. The manufacture and properties of niosome vesicles produced by both bulk and microfluidic methods were studied and compared to hydrophobic cinnarizine entrapment into niosome formulation in the next chapter where the process parameters used in this chapter will be taken into consideration.

Paper relating to this chapter:

Yeo, L.K., Chaw, C.S. and Elkordy, A.A. (2019). The effects of hydration parameters and co-surfactants on methylene blue-loaded niosomes prepared by the thin film hydration method. *Pharmaceuticals*, 12(12):46.

Chapter Four:

4. Manufacturing of niosomes containing cinnarizine as a model poorly water-soluble drug

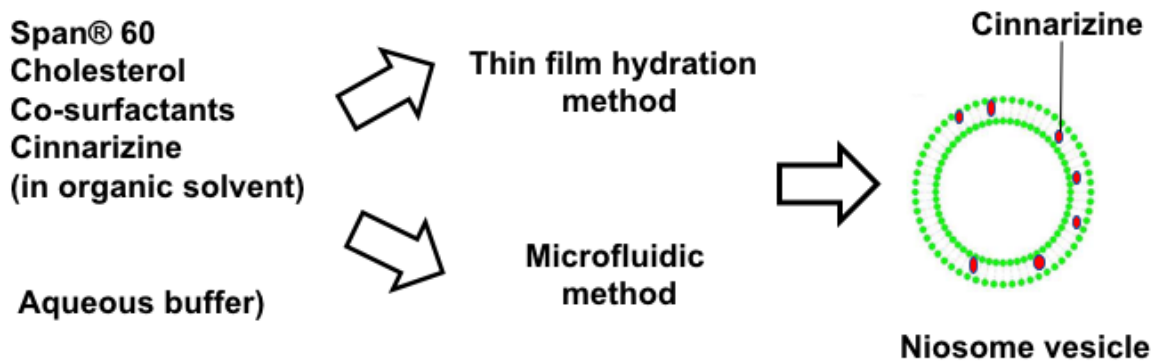


Figure 4-1: Graphical abstract for manufacturing of niosomes containing cinnarizine as a model poorly water-soluble drug.

4.1. Overview

For a drug to exert its therapeutic action, the drug must be firstly absorbed into the systemic circulation and distributed from its administration site except for intravenous route of administration. Upon reaching the systemic circulation, the drug may bind to plasma protein or remain freely to be distributed to its site of action. Apart from the physiological condition of the gastrointestinal tract (GIT) for oral formulations, there are a variety of factors including the drug properties and formulation factors, that can affect the formulation characteristics and performances. In particular, it is challenging to formulate poorly water-soluble drugs due to the fact that they must first be dissolved in the physiological fluid to be able to be absorbed into the bloodstream. Administration of oral dosage forms of solid-state drug presents the risk of adverse drug and subtherapeutic effects. Consequently, a dose increment is needed to achieve the intended therapeutic level, but it also increases the risk and intensity of adverse drug effects, which affects patient adherence and clinical outcome. However, due to limited solubility in gastrointestinal pH and precipitation of the poorly water-soluble drug, formulation design of a drug product with high drug load is generally difficult and dose escalation is causing toxicity side effects (Kawabata et al., 2011).

According to Kalepu and Nekkanti (2015), poorly water-soluble drugs are increasing in numbers with about 40% of the marketed drugs and nearly 90% of new drug molecules in the pharmaceutical development pipeline. They are drugs with low aqueous solubilities of lower than 100 µg/mL which often show limited dissolution to absorption (Hörter and Dressman, 2001). These poorly water-soluble drugs are increasingly a problem prompting pharmaceutical companies to explore formulation strategies on improving the intrinsic properties of the drug for enhanced dissolution

and bioavailability. Increasing aqueous solubility of the drug leads to a higher drug dissolution rate for absorption and enhanced bioavailability. Various approaches have been reported to improve solubility and dissolution of poorly water-soluble drugs through techniques such as salt formation, physical size reduction (i.e. micronization and nanosizing), self-emulsification, complexation, amorphous solid dispersion, and lipid-based systems (e.g. liposomes and niosomes) (Boyd, Christel A.S. Bergström, et al., 2019). Increasing solubilisation in the gastrointestinal tract not only enhance drug absorption for increased oral bioavailability but potentially reduce the dose required.

Cinnarizine was used as the model of poorly water-soluble drug in this chapter. The chemical structure and formula of cinnarizine are shown in Figure 4-2. It is classified as a class II drug in the Biopharmaceutical Classification System (BCS) with high permeability and low solubility. The weak base drug (Log P 5.6; pK_a 1.95 and 7.8) has a poor aqueous solubility, which is practically insoluble in water with a solubility of 20 µg/mL in water (Berlin et al., 2014). Cinnarizine is a piperazine derivative with two tertiary amine groups of which one tertiary amine group ionises at low pH where it remains dissolved and stable in which the degradation of cinnarizine does not occur readily (Tokumura et al., 1985).

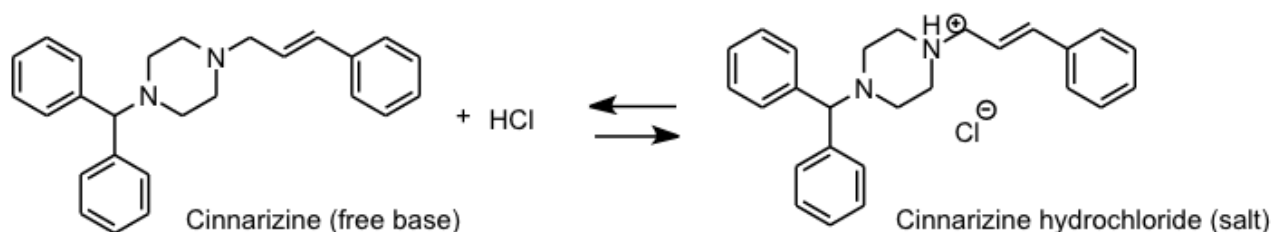


Figure 4-2: Structure of cinnarizine (C₂₆H₂₈N₂) in free base and salt forms (Chemdraw).

Commonly, cinnarizine hydrochloride is taken orally in a tablet form that usually results in a very slow absorption and a wide inter-individual variation (Cinnarizine 15 mg Tablets - SmPC, 2021). After oral administration, drug absorption is relatively slow with peak serum concentrations occurring after 2.5 to 4 hours from the upper gastrointestinal tract (stomach) with a narrow absorption window owing to its highly pH-dependent aqueous solubility. Variation in absorption is dependent on individual's gastric acidity where the cinnarizine is rapidly dissolved in the acidic gastric acid content. Castaneda Hernandez et al. (1993) reported that the elimination half-life for cinnarizine ranges from 4 to 24 hours, thus frequent dosing is needed.

Apart from sustained release properties and drug protection from degradation within the harsh gastrointestinal environment, solubilisation of poorly water-soluble drug within niosomal bilayers enhances oral bioavailability (Mahale et al., 2012). The low aqueous solubility drug (cinnarizine) was firstly dissolved with the surfactant/lipid in the solvent phase. Subsequently, niosome formation and encapsulation of the drug was performed simultaneously during the preparation process in thin film hydration method or nanoprecipitation process in microfluidic method. Entrapment and retainment of hydrophobic drugs are likely to remain associated with the membrane as it reforms in a spontaneous manner (Nguyen et al., 2015). Incorporation of poorly water-soluble drugs is not only dependent on the physicochemical properties of the drug, factors including bilayer composition, lipid alkyl chain length used and the method of preparations have also been shown to be contributing factors.

Conventionally thin film hydration is used as bulk method for manufacturing niosomes on hydration of a mixture of non-ionic surfactant with cholesterol (Baillie et al., 1985).

Following the hydration process, vesicles produced are typically multilamellar and heterogeneous in size requiring size reduction methods such as homogenisation, extrusion, and sonication. These processes are time-consuming and require high pressures and generate heat which can be damaging for drugs and excipients. Sonication method using either a probe sonicator or bath sonicator is often quick and simple method at laboratory scale as a top-down approach.

In comparison, microfluidic-based niosome manufacturing has been explored as a bottom-up approach. The microfluidic technique NanoAssemblr™ Benchtop from Precision Nanosystems Inc. was employed for the production of niosomes. The system is a computerised instrument with syringe pump platform which controls the mixing of miscible fluids within a specially designed micromixer cartridge. The cartridge consists of microchannels partly embedded with grooves pattern of a staggered herringbone micromixer (SHM) feature to facilitate mixing process. By changing the system parameters and controlling the intrinsic properties of the formulation, the manufacturing of niosomes using microfluidics was evaluated by changing influencing factors: the total surfactant/lipid concentration, total drug concentration, the total flow rate, and the flow rate ratio between aqueous and organic phases.

Vesicle membrane properties such as thickness and the level of fluidity are determined by the formulation compositions and drug characteristics. Vesicle membrane composition can affect both drug partitioning and drug encapsulation efficiency of lipophilic drugs as these drugs are embedded within the membrane bilayer, and their encapsulation depends on the solubility in the bilayer membrane (Eloy et al., 2014).

The physicochemical characteristics of vesicles were reported to be linked to the manufacturing method relating to the amount of drug encapsulated (Xu, Khan and Burgess, 2011). Cholesterol has been shown to enhance the stability of vesicles by filling space within bilayer membrane and has led to reduction in bilayer drug loading (Ali et al., 2010). Moreover, it is reported that the formation of hydrogen bonding interaction between the entrapped drug and niosome membrane had influence on the encapsulation efficiency and release of drug (Hao and Li, 2011).

In this chapter, characterisation of niosomes was performed including for physical properties using Fourier transform infrared spectroscopy to study drug-excipient interactions, differential scanning calorimetry for thermal properties, transmission electron microscopy for morphological and intrinsic properties of niosome vesicles. Dynamic light scattering technique was used in the measurement of average vesicle size and distributions, from niosomes manufactured by thin film hydration and microfluidic methods. Other properties monitored were drug encapsulation efficiency and in vitro drug release profile of the niosomes.

This chapter focused on the encapsulation of a hydrophobic drug within niosomes using thin film hydration method and microfluidic method for simultaneous niosome manufacturing and drug encapsulation. Apart from the manufacturing methods, different hydrophilic co-surfactants for formulation compositions have been investigated. The effect of manufacturing methods and formulation compositions on niosome characteristics were demonstrated and evaluated.

4.2. Aims and Objectives

This chapter aimed to study and report the manufacturing, formulation and properties of niosome vesicles as nanocarriers to encapsulate cinnarizine as a model of poorly water-soluble drug. Manufacturing methods used were conventional thin film hydration method and microfluidic method comprised of different formulation compositions. The purpose of this chapter was to explore and understand the manufacturing and formulation effects on physicochemical properties of niosomes produced, with the aim of supporting future studies.

The objectives of this chapter were to:

- Prepare cinnarizine-encapsulated niosomes using thin film hydration method and microfluidic method.
- Investigate the morphological properties of niosome vesicles prepared using both methods by transmission electron microscopy.
- Characterise the physical interactions between formulation compositions of cinnarizine encapsulated niosome formulations by Fourier-transform infrared and differential scanning calorimetry techniques.
- Characterise and evaluate the effect of niosome manufacturing methods and different formulation aspects on the physicochemical properties of niosomes (size distribution and encapsulation efficiency).
- Demonstrate a direct comparison of the characteristics of niosomes prepared using thin film hydration and microfluidic methods.

4.3. Results and Discussion

4.3.1. Vesicle size distribution and encapsulation efficiency: Effect of surfactant/lipid concentrations and sonication on niosomes manufactured by thin film hydration method

In Table 4-1, thin film hydration method used for the manufacturing of niosomes composed of different compositions had revealed heterogeneous dispersions of large multilamellar vesicles with a wide distribution (polydispersity index of more than 0.6). Two-fold increase in vesicle sizes can be seen with increasing the final total surfactant/lipid concentration within the formulation system from 10 or 20 mg/mL to 40 mg/mL. Despite a homogeneous thin film was obtained for each of the formulation, the conventional bulk method where the hydration process of the thin film involves agitation in a water bath at a temperature above its phase transition temperature, was not sufficient for producing a desirable homogeneous niosome dispersion. In the effort to reduce vesicle sizes and their distributions, TFH niosomes were subjected to sonication to enhance their characteristics. In Table 4-2, sonication process revealed a significant reduction in vesicle size can be seen across all niosome formulations with no notable difference between different surfactant/lipid concentrations. However, the size distributions of all sonicated niosome were remained high (polydispersity index of more than 0.7). Interestingly, the encapsulation efficiencies decreased with increasing total surfactant/lipid concentrations in S60:Cho:ELP niosomes and S60:Cho:RH40 niosomes. Whereas, the highest encapsulation efficiencies were obtained at 20 mg/mL total surfactant/lipid concentration in S60:Cho:HS15 niosomes.

Table 4-1: Effect of different final surfactant/lipid concentrations used on niosome size and distribution in TFH-based niosomes comprised of different formulation compositions, without sonication as post-preparation processing technique for size reduction.

Thin film hydration without sonication			
Final drug concentration at 0.5 mg/mL			
Final surfactant/lipid conc (mg/mL)	Formulation	Size (nm)	PDI
10	S60: Cho: ELP	4607 ± 795	0.59 ± 0.04
	S60: Cho: RH40	3166 ± 569	0.88 ± 0.21
	S60: Cho: HS15	3232 ± 435	0.87 ± 0.16
20	S60: Cho: ELP	3410 ± 485	0.77 ± 0.20
	S60: Cho: RH40	4533 ± 711	0.70 ± 0.28
	S60: Cho: HS15	4759 ± 834	0.84 ± 0.16
40	S60: Cho: ELP	7420 ± 1392	0.59 ± 0.01
	S60: Cho: RH40	7383 ± 997	0.70 ± 0.03
	S60: Cho: HS15	4436 ± 351	1.00 ± 0.00

Data are expressed as mean ± standard deviation from three independent experiments (n=3).

* All S60: cholesterol formulations of all surfactant/lipid concentrations were omitted as no formation of niosome were shown due to non-homogenous distorted thin film formed.

Table 4-2: Niosome characteristics for sonicated TFH-niosome formulations at different final total surfactant/lipid concentrations before purification process.

Thin film hydration with sonication				
Final drug concentration at 0.5 mg/mL				
Final surfactant/lipid con (mg/mL)	Formulation	Size (nm)	PDI	EE %
10	S60: Cho: ELP	430.5 ± 30.5	0.86 ± 0.08	49.2 ± 6.8
	S60: Cho: RH40	429.2 ± 17.9	0.90 ± 0.03	41.1 ± 15.6
	S60: Cho: HS15	556.1 ± 33.5	0.89 ± 0.05	20.5 ± 6.2
20	S60: Cho: ELP	477.6 ± 43.2	0.76 ± 0.05	32.1 ± 6.9
	S60: Cho: RH40	511.0 ± 62.9	0.93 ± 0.09	31.5 ± 16.1
	S60: Cho: HS15	389.3 ± 19.7	0.77 ± 0.02	26.5 ± 10.6
40	S60: Cho: ELP	543.9 ± 34.4	0.73 ± 0.11	31.3 ± 9.6
	S60: Cho: RH40	391.9 ± 26.5	0.79 ± 0.05	19.7 ± 3.6
	S60: Cho: HS15	877.9 ± 89.6	0.79 ± 0.14	20.6 ± 4.3

Encapsulation efficiencies (EE %) were calculated for all purified and sonicated niosome formulations. Data are expressed as mean ± standard deviation from three independent experiments (n=3).

4.3.2. Vesicle size distribution and encapsulation efficiency: Effect of TFR and FRR on the vesicle size and distribution of MF niosomes

To the best of our knowledge, there are no previous study on niosome formulation encapsulating cinnarizine using microfluidic method as a bottom-up approach of manufacturing. Other than the formulation parameters, niosome characteristics are dependent on the manufacturing parameters i.e. total flow rate (TFR) and flow rate ratio (FRR) between aqueous and organic phases. These manufacturing parameters are crucial in the process of rapid mixing within the micromixer to induce nanoprecipitation process for vesicle formation, and hence determining the characteristics of vesicles.

To investigate the effect of TFR on niosomes, S60:Cho:ELP formulation composition was used. In Table 4-3, the results showed that highly homogeneous dispersions of niosomes were manufactured. The increase in TFR at constant FRR of 4:1 showed a decrease in average vesicle sizes as a result of increasing mixing rates. Increasing the polarity change in the mixing process by increasing the FRR (from 1:1 to 9:1) at constant TFR of 12 mL/min showed to reduce the average vesicle sizes, with one exception on FRR of 3:2 showing the largest average vesicle sizes (Table 4-4).

The volumetric difference between aqueous and miscible organic phases triggers the nanoprecipitation process during the vesicle formation where the drug encapsulation occurred simultaneously. The larger the difference, the higher the polarity change. Increased in the change in polarity increased the encapsulation efficiencies of the hydrophobic drug in the vesicles. Notably, the highest drug encapsulation showed at FRR of 4:1, followed by a decrease encapsulation in the highest change in polarity at FRR of 9:1 (Table 4-4).

In Figure 4-3, higher FRRs showed no difference in vesicle size change upon refrigerated storage over 4-week period. In contrast, lower FRRs showed two-fold increase in average vesicle sizes.

Table 4-3: Effect of total flow rate on niosome size and distributions post-cartridge.

Span® 60: Cholesterol: Cremophor® ELP niosomes		
Initial total surfactant/lipid concentration at 100 mg/mL		
Initial drug concentration at 2.5 mg/mL		
Flow rate ratio (aqueous: organic) at 4:1		
Total Flow Rate (mL/min) [aqueous: organic]	Size (nm)	PDI
2 [1.6: 0.4]	213.2 ± 3.7	0.6 ± 0.03
4 [3.2: 0.8]	224.9 ± 2.5	0.6 ± 0.04
6 [4.8: 1.2]	192.0 ± 1.3	0.4 ± 0.01
8 [6.4: 1.6]	175.3 ± 2.0	0.7 ± 0.02
10 [8: 2]	171.5 ± 0.9	0.6 ± 0.02
12 [9.6: 2.4]	182.0 ± 1.0	0.3 ± 0.02

Data are expressed as mean ± standard deviation from three independent experiments (n=3).

Table 4-4: Effect of flow rate ratio (aqueous: organic) on niosome size and distribution post-cartridge; encapsulation efficiency post-purification.

Span® 60: Cholesterol: Cremophor® ELP niosomes			
Initial total surfactant/lipid concentration 100 mg/mL			
Initial drug concentration 1.25mg/mL			
Total flow rate at 12 mL/min			
FRR (aqueous: organic)	Size (nm)	PDI	EE %
1:1	282.5 ± 4.4	0.60 ± 0.05	27.1 ± 2.3
3:2	376.6 ± 14.0	0.20 ± 0.08	28.8 ± 1.2
3:1	225.0 ± 2.3	0.20 ± 0.02	34.7 ± 0.8
4:1	182.0 ± 1.0	0.30 ± 0.02	78.9 ± 1.6
9:1	125.8 ± 1.9	0.10 ± 0.01	49.2 ± 3.5

Data are expressed as mean ± standard deviation from three independent experiments (n=3).

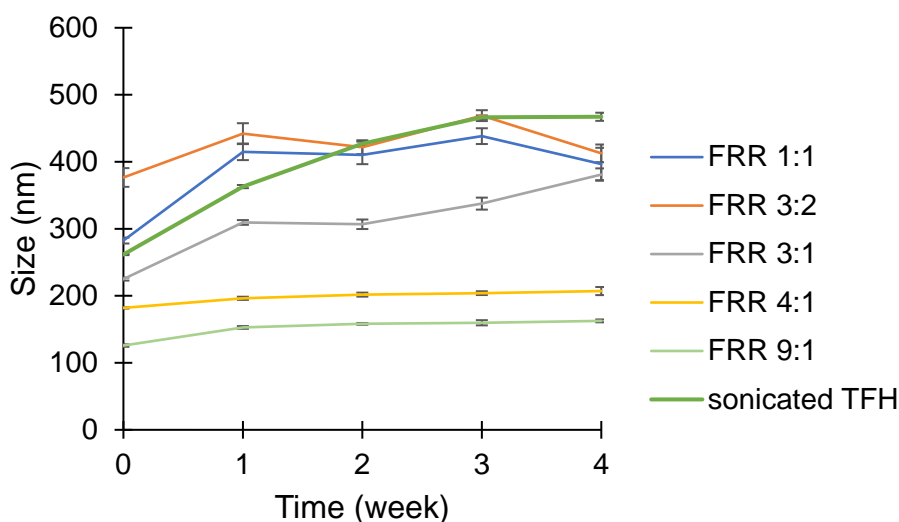


Figure 4-3: Line curves showed size changes upon refrigerated storage for Span® 60: cholesterol: Cremophor® ELP niosomes prepared by using microfluidic at different flow rate ratios (FRR) and the same formulation prepared using thin film hydration followed by sonication ($n=3$).

4.3.3. Vesicle size distribution and encapsulation efficiency: Effect of loading drug on microfluidic-based niosome characteristics

To investigate the effect of loading drug concentration on niosome characteristics, empty microfluidic-based niosomes (no drug) were compared with drug-loaded microfluidic-based niosomes using two initial drug concentrations for direct loading under constant manufacturing process. Results showed similar drug encapsulation efficiencies regardless of niosomes of all formulation compositions, the loading drug amount and the average size distributions (Table 4-5).

At higher loading drug amount, S60:Cho:ELP niosomes showed a notable decrease in average vesicle size. Similarly, the vesicle size of S60:Cho:HS15 niosomes decreased with increased loading drug amount. In contrast, the incorporation of cinnarizine into S60:Cho:RH40 niosomes revealed an increase in vesicle size. The decrease in average vesicle sizes might be explained due to the interactions between

the drug and excipients, at the same time, facilitating the drug encapsulation during the mixing process.

Table 4-5: Effect of cinnarizine loading characteristics of microfluidic-based niosomes.

Total flow rate at 12 mL/min; flow rate ratio (aqueous: organic) at 4:1					
Final total surfactant/lipid concentration at 20 mg/mL					
Theoretical final cinnarizine concentration (mg/mL)	Formulation	Size (nm)	PDI	Zeta potential (mV)	EE %
0	S60: Cho	176.6 ± 1.7	0.1 ± 0.01	-2.37 ± 0.69	n/a
	S60: Cho: ELP	312.3 ± 12.9	0.1 ± 0.03	-1.98 ± 1.12	
	S60: Cho: RH40	171.4 ± 2.7	0.2 ± 0.01	-2.06 ± 1.32	
	S60: Cho: HS15	364.9 ± 11.2	0.1 ± 0.01	-2.12 ± 1.19	
0.25	S60: Cho	186.8 ± 3.3	0.1 ± 0.02	-1.99 ± 1.03	68.6 ± 2.1
	S60: Cho: ELP	328.9 ± 12.2	0.1 ± 0.03	-2.09 ± 0.89	78.9 ± 1.6
	S60: Cho: RH40	212.0 ± 4.2	0.2 ± 0.01	-1.85 ± 1.56	78.4 ± 1.1
	S60: Cho: HS15	326.4 ± 5.2	0.1 ± 0.01	-2.37 ± 1.19	79.1 ± 0.6
0.50	S60: Cho	180.5 ± 2.7	0.2 ± 0.01	-2.29 ± 1.17	74.5 ± 2.3
	S60: Cho: ELP	182.0 ± 1.0	0.3 ± 0.02	-1.88 ± 1.39	76.6 ± 1.9
	S60: Cho: RH40	214.5 ± 9.2	0.2 ± 0.01	-1.99 ± 1.77	74.8 ± 0.5
	S60: Cho: HS15	306.7 ± 8.1	0.1 ± 0.02	-2.01 ± 1.55	81.7 ± 0.9

Data are expressed as mean ± standard deviation from three independent experiments (n=3). Not applicable (n/a).

4.3.4. Vesicle size distribution and encapsulation efficiency: Effect of manufacturing methods and formulation compositions on niosome characteristics

All cinnarizine-entrapped niosome formulations manufactured by thin film hydration method and microfluidic method in a drug-to-surfactant/lipid ratio at 1:40 via direct simultaneous loading of the drug during the formation of vesicles. Figure 4-7 showed the average vesicle size changes in microfluidic-based niosomes upon refrigerated storage over 4-week period. Both S60:Cho:RH40 niosomes and S60:Cho:HS15 niosomes had shown almost 1.5-fold increase in average vesicle sizes over the 4-week period. At the same time, S60:Cho niosomes and S60:Cho:ELP niosomes showed no noticeable difference in the change of average vesicle sizes over different storage temperatures over 4 weeks period (Figure 4-4). This suggests that the microfluidic-based niosome vesicles were stable with vesicle sizes less than 300 nm.

Table 4-6: Effect of manufacturing methods and formulation compositions on niosome characteristics.

Final surfactant/lipid concentration at 20 mg/mL						
Final cinnarizine concentration at 0.5 mg/mL						
Formulation	Size (nm)		PDI ***		EE% ***	
	TFH*	MF	TFH*	MF	TFH*	MF
S60: Cho	**	180.5 ± 2.7	**	0.2 ± 0.01	**	74.5 ± 2.3
S60: Cho: ELP	477.6 ± 43.2	182.0 ± 1.0	0.76 ± 0.05	0.3 ± 0.02	32.1 ± 6.9	76.6 ± 1.9
S60: Cho: RH40	511.0 ± 62.9	214.5 ± 9.2	0.93 ± 0.09	0.2 ± 0.01	31.5 ± 16.1	74.8 ± 0.5
S60: Cho: HS15	389.3 ± 19.7	306.7 ± 8.1	0.77 ± 0.02	0.1 ± 0.02	26.5 ± 10.6	71.8 ± 0.9

Data are expressed as mean ± standard deviation from three independent experiments (n=3).

* All TFH-based niosomes after subjected to sonication process.

** All S60: cholesterol formulations of different surfactant/lipid concentrations were omitted as no formation of niosome shown due to non-homogenous distorted thin film formed.

*** significantly different ($p < 0.05$).

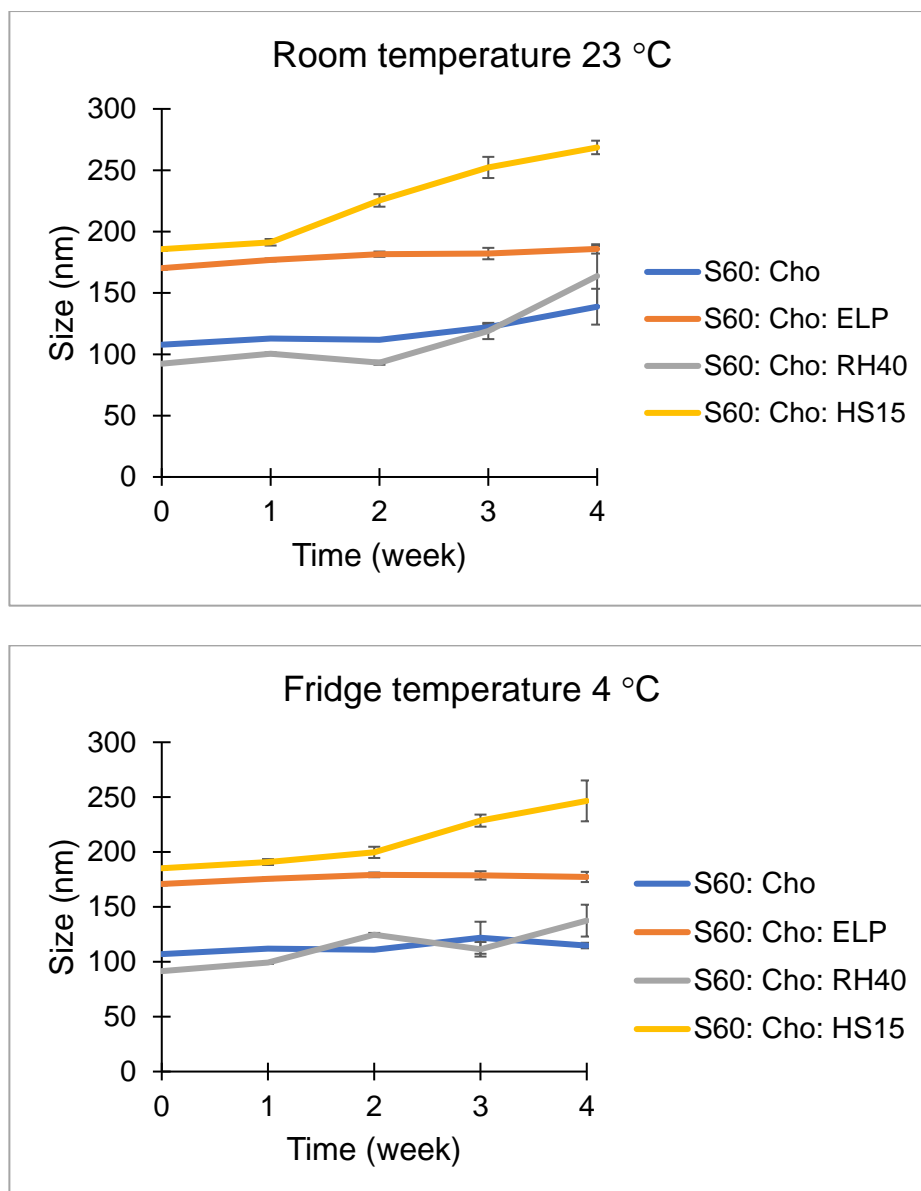


Figure 4-4: Line curves showed size changes upon room temperature (23 ± 2 °C) and refrigerated storage (4 ± 2 °C) for purified microfluidic-based niosomes comprised of different formulation compositions.

4.3.5. Vesicle size distribution and encapsulation efficiency: Effect of manufacturing methods and total surfactant/lipid concentrations on niosome characteristics

Table 4-7 presents the influence of expected final total surfactant/lipid concentrations on vesicle size and encapsulation efficiency of S60:Cho:ELP niosomes manufactured by thin film hydration and microfluidic methods.

In sonicated TFH-based niosomes, average vesicle size increased but encapsulation efficiencies decreased with increasing final total surfactant/lipid concentration. In contrast, MF-based niosomes showed an increase in average vesicle size with increasing final total surfactant/lipid concentration at constant total flow rate of 12 mL/min. The highest final total surfactant/lipid concentration at 40 mg/mL showed the lowest encapsulation efficiency. This might be due to the high surfactant/lipid components mixture leading to a change in self-assembly behaviour of surfactant/lipid components and resulted in less efficient and/or insufficient mixing within the microfluidic microchannels, leading to the highest average vesicle sizes. The highest encapsulation efficiency was shown in MF-niosomes of 20 mg/mL final total surfactant/lipid concentration. This revealed that the impact of total surfactant/lipid concentration for an efficient mixing between miscible organic phase (containing a mixture of dissolved surfactant/lipid components and hydrophobic drug) and aqueous buffer in microfluidic method. As microfluidic method enables a controlled process for reproducible manufacturing of nanoparticles, the surfactant/lipid quantification and recovery study will be followed in Chapter 5.

Table 4-7: Niosome characteristics for sonicated TFH-based niosomes and microfluidic-based niosomes at different final total surfactant/lipid concentrations.

Span® 60: Cholesterol: Cremophor® ELP niosomes						
Final drug concentration at 0.5 mg/mL						
Total flow rate of 12 mL/min in microfluidic mixing						
Flow rate ratio (aqueous: organic) at 4:1						
Final surfactant/lipid concentration (mg/mL)	Size (nm)		PDI		EE%	
	TFH	MF	TFH	MF	TFH	MF
10	430.5 ±	125.8 ±	0.86 ±	0.10 ±	49.2 ±	49.2 ±
	30.5	1.9	0.08	0.01	6.8	3.5
20	477.6 ±	182.0 ±	0.76 ±	0.30 ±	32.1 ±	76.6 ±
	43.2	1.0	0.05	0.02	6.9	1.9
40	543.9 ±	376.6 ±	0.73 ±	0.20 ±	31.3 ±	28.8 ±
	34.4	14.0	0.11	0.08	9.6	1.2

4.3.6. Effect of manufacturing method on drug release

Following drug encapsulation, *in vitro* drug release from the purified niosome vesicles manufactured by thin film hydration method and microfluidic method were performed via dialysis method. Amount of drug quantified and expressed as % cumulative release in relation to the total amount of drug encapsulated were calculated. Results showed that an initial drug release of about 10 % was similar and independent of the manufacturing method, and followed by continuous release of a further 40% of the encapsulated drug over 6 h (Figure 4-5). Subsequent drug release up to 24 h showed a higher release from TFH-niosomes than MF-niosomes. Similarly, a previous study demonstrated a slow drug release of Span® niosomes encapsulating a model hydrophobic drug that was prepared by thin film hydration method at both pH 2 and

pH 7.4 (Jadon et al., 2009). The incorporation of cholesterol into the membrane bilayer contributed to a more condensed and less porous membrane bilayer. Encapsulation and release were reported to be influenced greatly by the hydrogen binding interaction intensity (Hao and Li, 2011). The study suggested that the stronger the hydrogen binding between the encapsulated drug and membrane bilayer components, the higher entrapment efficiency and slower release rate. Similarly, MF-niosomes showing twice higher encapsulation efficiencies than TFH-niosomes (Table 4-7) demonstrated a notably slower release over 24-hour period.

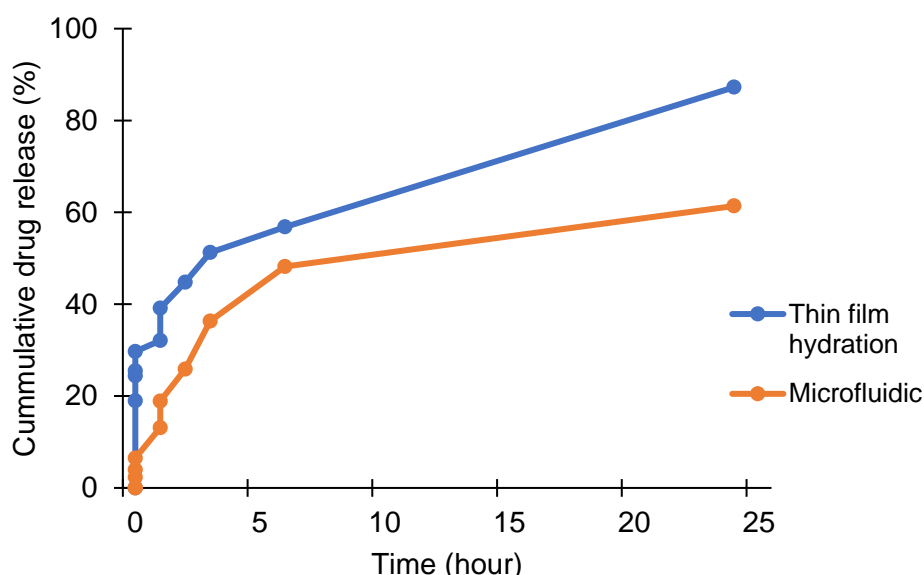


Figure 4-5: In vitro drug release plot shows the cumulative drug release over 24 hours period in simulated gastric fluid without enzymes (pH 1.2 and 37 °C) for cinnarizine-loaded S60:Cho:ELP niosomes manufactured by thin film hydration and microfluidic methods. Initial drug concentration used was 0.5 mg/mL. Error bars have been omitted intentionally for the clarity of the graph.

4.3.7. Morphological properties of niosome vesicles

After initial observation using optical microscopy, niosomes were studied using transmission electron microscopy (TEM) to investigate the morphological properties of vesicles manufactured by thin film hydration (TFH) method or microfluidic (MF) method. TEM images taken (Figure 4-6) verified the small vesicles manufactured by

microfluidics, in agreement with the average sizes of vesicles obtained via dynamic light scattering technique (<350 nm). There was no notable difference in images obtained for empty niosome vesicles and cinnarizine-loaded niosome vesicles. Similarly, for sonicated TFH-based niosome vesicles (Figure 4-7), they were generally larger in average sizes in comparison to MF-based niosome vesicles. All vesicle sizes taken were corresponded to measurements obtained by using dynamic light scattering technique.

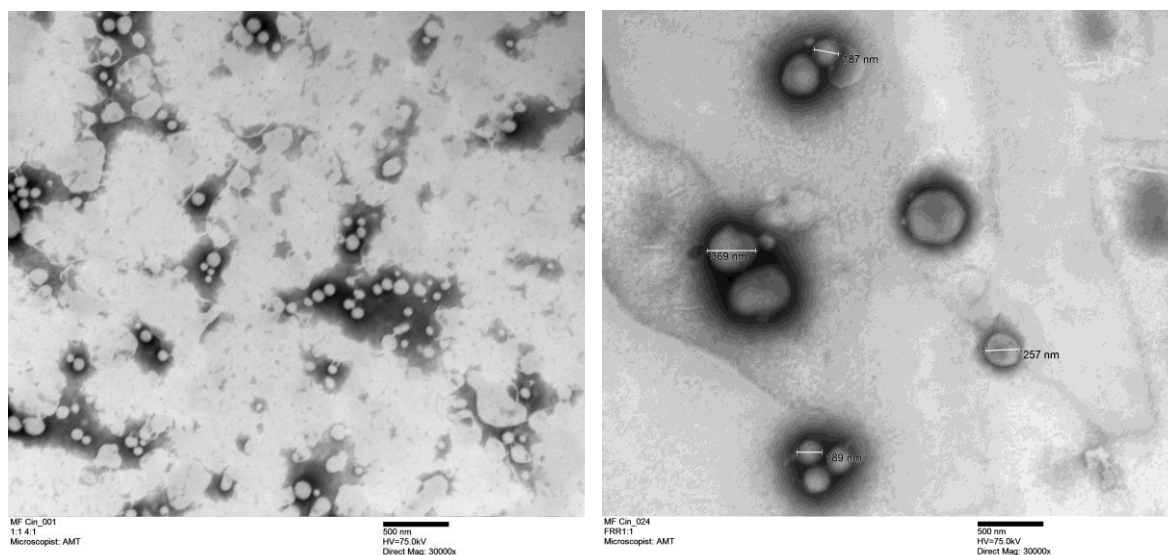


Figure 4-6: Transmission electron microscopy images obtained of (left) S60: Cho MF-niosomes (TFR12 mL/min, FRR4:1); (right) S60: Cho: ELP MF-niosomes (TFR 12mL/min, FRR 1:1).

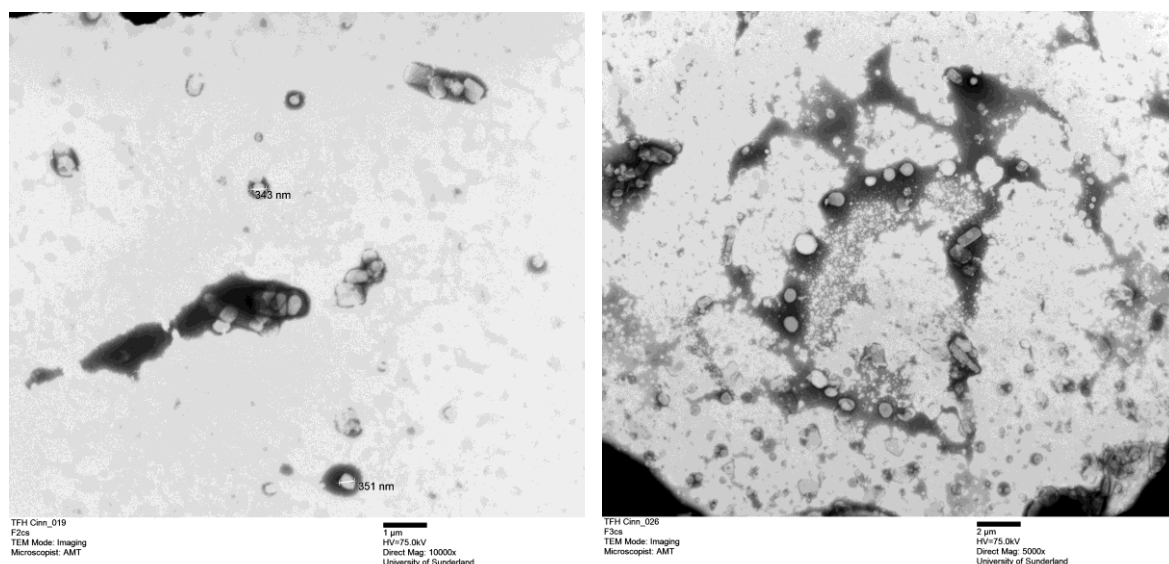


Figure 4-7: Transmission electron microscopy images obtained of (left) S60: Cho: ELP sonicated TFH-niosomes; (right) S60: Cho: RH40 sonicated TFH-niosomes.

4.3.8. Fourier-transform infrared (FTIR) spectroscopy

Fourier-transform infrared (FTIR) was used as an analysis technique for the identification of raw materials by determining principle peaks of characteristic functional groups and their changes within specific printing area (Griffiths and De Haset, 2007). To identify the interaction between the formulation excipients and entrapped drug, FTIR spectra of individual raw ingredients and freeze-dried niosomes were taken to evaluate their interactions and compatibilities as a formulation entrapping cinnarizine. The principal peaks and assignment for the major infra-red absorption bands of cinnarizine in its free base form were observed and shown in Table 4-8 (from Figure 4-7B). Niosome formation incorporating non-ionic surfactant, cholesterol and co-surfactant for all formulations showed similar peaks comparing empty niosomes and cinnarizine-entrapped niosomes, indicating no effect of encapsulated drug on niosome formulation interactions. Among all cinnarizine-entrapped niosomes, disappearance of the principal peaks of cinnarizine (CN stretch

and C=C aromatic stretch) was shown in formulations composed of Cremophor® ELP or Solutol® HS15, indicating well incorporation of cinnarizine within these vesicles. Similar spectra were shown for microfluidic-based niosomes composed of Cremophor® ELP demonstrated well incorporation of cinnarizine, suggesting that the hydrophobic drug incorporation is independent of niosome manufacturing methods. As for niosomes composed of Cremophor® RH40, the presence of cinnarizine principle peak (C=C stretch) revealed that the drug was not incorporated well within the vesicles, this incompatibility detected might be due to its high molecular weight and hydrophilicity inhibiting the entrapment of hydrophobic cinnarizine within vesicle bilayers.

Table 4-8: Principal peaks with respective assignments of pure cinnarizine in its free base form.

Frequency (cm⁻¹)	Assignments
2959	CH stretching (aromatic, alkene, monosubstituted)
2936	CH stretch (aliphatic alkane)
1597	C=C aromatic stretch
1490 and 1448	CH ₂ stretch (aliphatic alkane)
1134	CN stretch
999 and 962	=CH out of plane (aromatic, alkene)

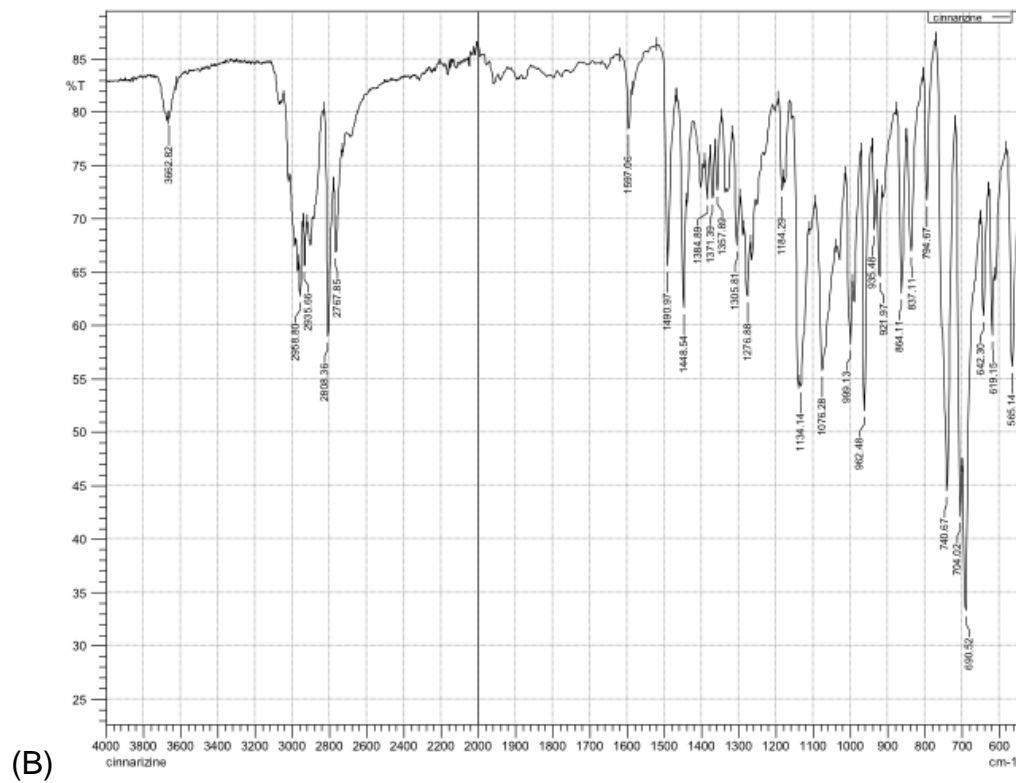
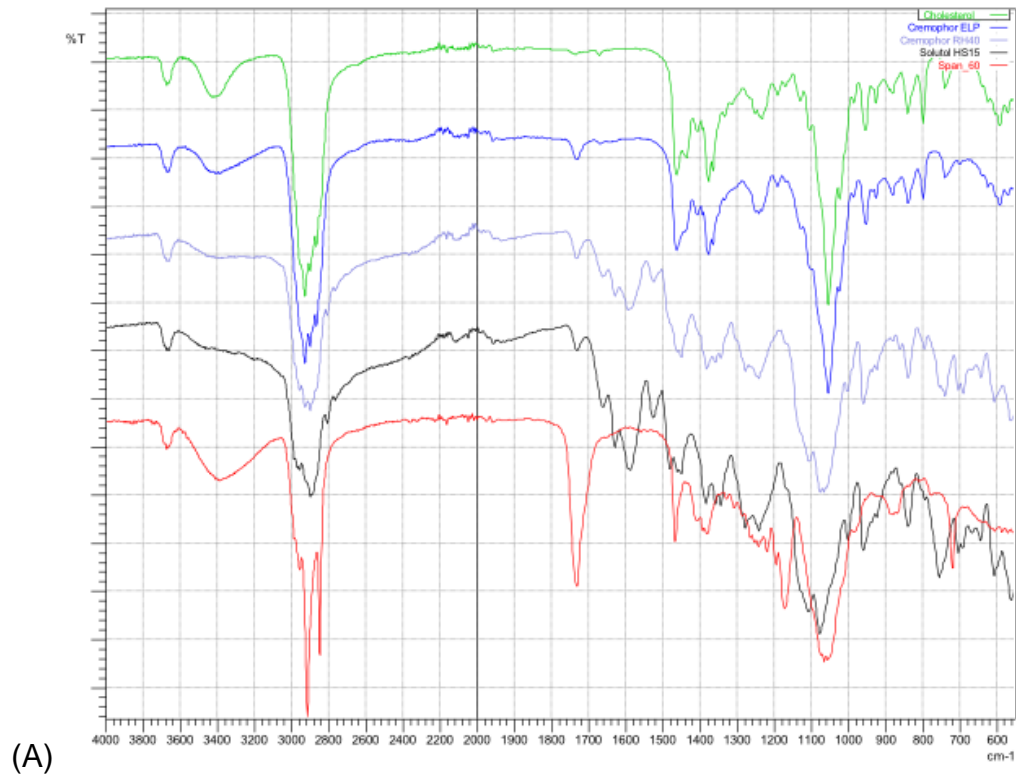


Figure 4-8: FTIR spectra for (A) individual pure ingredient: cholesterol (green), Cremophor® ELP (blue), Cremophor® RH40 (purple), Solutol® HS15 (black) and Span® 60 (red); (B) pure cinnarizine base.

4.3.9. Differential scanning calorimetry (DSC)

Differential scanning calorimetry (DSC) heat flow curves were generated for all pure raw ingredients used in preparing niosomes composed of different formulation compositions for which their thermal characteristics i.e. melting temperatures and enthalpy change were observed. During manufacturing process for niosome formation, the input of external energy in the form of mechanical agitation in water bath or rapid mixing within the staggered herringbone micromixer can influence the niosome characteristics in terms of their thermal behaviours and physical properties.

A sharp endothermic peak at 123.05 °C can be observed on the DSC thermograph for pure cinnarizine, showing its melting point in its crystalline drug form. This endothermic peak was seen demolished (in S60: Cho: ELP niosomes; Figure 4-9B) or broadened and shifted to a lower temperature (Figures 4-9C and 4-9D), suggesting changes in the structure arrangement as drug incorporation into niosome vesicles and the transformation of crystalline form into an amorphous form. The use of mannitol as cryoprotectant to preserve the integrity of the vesicles during the freeze-drying process showed no effect on drug-excipient interaction of niosomes (Figure 4-10). This is in agreement with the formation of an amorphous matrix suggested that freeze-dried vesicles can be inter-dispersed avoiding fusion and aggregation in dispersion forms (Sebaaly et al., 2016).

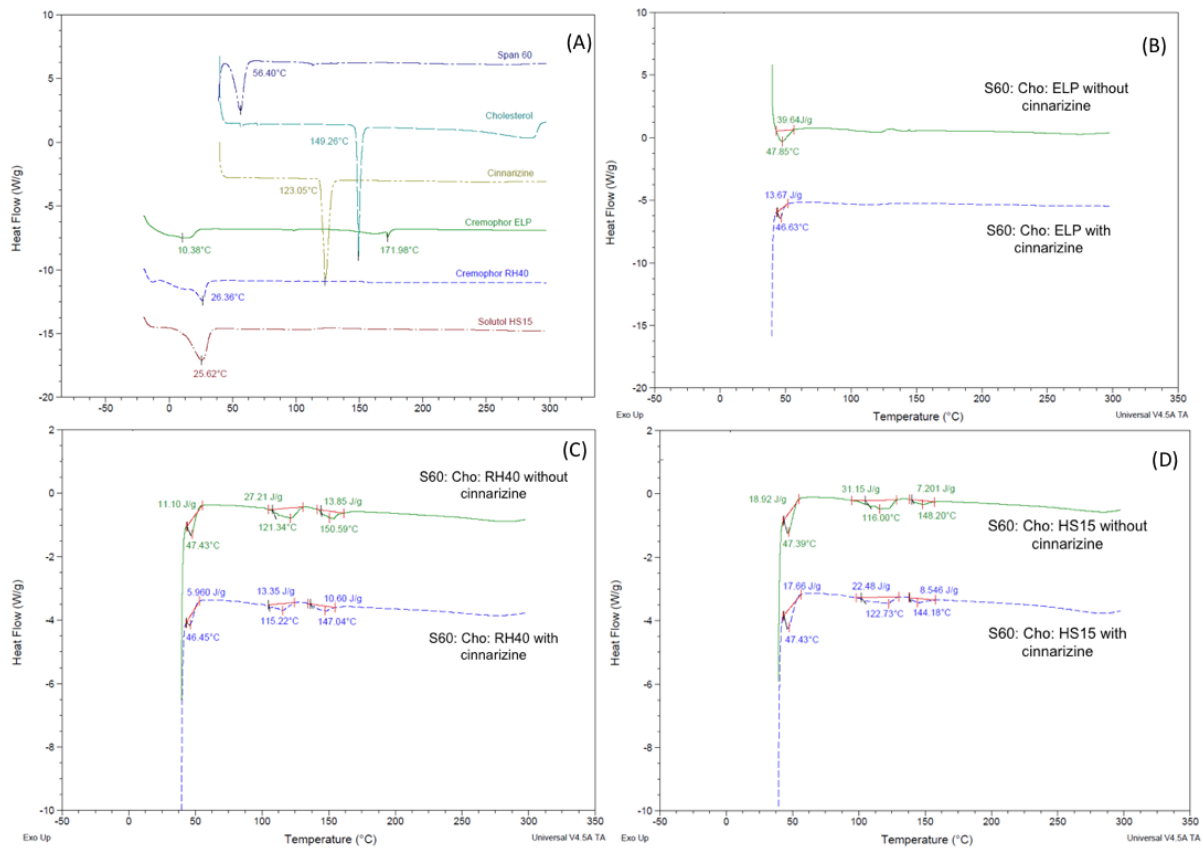


Figure 4-9: DSC thermograms (heat flow as a function of temperature; exothermic up) for (A) pure raw ingredients of niosome formulation composition; (B) S60: Cho: ELP TFH-niosomes; (C) S60: Chol: RH40 TFH-niosomes; and (D) S60: Cho: HS15 TFH-niosomes.

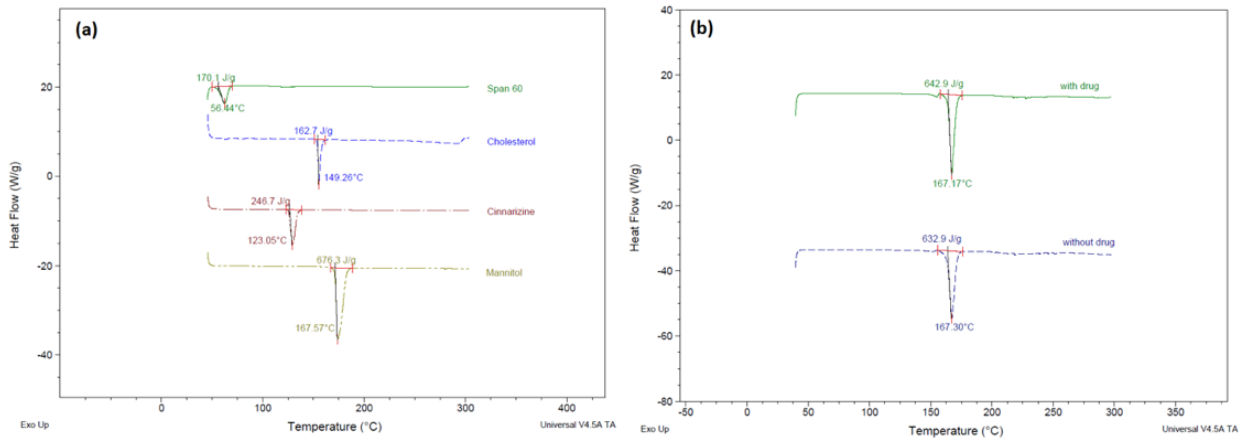


Figure 4-10: DSC thermograms for (a) pure main raw formulation ingredients; and (b) freeze-dried S60: Cho: ELP MF-niosomes with the addition of mannitol as lyoprotectant.

4.3.10. Effect of hydrophilic and hydrophobic drugs loading on niosome characteristics

Vesicle size and drug encapsulation efficiency of TFH-niosomes and MF-niosomes for hydrophobic drug (cinnarizine) and hydrophilic drug (methylene blue) were presented in Table 4-9. Regardless of niosome manufacturing method, the size and distribution of cinnarizine-entrapped niosomes were slightly larger compared to MB-entrapped niosomes. Interestingly, encapsulation efficiency was found to be independent of the vesicle size of niosomes for both hydrophilic and hydrophobic drugs.

It is noteworthy that the encapsulation efficiency of hydrophilic MB into niosomes showed no difference between the two manufacturing methods. This suggests that the influence of manufacturing method on hydrophilic drug encapsulation into niosomes is minimal. As for hydrophobic cinnarizine, two-fold increase in encapsulation efficiency can be seen clearly in the microfluidic-based niosomes compared to thin film hydration method. This can be explained through the difference in mixing between the two manufacturing methods. In bulk method, the extent of mixing during the hydration process of the film could be insufficient and less effective in comparison to the microfluidic method where the efficient mixing occurs between the aqueous phase and miscible organic solvent containing the hydrophobic drug.

Table 4-9: Physicochemical properties of niosomes encapsulated with cinnarizine (CIN) and methylene blue (MB).

Span® 60: cholesterol: Cremophor® ELP niosomes						
Final surfactant/lipid concentration at 20 mg/mL						
Final drug concentration at 0.5 mg/mL						
Preparation method	Size (nm)		PDI		EE%	
	CIN	MB	CIN	MB	CIN	MB
TFH-sonication	477.6 ±	301.1 ±	0.76 ±	0.46 ±	32.1 ±	18.7 ±
	43.2	12.3	0.05	0.12	6.9 **	3.5
MF	182.0 ±	112.6 ±	0.3 ±	0.24 ±	76.6 ±	14.9 ±
	1.0	1.0	0.02	0.01	1.9 * **	1.0 *

Data are expressed as mean ± standard deviation from three independent experiments (n=3).

* and ** show significant difference ($p < 0.05$).

4.4. Conclusion

This chapter demonstrated conventional thin film hydration and microfluidic manufacturing of niosomes to encapsulate cinnarizine as poorly water-soluble drug. Niosome characteristics have been shown influenced by manufacturing methods and formulation compositions. In comparison to bulk method, microfluidic method provides a platform where all required excipient components to mix effectively and efficiently within a single-phase system. Interactions between drug and excipients were analysed through their physical and thermal properties as well as evaluation on niosome vesicle size and encapsulation efficiency. The interactions within manufactured niosome vesicles contributed to the slow release of cinnarizine in the simulated gastric fluid. Further drug absorption enhancement via mucoadhesion is followed in the next chapter focusing on the incorporation of mucoadhesive biopolymers to prolong gastric retention for drug absorption.

Paper relating to this chapter:

Yeo, L.K., Olusanya, T.O.B., Chaw, C.S. and Elkordy, A.A. (2018) Brief effect of a small hydrophobic drug (cinnarizine) on the physicochemical characterisation of niosomes produced by thin-film hydration and microfluidic methods. *Pharmaceutics*, 10(4):185.

Chapter Five:

5. Mucoadhesion study

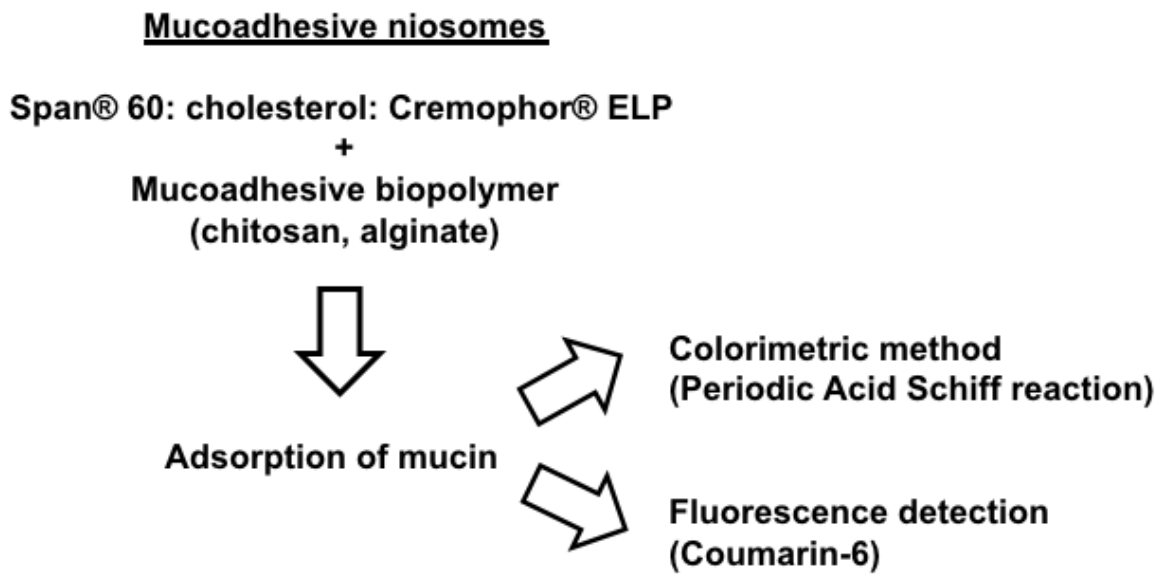


Figure 5-1: Graphical abstract for mucoadhesion study.

5.1. Overview

Mucoadhesion is the interaction between the drug carrier and the mucus gel layer on mucosa surfaces, where the dosage form can release drug slowly at a specific site of absorption for over a prolonged period. Mucoadhesion shows a promising approach in increasing the retention of orally administered dosage forms in the gastrointestinal tract for increased absorption and oral bioavailability (Peppas et al., 2009). Adherence to the mucosal surface allows for delayed transit time and localised the drug to the absorptive surfaces (Dhawan et al., 2004; George and Abraham, 2006).

This approach enables maximal absorption for drugs with a narrow absorption window, by overcoming the challenge of a short transit of the therapeutic formulation in the dynamic physiological environment within the gastrointestinal tract. This is particularly noteworthy for weakly basic drugs as they generally show poor oral bioavailability due to erratic absorption owing to their poor solubilities in the gastrointestinal tract. Weakly basic drugs generally exhibit high gastric solubility, and then a rapid decrease in drug solubility that results in drug precipitation following the gastric emptying to the intestinal fluid in the gastrointestinal tract (Zheng et al., 2020). With a decrease in the gastrointestinal transit rate of the drug delivery system by attachment to the mucosal layer, thereby increasing the overall time for drug absorption to occur (MacAdam, 1993). In addition, the mucoadhesive drug delivery system helps to improve formulation stability to allow the encapsulated drug to remain solubilised for improved drug dissolution and oral absorption (Ibrahim et al., 2019).

As oral administration remains the most preferred and convenient route of taking medication, it is important to overcome factors that limit oral bioavailability. Besides

the physiological and physicochemical properties that affect drug absorption, drug dissolution and gastrointestinal permeability are the critical parameters controlling the rate and extent of drug absorption upon oral administration. Orally administered dosage forms must be firstly solubilised in the gastrointestinal tract for the process of absorption to the systemic circulation. Drug solubilised in the colloidal phases has been reported to be more readily available for absorption and favours *in vivo* drug exposure (Sassene et al., 2015). In addition to increased solubilisation, encapsulation of poorly water-soluble drugs into the bilayer of niosomes offers drug protection from degradation and controls its pharmacokinetic profile to improve its therapeutic efficacy. Similarly, an improved oral bioavailability of alendronate has been shown in a study of mucoadhesive liposomal delivery system (Han et al., 2012).

The mucosal lining of the gastrointestinal tract covered by a viscous layer of mucus that consists of mucin glycoproteins, lipids and mostly water. Generally, mucin aggregates are formed through hydrophobic interactions between non-polar groups, hydrogen bonding between sugar units, and disulphide bonding between cysteine residues (Sogias et al., 2008). Mucins are negatively charged glycoproteins due to the presence of anionic sulfonic, sialic acids and ester sulphates. These physiological properties contribute to the nature of interactions between mucoadhesive biopolymers and mucin macromolecules within the mucosal layer at a molecular level. Main mucosal binding mechanisms include ionic and electrostatic interactions between the anionic mucus matrix components and a cationic biopolymer (Han et al., 2012). This can be seen in the chitosan-mucus interaction that leads to the formation of a viscous gel, which reduces the mucus clearance and increases the residence time of the drug in the mucosal absorption site for increased bioavailability (Jain et al., 2006; Prego et

al., 2005; Sogias et al., 2008). Furthermore, the stability of chitosan-coated nanoparticle was demonstrated based on the nanoparticle structure and previous study showed protection on entrapped drug in the simulated gastric fluid, preventing leakage of entrapped drug on exposure to highly acidic environment (Filipović-Grcić et al., 2001).

As mucous gels consist of gel-forming mucin and other non-mucin components, these non-mucin components can inhibit gel formation and affect the rheological properties of mucous gels (Pearson et al., 2000). Nevertheless, solution viscosity measurement can be useful to investigate the interactions between mucin solution with compounds for their mucoadhesive properties. If the mucin interacts with a polymer, mixtures of mucin-polymer would be expected to show synergism in which the specific viscosity of mucin/polymer increases in a concentration-dependent manner over and above the sums of the specific viscosity of the individual components (Rossi et al., 1995). The bio-adhesion bond strength between different biopolymer types with mucin were quantified by the viscometric method to evaluate the interactions between bio-adhesive polymers and mucin dispersion (Hassan and Gallo, 1990).

The understanding of mucin-polymer interactions within the physiological environment is essential. Besides the nature of interactions between biopolymer and mucin, the effective mucoadhesion of a polymer can be influenced by factors such as molecular weight, density of crosslinking, hydration level, and interaction with environment (variable physiological pH). Biopolymers such as chitosan and alginate have been studied for oral sustained release dosage forms, owing to their biodegradable, biocompatible and mucoadhesive properties (Sarmiento et al., 2007).

Chitosan is a cationic polysaccharide that is soluble in acidic medium with a mucoadhesive property (Sonia and Sharma, 2011). Moghassemi et al. (2015) reported the capability of chitosan as absorption enhancer that facilitated the paracellular transport of insulin-entrapped niosomes through an intestinal model, revealing sustained and controlled release pattern. Adsorption process is expected to be dominated by electrostatic interaction between cationic chitosan polymer and the anionic sulfonic and sialic acid residues within the mucus matrix (Han, Shin and Ha, 2012).

Alginate is an anionic linear polysaccharide comprises of binary copolymer mannuronic acid (M) and guluronic acid (G) residues. Sodium alginate precipitates and forms an insoluble gel form in the present of stomach acid. As a result, a hydrocolloidal layer of high viscosity is formed due to gelation and raft forming properties of alginate (Essa et al., 2021).

Here, the work in this chapter describes and explores the utilisation of biopolymers with niosomes (nanocarriers) as a mucoadhesive approach in order to increase the retention of the nanocarriers within the gastric environment for a sustained release of encapsulated drug. The zeta potential of mucoadhesive biopolymer coated niosomes were measured to evaluate their interactions with mucin dispersions. Adsorption of mucin on mucoadhesive niosomes and the adsorption of mucoadhesive niosome formulation onto gastric mucosa surface were investigated using colorimetric and fluorescence approaches, respectively. Periodic acid-Schiff (PAS) was employed as colorimetric assay to determine mucin concentrations. Fluorescence assay was

applied to measure the content of the entrapped fluorescent coumarin-6 within biopolymer-coated niosomes adhered to mucosa surfaces.

The instabilities of vesicular formulations in aqueous dispersion are mainly due to chemical (e.g. oxidation and hydrolysis) and physical (aggregation, precipitation and phase separation) degradation, resulting in shorter product half-life and loss of efficacy for the intended performance. Dehydration of nanoparticulate dispersions have been studied in order to improve the formulation products with prolonged shelf life and expected efficacy upon administration (Trenkenschuh and Friess, 2021).

5.2. Aim and Objectives

This chapter aimed to explore the use of mucoadhesive biopolymers for preparation of mucoadhesive niosomes delivery system to encapsulate poorly water-soluble drug e.g. cinnarizine, for an extended drug release at its site of absorption in the stomach. This work focused on two biopolymers: (1) chitosan of different molecular weights (low molecular weight and highly viscous) and (2) alginate suspension.

To achieve this purpose, the main objectives were to:

- Determine the bulk fluid behaviour and intermolecular interactions of mucoadhesive biopolymers through measurement of their viscosities using a direct indicating viscometer.
- Characterise and evaluate the influence of different mucoadhesive biopolymers on the physicochemical properties of mucoadhesive niosomes and their mucoadhesive properties between mucin and coated niosomes.
- Assessment of mucoadhesion by measuring and quantifying free mucin after adsorption process of mucin on niosomes.
- Investigate and understand the mucoadhesion interactions between gastric mucosal surface and mucoadhesive biopolymer coated niosome suspension.

5.3. Results and Discussion

5.3.1. Bulk behaviour of mucoadhesive biopolymer solution: viscosity

In order to determine the bulk fluid behaviour of mucoadhesive biopolymers, their viscosities were assessed by viscometric method using a direct indicating Brookfield viscometer. This bulk rheological measurement helps to provide mechanical information and also the nature of intermolecular interactions of mucoadhesive biopolymers involved in this work.

All biopolymer dispersions (chitosan and alginate) used in this study exhibits non-Newtonian fluid properties (flow curves shown in Figure 5-3). All data obtained were best fitted to Herschel Bulkley rheological model to calculate the rheological parameters directly for interpreting rheological properties. Based on the non-linear model, measured viscosities were calculated from the lowest (low molecular weight chitosan) to the highest viscosity (alginate suspension) (Table 5-1). Overall, all three mucoadhesive biopolymer dispersions showed shear thinning behaviour (Figure 5-2) that can be seen in non-Newtonian fluids whose viscosity decreases as the rate of shear increases (Lam and Jefferis, 2014). Herschel-Buckley model relates the shear stress to the shear rate by the equation as follows (Mullineux, 2008):

$$\tau = \tau^0 + K \dot{\gamma}^n \quad \text{Equation 5.1}$$

where τ^0 is the yield stress of the material, K is the consistency factor, and n is the flow behaviour index.

The yield stress was investigated from the linear fitting of the flow curves. Yield stress is a threshold stress to be exceeded for the fluid to flow or deform (Chhabra, 2010).

As low yield stress values were obtained in both low molecular weight and highly viscous chitosan dispersions ($< 0.05 \text{ N/m}^2$), the magnitude of the external yield stress can easily exceed the threshold stress. Both chitosan dispersions exhibited shear-thinning characteristics in which their viscosity decrease with increasing shear where the fluid will show a constant viscosity until a large decrease in viscosity at a critical shear rate (Figure 5-2). On the other hand, the rheological profile for alginate suspension where a hysteresis loop can be seen clearly in which the shear rate was increased at a constant rate from 0 to 45 sec^{-1} (maximum value) and then reduced at the same rate to zero again, presenting thixotropic behaviour. Its viscosity gradually decreased at constant shear rate as the internal structural linkages were broken down with times. It exhibited thixotropic fluid nature that the fluid eventually reaching a dynamic equilibrium state when the rates of break down and rebuild are balanced (Chhabra, 2010).

Flow behaviour index for low molecular weight chitosan dispersion is greater than 1, indicating a dilatant fluid nature, whereas the highly viscous chitosan dispersion exhibited more Newtonian fluid behaviour as its flow index value is closer to 1. As for alginate suspension, flow index revealed a visco-plastic behaviour.

The role of mucin in the gelation of mucus is owing to its viscoelastic properties. The viscosity of mucin increases with decreasing pH from 7 (solution state) to 2 (gel state) as a result of molecular conformational change and aggregation of the mucin (Bansil et al., 1996). This is due to more interactions as the hydrophobic interior of the mucin molecule opens up at acidic pH and forming aggregates through intermolecular interactions.

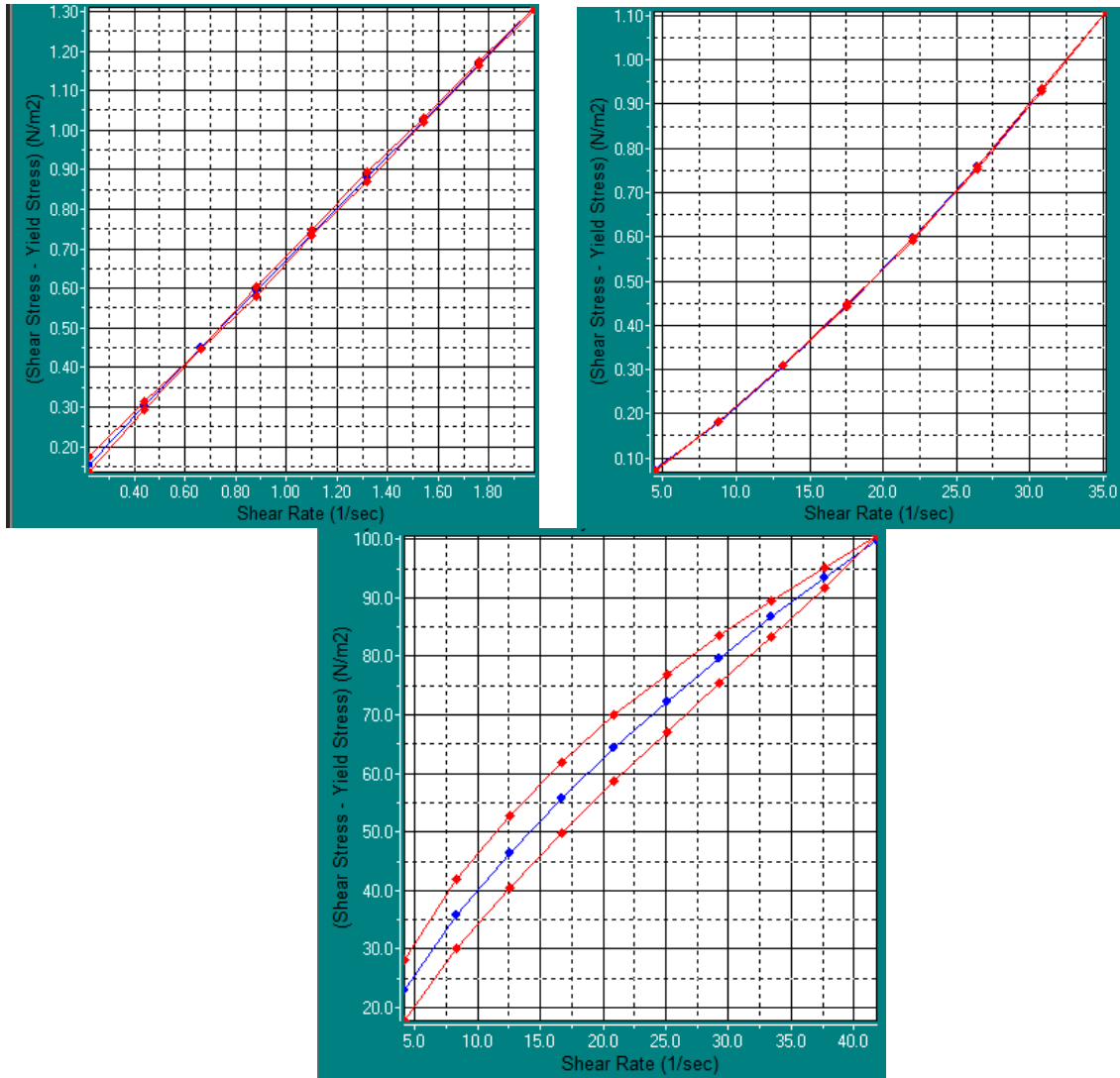


Figure 5-2: Herschel Bulkley flow curves for 0.6 % w/v CS LMW (top left); 1.25 % w/v CS HV (top right); and Gaviscon® alginate suspension (bottom). Raw data shown in red and fitted curve shown in blue.

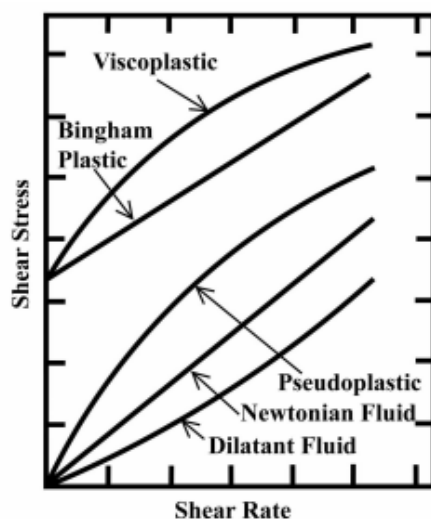


Figure 5-3: Flow curves for different types of non-Newtonian fluid behaviours. (Adapted from Chhabra, 2010).

Table 5-1: Rheological data of mucoadhesive biopolymer dispersions based on Hershel Bulkley model ($n = 3 \pm SD$).

Biopolymer ^a	Consistency index ^b	Flow index	Yield stress (N/m ²)	Confidence of fit (%)
CS LMW	10.4 ± 0.3	1.31	0.05	100.0
CS HV	679.7 ± 9.0	0.96	0.00	99.9
GAV alginate	7702.3 ± 1384.2	0.68	6.64	98.4

^a CS LMW (1.25 %w/v chitosan low molecular weight); CS HV (0.6% w/v chitosan highly viscous); GAV (Gaviscon® alginate suspension).

^b Consistency index is numerically equal to viscosity (mPa.s) at shear rate of 1 s⁻¹.

5.3.2. Bulk behaviour: Influence of the mucoadhesive biopolymer on zeta potential of mucin dispersion and manufactured niosomes

The extent of drug binding to mucin was evaluated in binding studies performed by diafiltration method (Bhat, Flanagan and Donovan, 1996). The authors reported a low magnitude of binding constants between drugs and mucins, and concluded that the binding of drugs to gastric mucins is non-specific in nature. However, the binding of

the drug to mucin can reduce the available free drug for absorption which affects bioavailability. On the other hand, several studies investigated the interactions between mucins and polymers (Dhawan et al., 2004; Grießinger et al., 2015; Peppas and Huang, 2004; Rossi et al., 1995). Interactions have been shown to modify the viscoelasticity characteristics of mucus layer and the characteristics of mucoadhesive nanoparticles. It has been reported that a decrease in zeta potential reduced the amount of mucin adsorbed onto the chitosan microspheres (Dhawan et al., 2004). Nevertheless, the interactions can affect the penetration and particle diffusion across the mucus layer, affecting the drug absorption and bioavailability.

Here, mucoadhesive properties of biopolymers and their interactions with mucin, with the incorporation of niosomes were studied and evaluated through zeta potential measurements of the bulk dispersions. Measured data on zeta potential relating to mucoadhesive biopolymers are presented in Table 5-2. Zeta potential measurements were analysed to characterise different mucoadhesive biopolymer types and their interactions with manufactured niosomes and prepared mucin dispersions. These interactions are as follows:

- Mucin-niosome interactions and mucin-biopolymer interactions.
- Biopolymer-niosome interactions.
- Mucin-biopolymer-niosome interactions.

Overall, the interactions between mucoadhesive biopolymer and niosomes can be seen through the changes in zeta potential measurements. There is no difference observed in measured zeta potential values between mucin dispersions and mucin-niosome mixtures (M1), both samples were given negative zeta potential values.

However, a significant change in zeta potential is observed for mucin-niosome mixtures (M1) and mucin-mucoadhesive niosome mixtures (M2 and M3), both showing a higher magnitude of positive and negative charges respectively. This can be explained due to the nature of positively charged chitosan and negatively charge alginate. It is observed that within the same biopolymer type (chitosan in M2 and M4), interactions between mixture components resulted in significant difference in zeta potentials, owing to the non-specific interaction that involves a physical entanglement between the mucin and chitosan (Rinaldi et al., 2020).

The presence of mucin in mucin-alginate-niosome (M3) showed a highly negative charge when compared to alginate-niosome mixture (M5). This synergistic effect on negative charge of mucin and alginate system could be due to more exposure of the negatively charged groups. This suggests that less interaction occurred between mucin and alginate owing to similar charges. Nonetheless, numerous studies reported that the polyelectrolyte nature alginate presents both mucoadhesion and floating mechanisms for oral drug delivery as a floating gastro-retentive in situ gelling (raft forming) system (Essa et al., 2021).

Table 5-2: Zeta potential measurement data of mucin dispersion (1 mg/mL), mucin-biopolymer mixtures and biopolymer-niosomes suspensions at pH 4.5. Preparation details shown in Section 2-5.

Composition	Zeta potential (mV)	
	no niosomes	with niosomes
Mucin dispersion (M1)	-7.16 ± 2.44	-7.37 ± 0.59** ***
Mucin: Chitosan (M2)	15.87 ± 6.55*	8.82 ± 0.82* **
Mucin: Alginate (M3)	-21.80 ± 0.61	-27.87 ± 0.50** *** ****
Chitosan (M4)	11.70 ± 3.02	14.43 ± 2.48***
Alginate (M5)	-32.07 ± 1.27*	-9.05 ± 2.07* ****
No mucin, no polymer	--	-2.85 ± 1.29

Data are expressed as mean ± standard deviation from triplicate experiments (n=3).
 * significantly different ($p < 0.05$) in the presence of niosomes of the same biopolymer.
 ** significantly different ($p < 0.05$) in the presence of niosomes with mucoadhesive biopolymers.
 *** significantly different ($p < 0.05$) between mucin-niosome and chitosan-niosome; between mucin-niosome and mucin-alginate-niosome.
 **** significantly different ($p < 0.05$) between mucin-alginate-niosome and alginate-niosome.

5.3.3. Adsorption of mucin on manufactured mucoadhesive niosomes

Mucin glycoproteins are the gel-forming component of mucus that are secreted from epithelial cells covering all mucosal surfaces. Despite only accounting for less than 3 % of mucin molecules in the mucus layer, these glycoproteins are crucial components of the mucus that are comprised of block copolymers with branched and unbranched chain residues in the protein backbone (Peppas and Huang, 2004). Therefore, it is important to understand and determine the adsorption interactions of mucin-niosomes for the assessment of mucoadhesion. In order to investigate the mucoadhesive properties of mucoadhesive niosomes, mucin adsorption (binding efficiency) was determined by quantifying the concentration of free mucin in the supernatant, after an incubation process with uncoated and biopolymer-coated formulations and followed by centrifugation process (Section 2.5.1.). The quantification of free mucin available

was based on the Periodic-Acid Schiff (PAS) colorimetric method (Section 2.2.3.3.) (Alam et al., 2016; Mantle and Allen, 1978).

Following a maximum absorbance at 555 nm obtained using scanning mode by xMark microplate spectrophotometer, the calibration curve of mucin standard dispersions (Figure 5-4) was generated by using a spectrophotometer, and used for quantification of free mucin in the supernatant before calculating the mucin binding efficiency (%) using the mucin adsorption equation (Equation 2.6 in Section 2.5.1.).

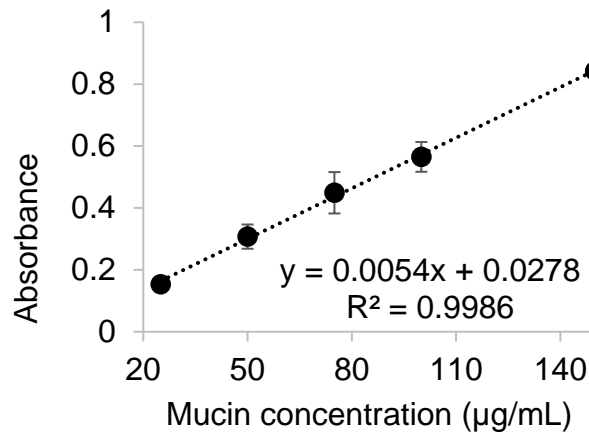


Figure 5-4: Calibration of mucin standard dispersions (25 to 150 µg/mL) using PAS colorimetric method (colourless to magenta) by ultraviolet spectrophotometer at 555 nm.

Mucoadhesive properties of different polymer coating on niosomes were evaluated by studying the interactions between mucin solution and biopolymer-niosome suspensions. The interaction was determined by the amount of mucin adsorbed on the coated niosomes through measuring the amount of free mucin after incubation process and then under agitation with the PAS reagent. When only the niosome was present in the suspension with mucin, free mucin detected in the supernatant was less than 45%, revealing interaction between mucin and niosomes (Table 5-3). High mucin

binding efficiencies can be seen in all mucoadhesive niosomes where available free mucins to react with PAS reagent were notably reduced. Those interactions within mucin-polymer-niosomes could be non-specific and physically entangled and precipitated as reported by Rinaldi et al. (2020). This suggests that potential prolonged gastric retention to allow drug absorption in the stomach from the mucoadhesive niosomes.

Table 5-3: Mucin binding efficiency (%) of mucoadhesive niosomes.

Composition ^a	% Mucin binding efficiency ^b
Niosomes (no polymer)	56.4 ± 2.2*
CS LMW niosomes	94.2 ± 0.4*
CS HV niosomes	89.6 ± 0.6*
GAV niosomes	93.2 ± 0.9*

^a CS LMW (1.25 %w/v chitosan low molecular weight); CS HV (0.6% w/v chitosan highly viscous); GAV (Gaviscon® alginate suspension).

^b Expressed in mean ± standard deviation from triplicate experiments (n=3).

*significantly different (p < 0.05) between niosomes with no polymer and polymer-niosome suspensions.

5.3.4. Adsorption of mucoadhesive niosomes on gastric mucosa

The characteristics of coumarin-6 entrapped niosomes manufactured by using microfluidic method were shown in Table 5-4. Subsequently, niosomes were incorporated with mucoadhesive biopolymers (chitosan and alginate) according to Section 2.5. to produce mucoadhesive niosomes. The interactions between mucoadhesive niosomes and gastric mucosal surface were investigated to assess and evaluate the mucoadhesive properties of mucoadhesive niosomes by an *in vitro* wash-off method (Beri et al., 2013). Mucoadhesive niosomes were entrapped with coumarin-6 as fluorescent agent. By using HPLC with fluorescence detection technique, coumarin-6 calibration curve was generated and the amount of coumarin-6 was calculated at predetermined time intervals over a six-hour period from the *in vitro* gastric mucosa surfaces.

Table 5-4: Summary of the physicochemical properties of microfluidic-based niosomes (without and with coumarin-6 entrapped). Niosome formulation studied was comprised of Span® 60: cholesterol: Cremophor® ELP.

Niosomes	Size (nm)		Zeta potential (mV)	EE (calculated loaded concentration, µg/mL)
	Before filtration (PDI)	After filtration (PDI)		
No drug	322.8 ± 10.4 (0.2 ± 0.09)	192.3 ± 2.1 (0.2 ± 0.07)	-2.79 ± 0.29	--
C-6	321.9 ± 6.3 (0.2 ± 0.10)	199.7 ± 1.2 (0.2 ± 0.09)	-2.85 ± 1.29	8.13 ± 3.56 % (1.6 ± 0.7 µg/mL)

All were expressed in mean ± standard deviation from triplicate experiments (n=3).

Coumarin-6 calibration HPLC with fluorescence detection

By using high-performance liquid chromatography (HPLC) with fluorescence and ultraviolet detection modes, coumarin-6 was detected at 5.2 min and 5 min, respectively (Figure 5-5). Calibration plot for coumarin-6 was generated with a linear equation shows $y = 8.3462x + 9.9611$ and a linear regression coefficient of 0.9705 (Figure 5-6).

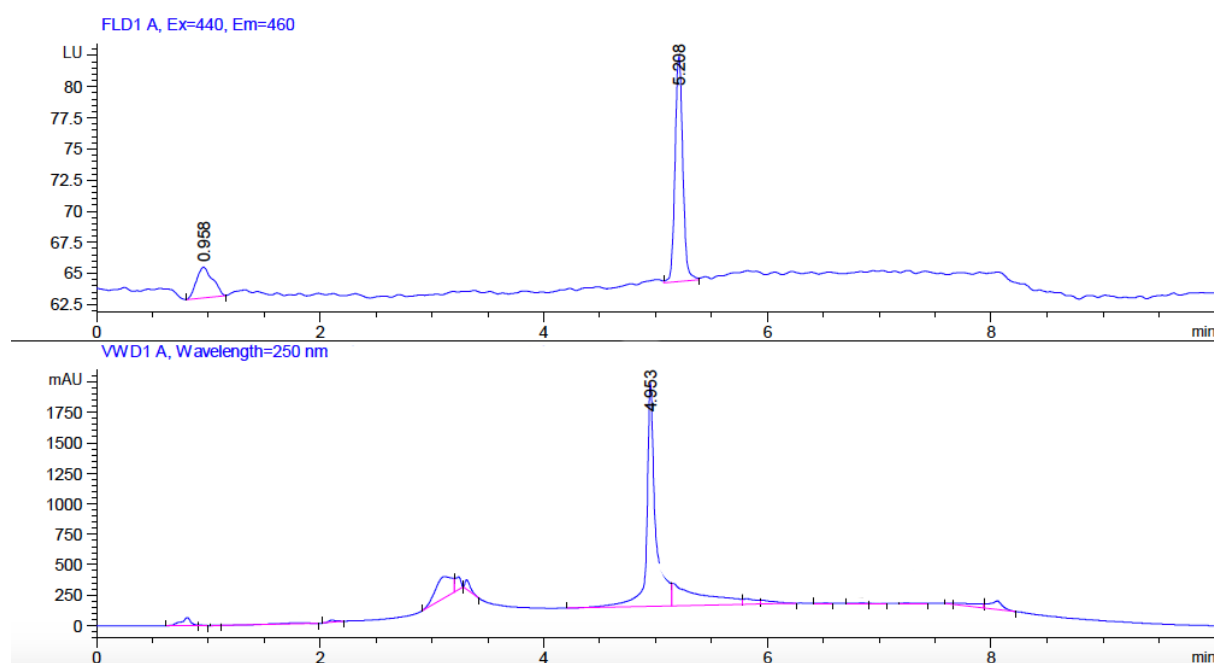


Figure 5-5: Chromatogram of coumarin-6 (10 µg/mL) detected at 5.2 min (fluorescence detection: excitation wavelength at 440 nm and emission wavelength at 460 nm, top) and at 5 min (ultraviolet detection: wavelength at 250 nm, bottom).

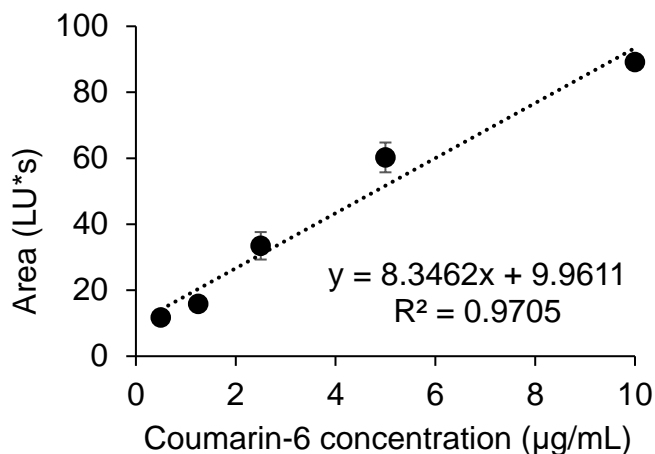


Figure 5-6: Calibration plot for coumarin-6 standard concentration (0.5 to 10 µg/mL) based on fluorescence detection. (Luminescence unit per second, LU*s)

Recovery analysis of coumarin-6

Recovery analysis on coumarin-6 entrapped mucoadhesive niosomes by HPLC with fluorescence detection was performed at pre-determined intervals over a six-hour period. This was taken into consideration that the mucus clearance mechanism in the gastro-intestinal tract usually occurs within 1 to 4 hours turnover time (Murgia et al., 2018). Quantification of coumarin-6 entrapped in microfluidic-based mucoadhesive niosomes were recovered from gastric mucosa surfaces treated with the mucoadhesive niosomes and wash-off method. Untreated mucosa (without niosome was used as a negative control – no coumarin-6 and no mucoadhesive polymer), treated mucosa with empty mucoadhesive niosomes (no coumarin-6 entrapped) and treated mucosa with non-mucoadhesive niosomes (no mucoadhesive polymer) were used to compare with mucoadhesive niosomes (Uthaiwat et al., 2021).

Figure 5-7 shows the percentage recovery of coumarin-6 of mucoadhesive niosomes on gastric mucosa surface over six hours period. It is important to note that all

percentage recoveries of coumarin-6 on gastric mucosa were supported by the percentage recoveries of coumarin-6 in the simulated gastric fluid (SGF) where the gastric mucosa tissue specimens immersed in. Notably, the decrease in percentage recovery of coumarin-6 from 1.5 hours onwards suggested more niosomes were in the SGF than adsorbed onto gastric mucosa surface for niosomes without mucoadhesive coat. This can be explained that niosome without biopolymer incorporation had less interaction with mucosa surface and therefore less adsorption onto gastric mucosa. In contrast, when the niosomes incorporated with mucoadhesive biopolymers (chitosan and alginate), there were strong interactions and more adsorption onto gastric mucosa, as shown with high percentage recoveries, which means almost complete recovery of coumarin-6 throughout the six-hour period.

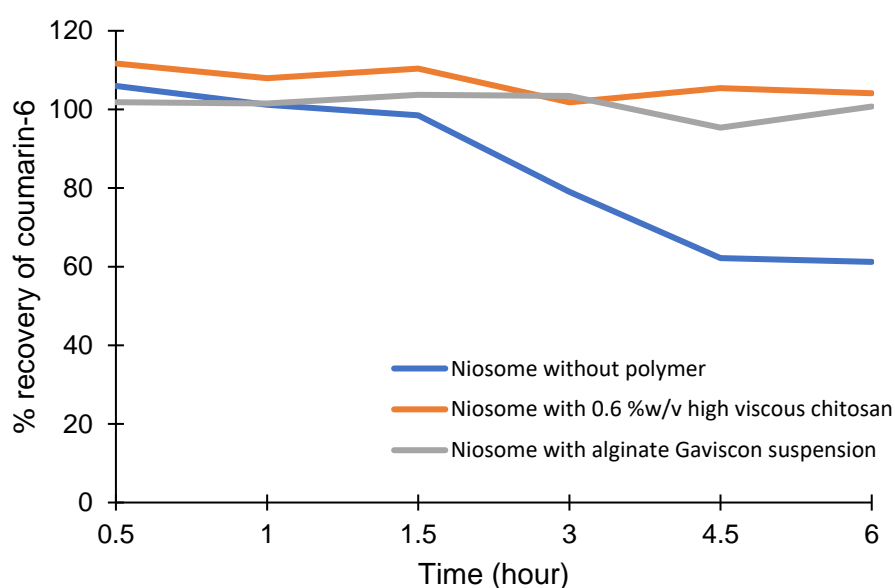


Figure 5-7: Percentage recovery of coumarin-6 at predetermined time intervals. Plot showed average of percentage of coumarin-6 recovered from two independent batches.

5.4. Conclusion

Mucoadhesion has been a promising approach in drug delivery system to essentially enhance drug absorption by prolonging mucosal adherence time to allow prolonged contact of vesicles with epithelia and retention in the gastrointestinal site of absorption. Subsequently enhancing opportunities for oral absorption of either the vesicles or the payloads.

This chapter provides the bulk properties of mucoadhesive polymer dispersions through rheological measurements for a better understanding on intermolecular interactions with biopolymer dispersion potentially acts as bulking agent in the oral formulation of niosome suspension. Within this chapter, the mucin interactions with mucoadhesive biopolymers and niosomes were studied through zeta potential measurements.

While the interaction with mucus layer is important as absorption enhancement approach, binding to the mucus (via mucoadhesion) in the hope to allow sustained release of drug for absorption, does not necessarily mean all drug is in its free form available for drug absorption and get fully absorbed. Despite of this, it is important to explore and understand the all possible interactions of mucins, biopolymers and drug nanocarriers. Ultimately better promote understanding on gastro-retention and developability of dosage forms.

Chapter Six: Recovery study

6. Recovery study

6.1. Overview

Given that the formulation composition in nanoparticulate systems is crucial for their characteristics, quantification of formulation composition component is a key indicative feature. Previous studies have demonstrated rapid and effective quantification of lipid concentration within drug-free liposomes (Roces, 2016), protein-loaded liposomes (Forbes et al., 2019), and protein-loaded nanoparticles (Roces, 2020). However, niosome formulations manufactured by using microfluidic mixing method as a bottom-up manufacturing approach, have not been investigated for the correlation between their formulation components and the advanced manufacturing method.

In order to determine the niosomes' outcome, it is important to assess the reproducibility and consistency on the manufacturing method of niosomes. This chapter focuses on the formulation component recovery of the microfluidic-based niosomes. Using modified high performance liquid chromatography-evaporative light scattering detection (HPLC-ELSD) method (Roces et al., 2016), the quantification of the surfactant/lipid content within microfluidic-based niosomes was performed. Main formulation components of niosomes in this study were non-ionic surfactant (Span® 60) and lipid (cholesterol). The method allows separation of surfactant/lipid mixture that dissolved in organic solvent for direct detection of these non-volatile compounds regardless of their functional groups that are lacking ultraviolet chromophores. Owing to the measurement of scattered light, the detector response is independent from the optical properties (ultraviolet absorption) of the compounds. In addition, the HPLC-ELSD method offers high sensitivity and minimal effect on the baseline stability regardless of rapid changes in eluent composition in gradient elution.

Operational principle of ELSD (Agilent ELSD manual):

Evaporative light scattering detector allows direct detection of all non-volatile compounds regardless of their functional group or chromophore because the principle of operation is based on measurement of scattered light and has been found useful as a detector in structure determination of compounds with poor UV chromophores. The mobile phase from the column is nebulised and passed through a beam of light. Any particles within the sample that are not volatilised will pass through the beam, and the resulting scattered light is detected. Volatile components are not detected, and quantification requires attention as response curves may not be linear. However, it is sensitive and can be used under gradient elution and for non-UV components.

Nebulisation: Inlet eluent stream passes through the heated nebuliser and is mixed with the incoming nebuliser gas stream. The mixed stream is then dispersed uniformly as nebulised droplets passing into the evaporator section.

Evaporation: As nebulised droplets travelled through the evaporation section, the solvent is evaporated leaving a stream of dry particles (analyte).

Detection: Light is passed through the instrument at right angles to the direction of particle flow. In the optical chamber, the mist of solute particles passes through the light path scatter light to a photosensitive device. The signal is amplified and a voltage output provides the concentration of the solute particles passing through the light in real time.

6.2. Aim and Objectives

Microfluidics was assessed as a bottom-up manufacturing method for niosomes to better understand the correlation between microfluidics as manufacturing method, and the manufactured niosome outcome and characteristics.

To achieve this aim, the main objectives of this chapter were to:

- Demonstrate the modified HPLC-ELSD method in the recovery and quantification of formulation components of microfluidic-based niosomes.
- Investigate the influence of the presence of small molecule drug (cinnarizine) in the lipid mixture on the lipid analysis using the modified HPLC-ELSD method.
- Investigate the influence of the presence of hydrophilic co-surfactant (Cremophor® ELP) in the lipid mixture on the lipid analysis using the modified HPLC-ELSD method.
- Investigate the effect of gel chromatography as purification method on the physicochemical properties of microfluidic-based niosomes.
- Evaluate the effect of ethanol dilution on microfluidic-based niosomes.

6.3. Results and Discussion

In order to demonstrate the separation, identification, and quantification of lipid components by using modified HPLC-ELSD method, each individual lipid compound and lipid mixtures of known concentration were firstly dissolved in organic solvent (Section 2.6.2.) to be injected independently into the system. The total surfactant/lipid concentration of niosome component prepared was 2 mg/mL and the concentration of each component prepared was 1 mg/mL individually, and combined as a surfactant/lipid mixture (Section 2.6.2.). Of these, Figure 6-1 shows distinctive individual elution peaks of the known surfactant/lipid mixture comprising Span® 60 (sorbitan stearate), cholesterol, glyceryl monostearate (GMS), and dipalmitoyl phosphatidylcholine (DPPC) in a tandem arrangement, established by using the modified HPLC-ELSD method from Roces et al. (2016).

In Figure 6-1, the order of elution can be seen with retention times at 6 min for GMS, 10 min for cholesterol, and 11 min for DPPC, respectively. These distinctive elution peaks were well separated and showed high and sharp peaks. All components from the surfactant/lipid mixture were shown to be eluted within 15 min analysis time. Interestingly, it is clear that Span® 60 was close to being not detected in the same run as with the other three lipids (GMS, cholesterol, and DPPC) that were also presented in the surfactant/lipid mixture. This suggested that the presence of other lipid compounds might affect the detection sensitivity of Span® 60 due to the interaction with other lipid compounds within the lipid mixture. It is important to understand the influence of potential interactions as it could affect the feasibility of using the HPLC-ELSD method for quantification of each composition component within a formulation mixture. Furthermore, it is worth noting that verification of each lipid compound

recovery on the employed HPLC-ELSD method without initial lipid extraction prior to measurements, was carried out by verifying concentrations of lipid at ratios defined prior to formulation preparation (Section 6.3.3.).

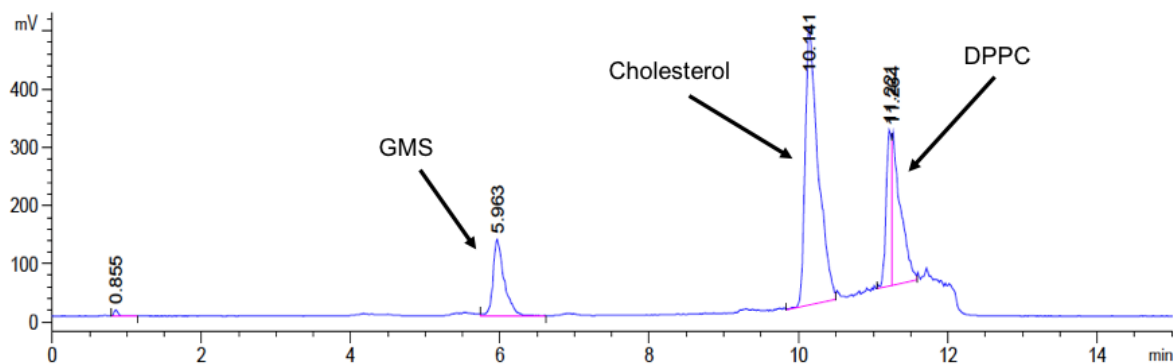


Figure 6-1: Chromatogram showing distinctive peaks for glyceryl monostearate (GMS), cholesterol, and dipalmitoyl phosphatidylcholine (DPPC). Response of detection measured in voltage (mV) for 15 min run time.

In order to demonstrate the detectability of Span® 60 by using the method, a range of Span® 60 standard solutions (from 0.1 to 2.0 mg/mL) were run independently (n=3) to construct a calibration plot for linearity assessment and evaluation (Section 6.3.1.). After taking account of the blank chromatogram, the response peaks obtained on the chromatogram for Span® 60 standard were shown in Figure 6-2, in which three response peaks were clearly shown with good resolution. These obtained peaks can be explained owing to the fact that Span® 60 (sorbitan stearate) is comprised of fatty acid fractions at approximately equal stearic acid (C18:0) and palmitic acid (C16:0).

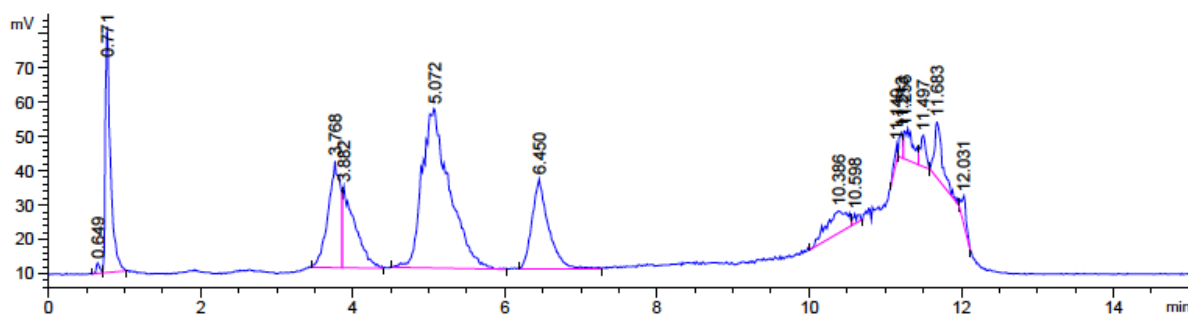


Figure 6-2: Chromatogram of Span® 60 standard at (concentration 2.0 mg/mL) showing three response peaks (retention times at 3.8 min, 5.1 min, and 6.5 min).

On the other hand, a single elution peak for cholesterol can be seen using cholesterol standard solution at 1.0 mg/mL concentration (Figure 6-3). As cholesterol was used as main component alongside Span® 60 at equimolar composition in this work to manufacture niosomes, the surfactant/lipid mixture of cholesterol and Span® 60 was eluted and analysed for the detectability of both components using the modified method. Both Span® 60 and cholesterol were separated and detected (Figure 6-4) using the modified method for quantification. At equimolar composition, the peak responses obtained for Span® 60 were noticeably insignificant alongside the distinctive sharp cholesterol peak at 10 min. Therefore, it is important to construct and utilise the cholesterol calibration curve for linearity assessment and evaluation (Section 6.3.2.).

Despite the low detection sensitivity for Span® 60, this work clearly demonstrated that the employed HPLC-ELSD method is applicable for use in separation, identification and quantification of individual formulation component used to manufacture niosomes. Other than component recovery, niosome formulation recovery was assessed using the HPLC-ELSD method (Section 6.3.6.) to study the effect of gel purification on

microfluidic-based niosomes. All percentage recovery calculations were based on the found and theoretical concentrations of analyte (Equation 6.1).

$$\text{Recovery (\%)} = \frac{\text{Found concentration } \left(\frac{\text{mg}}{\text{mL}}\right)}{\text{Theoretical concentration } \left(\frac{\text{mg}}{\text{mL}}\right)} \times 100 \quad \text{Equation 6.1}$$

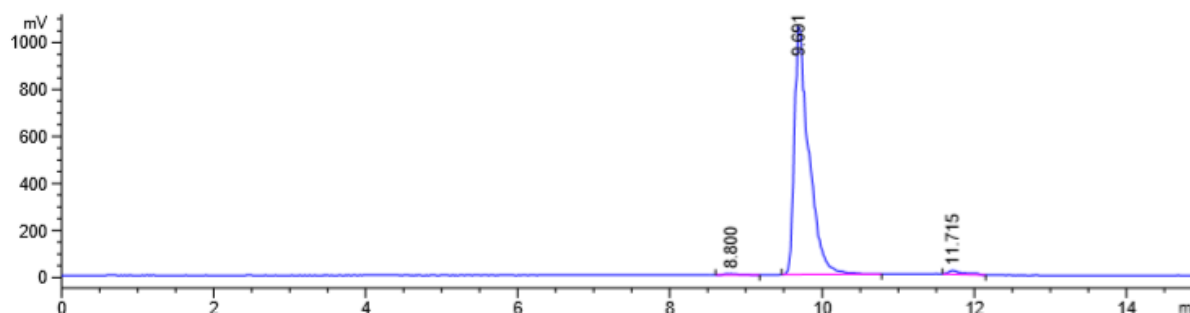


Figure 6-3: Chromatogram of cholesterol standard at 1.0 mg/mL.

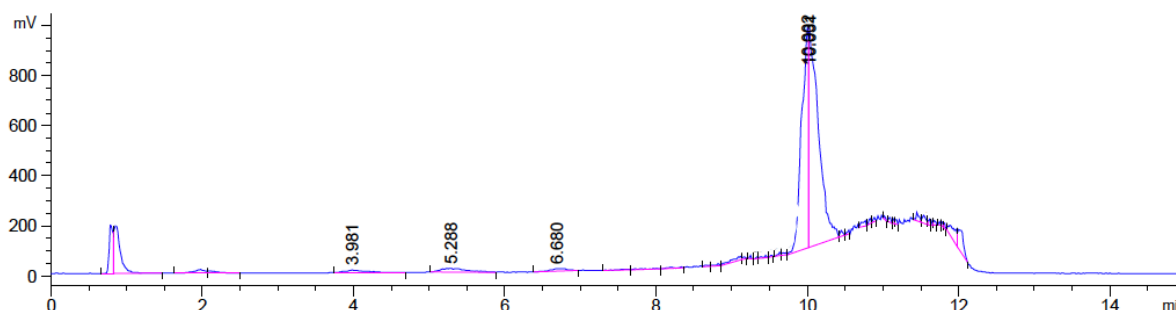


Figure 6-4: Chromatogram showing distinctive peaks for Span® 60 (retention times at 3.9 min, 5.2 min, and 6.6 min) and cholesterol (retention time at 10 min). Equimolar composition of Span® 60 and cholesterol was used (total lipid content at 2.0 mg/mL). Molecular mass of Span® 60 is 430.62 g/mol and molecular mass of cholesterol is 386.65 g/mol.

6.3.1. Span® 60 calibration

Based on Figure 6-2, the total responses from the three peaks obtained for Span® 60 were used as the peak area for calibration plot (Figure 6-5) owing to its fatty acid composition distributions. This is in agreement with previous studies on the

quantification determination of the distribution of sorbitan esters of fatty acids where the separation of individual sorbitan mono-, di- and tri-ester fractions was achieved with good resolution by using reversed phase liquid chromatography (Wang and Fingas, 1994a, 1994b). Despite this, accurate and reliable quantification of the non-ionic surfactant is a big challenge due to the nature of Span® 60 that comprised of different fatty acid compositions.

In order to quantify the non-ionic surfactant, calibration curve of calculated mean and standard deviation of peak responses for each known concentration of Span® 60 (0.1 to 2.0 mg/mL) was plotted for linearity assessment. Linear response factor was achieved due to the fact that ELSD technique is independent of molecular weight of the non-volatile analyte (Bear, 1988). Equation generated was $y = 984.46x - 148.06$, with a linear regression coefficient of 0.9777 (Figure 6-5). Table 6-1 outlines the percentage of relative standard deviation (%RSD) and recovery for Span® 60 standard solutions (n=3). Overall, the %RSD was found within acceptable values at less than 10 % and percentage recovery ranging from 90 – 110 % (Shabir, 2005), showing good reproducibility across the three concentrations investigated (0.5, 1.0 and 1.5 mg/mL).

Table 6-1: Evaluation of %RSD and recovery during calibration of Span® 60.

Concentration standard (mg/mL)	Average found concentration (mg/mL)	%RSD	Recovery (%)
0.5	0.4569	8.4	91.4 ± 7.6
1.0	1.0065	2.8	100.7 ± 2.8
1.5	1.4327	0.2	95.5 ± 0.2

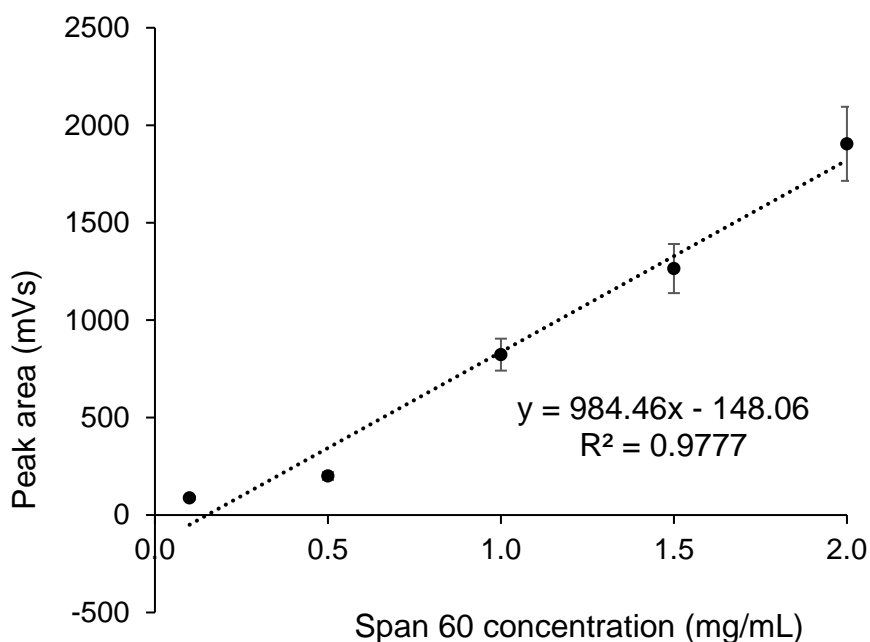


Figure 6-5: Linear calibration plot of Span® 60 standards (0.1 to 2.0 mg/mL) was constructed to quantify Span® 60 concentration.

6.3.2. Cholesterol calibration

At higher cholesterol concentration (above 2.0 mg/mL), overshooting of the elution peak can be seen, therefore respective dilution of the standards (0.05 to 2.0 mg/mL) was used for linearity assessment and for quantification of cholesterol concentration used within niosomes. Mean and standard deviation of peak area for each concentration was calculated and plotted, the resulting calibration plot showed a linear regression coefficient of 0.99 and equation was $y = 14380x - 958.74$ (Figure 6-6). Table 6-2 outlines the %RSD and recovery for cholesterol standard solutions (n=3). For all three cholesterol concentrations, the found %RSD values were within acceptable values of less than 10 % and percentage recovery ranging from 90 – 110 % (Shabir, 2005).

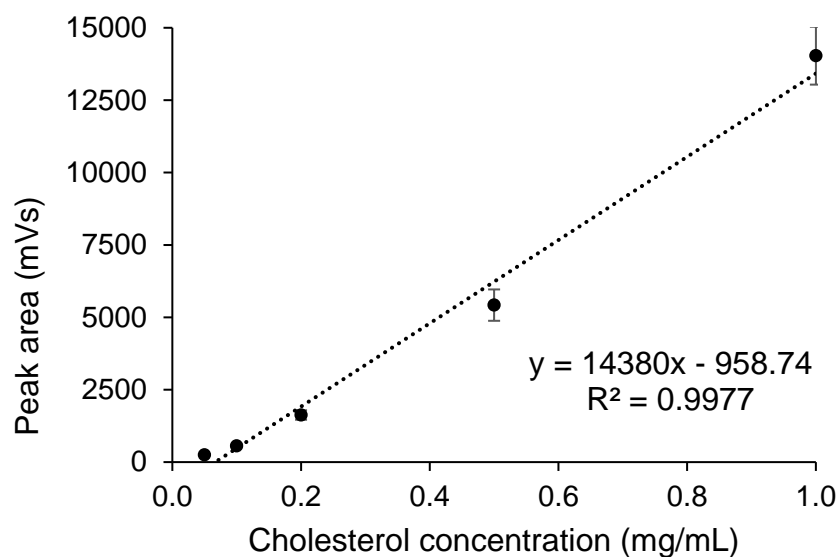


Figure 6-6: Linear calibration plot of cholesterol standards (0.05 to 1.0 mg/mL) was constructed to quantify cholesterol concentration.

Table 6-2: Evaluation of %RSD and recovery of cholesterol during calibration of cholesterol standard solutions.

Concentration standard (mg/mL)	Average found concentration (mg/mL)	%RSD	Recovery (%)
0.5	0.4648	7.2	93.0 ± 6.6
1.0	1.0857	7.2	108.6 ± 7.8
2.0	1.9103	4.1	95.5 ± 3.9

6.3.3. Component recovery: Cholesterol recovery from surfactant/lipid mixture with presence of drug

Well separated peaks of Span® 60 and cholesterol in the lipid mixture can be seen in Figure 6-4. The employed HPLC-ELSD method demonstrates a rapid elution (15 minutes) of individual component (Span® 60 and cholesterol) with sufficient resolution and good efficiency. Cholesterol recovery from the surfactant/lipid mixture composed of Span® 60 and cholesterol were achieved within acceptable range between 90 and

110 % (Shabir, 2005). Independently, the presence of poorly water-soluble drug (cinnarizine) in the Span® 60/cholesterol mixture (drug to surfactant/lipid ratio at 1: 40) showed a lower recovery of cholesterol from the surfactant/lipid mixture in comparison to drug-free surfactant/lipid mixture (Table 6-3). This suggests that the recovery of cholesterol is independent of the presence of the hydrophobic drug used as it did not affect the use of the employed method for quantification.

Table 6-3: Evaluation of %RSD and recovery of cholesterol in the surfactant/lipid mixture of Span® 60 (S60) and cholesterol (CHO) at a total concentration of 2.0 mg/mL. Known drug (cinnarizine) concentration at 0.05 mg/mL.

Mixture composition	CHO known concentration (mg/mL)	Average found concentration (mg/mL)	%RSD	Recovery (%)
S60: CHO drug-free	0.95	1.01	2.31	105.86 ± 19.11
S60: CHO with drug	0.95	0.88	0.44	92.74 ± 3.57

6.3.4. Component recovery: Cholesterol recovery from lipid mixture with presence of Cremophor® ELP as co-surfactant

Low sensitivity in detection of Span® 60 obtained from the surfactant/lipid mixture with Cremophor® ELP was similar to the Span® 60 responses obtained in Figure 6-4. Therefore, the recovery of Span® 60 was omitted. However, the presence of Cremophor® ELP in the S60: CHO mixture has shown an impact on the estimation of cholesterol recovery, showing percentage recovery as high as 140 % (Table 6-4). This might be explained that Cremophor® ELP did not elute separately away from cholesterol, and that contributed to the calculated percentage recovery for cholesterol,

despite the fact that the response retention time for cholesterol remained the same as of the surfactant/lipid mixture without Cremophor® ELP at 10 min. To confirm the possible co-elution of Cremophor® ELP with cholesterol, separation of both components requires a different detection technique such as mass spectrometry in further study.

On the other hand, the presence of hydrophobic drug (cinnarizine) has showed no difference on the recovery of cholesterol from S60: CHO: ELP mixtures. The results revealed that the modified method was unable to separate Cremophor® ELP from cholesterol but eluted at the same time, of the surfactant/lipid mixtures with the presence of Cremophor® ELP regardless of the presence of drug.

Table 6-4: Evaluation of %RSD and recovery of cholesterol in the lipid mixture of Span® 60 (S60, cholesterol (CHO) and Cremophor® ELP (ELP) at a total lipid concentration of 2.0 mg/mL. Known drug (cinnarizine) concentration at 0.05 mg/mL.

Mixture composition	CHO known concentration (mg/mL)	Average found concentration (mg/mL)	%RSD	Recovery (%)
S60: CHO: ELP drug-free	0.66	0.91	1.06	138.48 ± 13.81
S60: CHO: ELP with drug	0.66	0.92	0.81	139.10 ± 17.46

6.3.5. Formulation recovery: Cholesterol recovery from microfluidic-based niosomes

Cholesterol recovery within microfluidic-based niosomes was expressed as in Equation 6.1. This was to calculate the cholesterol recovery percentage after taking

account of the dilution factors such as the flow rate ratio (during the manufacturing process) and sample-diluent ratio (for HPLC analysis). The found cholesterol concentration post microfluidic cartridge was considered based on the known concentration of cholesterol in the surfactant/lipid mixture stock prior to use in the microfluidics device for niosome manufacturing. Found cholesterol concentration is the determined concentration of cholesterol obtained in the steady state of the run in the microfluidics process, omitting the first and final output droplets of the microfluidic chip. All cholesterol recovery from microfluidic-based niosomes were performed in triplicate and assessed using the modified HPLC-ELSD method as described in Section 2.6.3.

In Table 6-5, the recovery analysis of cholesterol from the microfluidic-based niosomes using the modified HPLC-ELSD method showed good reproducibility with %RSD less than 1 % for niosome suspensions before and after gel filtration process. Due to the low detection sensitivity for Span® 60, the niosome recovery was based on the recovery analysis of cholesterol given that cholesterol molecules intercalating with Span® 60 molecules in the formation of niosome vesicles at equimolar ratio of both compounds were used. More discussion will be followed in the next section (Section 6.3.6.) with physicochemical characteristics of manufactured niosomes.

Table 6-5: Evaluation of recovery of cholesterol within microfluidic-based niosomes without drug encapsulation. Calculated theoretical total composition/cholesterol concentrations based on the initial total lipid concentration, the flow rate ratio for mixing, and dilution factor on filtration process and sample preparation. The total composition was Span® 60: cholesterol (1:1).

Sample	Theoretical total composition/cholesterol concentration (mg/mL / mg/mL)	Average found cholesterol concentration (mg/mL)	%RSD	% cholesterol recovered
S1 After microfluidic chip	10.0/3.3	1.11	0.12	33.6 ± 3.9
S2 After gel filtration	2.5/0.82	0.59	0.06	72.0 ± 4.1

6.3.6. Evaluation of microfluidics manufacturing: process and formulation recovery

Microfluidic mixing allows a controlled mixing of miscible solvents and nanoprecipitation of dissolved lipid compounds to form nanoparticles as the manufactured output. For niosomes manufacturing, Span® 60 as an amphiphilic molecule self-assembles to form vesicles, whereas cholesterol acts as membrane stabiliser that works by intercalating within the vesicle membrane. The assessment of microfluidic process for niosome manufacturing can be demonstrated through the quantification of recovered cholesterol after manufacturing of niosome.

For the microfluidics manufacturing process of nanoparticulate system, there are two key parameters in the mixing process – total flow rate and flow rate ratio, where both parameters have shown effects on process yield (Roces et al., 2016; Roces, Christensen and Perrie, 2020). Flow rate ratio determines the volumetric dilution of

the organic solvent that contains surfactant/lipid mixture as stock solution (known initial total surfactant/lipid concentration) during the microfluidic mixing process. To better understand the mixing process on the degree of utilising lipid compounds to form niosomes, cholesterol recovery within microfluidic-based niosomes was evaluated, in order to provide an insight for niosomes manufacture using microfluidics.

The recovered cholesterol after niosome manufacture using microfluidics without purification step includes free cholesterol and cholesterol from within formed niosomes. Interestingly, the percentage of cholesterol recovered obtained in this study was noticeably low at 33.6 % (S1 in Table 6-5), indicated a lower output and yield that might be explained due to the loss of starting components during the mixing process. Despite the fact that the microfluidic cartridge material is made up of cyclic olefin copolymer (COC) that is chemically inert in which it helps to minimise lipid loss to adsorption, the high lipid content can lead to precipitation and deposition within the staggered herringbone micromixer relating to the hydrophobicity nature of Span® 60 and cholesterol during the mixing process.

In order to remove non-entrapped drug and free component compounds from nanoparticle suspension, there have been a number of purification techniques that are commonly used such as dialysis, centrifugation, gel filtration, and tangential flow filtration. These techniques can influence the particle attributes in terms of size, distribution, and the vesicle recovery. To assess the effect of purification, measurement of particle size and size distribution of microfluidic-based niosomes after gel filtration was taken and also the assessment of niosome recovery based on the recovery of cholesterol using the modified HPLC-ELSD method.

The process of gel filtration involved dilution of the manufactured niosome suspension from the microfluidic system in the aqueous phase, before being disrupted for recovery analysis of cholesterol. The filtration removed free compounds by size exclusion, obtaining formed niosome vesicles only for cholesterol recovery study. Smaller niosomes are produced after gel filtration process, with a cholesterol recovery over 70 % (Table 6-6). The results show a significant influence ($p < 0.05$) of gel filtration on the physicochemical properties of microfluidic-based niosomes in terms of the average vesicle size and the percentage of cholesterol recovered.

Table 6-6: Physicochemical characteristics of microfluidic-based niosomes and their percentage recovery of cholesterol before and after gel filtration. For this study, microfluidic-based niosomes without drug were studied. The niosome composition was Span® 60: cholesterol (1:1).

	Size (nm)	PDI	% cholesterol recovered
Before gel filtration	322.8 ± 10.4	0.158 ± 0.024	33.6 ± 3.9
After gel filtration	192.3 ± 2.1	0.130 ± 0.012	72.0 ± 4.1

6.4. Conclusion

Apart from manufacturing process parameters such as TFR, FRR, and temperature, formulation parameters are important in relation to niosome characteristics. Microfluidics mixing enabled controlled nanoprecipitation reaction of formulation components for formation of vesicles, driven by molecular diffusional and chaotic advection mixing. In this chapter, the recovery analysis of microfluidic-based niosomes focusing on cholesterol recovery was assessed and quantified by the modified HPLC-ELSD method without an initial extraction process. This method generated

chromatograms showing well separated peaks of the formulation component (Span® 60 and cholesterol) to allow quantification, enabling the evaluation on microfluidics as manufacturing method for niosomes. However, low detection sensitivity was found for Span® 60 but did not show to affect the analysis of cholesterol by using the modified analysis method for niosome composition component and formulation recovery. Additionally, the inclusion of hydrophobic drug (cinnarizine) with niosome components did not influence the analysis of cholesterol. However, the inclusion of hydrophilic so-surfactant (Cremophor® ELP) was found to be co-eluted with cholesterol which requires further confirmation using mass spectroscopy technique.

Despite of high reproducibility on niosome manufacturing using microfluidic method employing the NanoAssemblr™ system, the manufacturing efficiency of niosome was low based on the recovery analysis of cholesterol from niosome suspension obtained post cartridge (Sections 6.3.5. and 6.3.6.). Additionally, the organic solvent content in the post-cartridge and post-filtration niosome suspensions might affect the recovery analysis of niosome formulation.

Overall, this work reported and verified the applicability of a rapid and reproducible HPLC-ELSD method to analyse the non-ionic surfactant (Span® 60) and lipid (cholesterol) simultaneously for quantification of typically non-volatile surfactant/lipid compounds within niosomes, in addition to other nanoparticles investigated in previous studies. This method enables quantification of surfactant/lipid content within niosome without having to perform time-consuming mass spectroscopic assays for determination of microfluidic manufacturing efficiency. The technique helped to evaluate the effectiveness of niosomes manufacturing using microfluidics by

assessing the recovery of cholesterol as the main component of niosomes, as well as the impact of gel filtration on the niosomes in terms of miscible organic solvent dilution in aqueous phase, which gives insights into consideration on future works on improving parameters on the production of niosomes in the overall process yield.

Chapter Seven: General conclusions and future work

7. General conclusions and future work

7.1. Effect of niosome manufacturing methods on characteristics of niosomes encapsulated with methylene blue and cinnarizine

In this study, niosomes of cinnarizine and methylene blue were prepared using the conventional thin film hydration and microfluidic methods. Based on each manufacturing method, the process and formulation variables affecting the niosomes characteristics - vesicle size, distributions and encapsulation efficiency were examined. With the initial studies using methylene blue as hydrophilic model drug, the effect of manufacturing method was explored and found to be significantly different on niosome characteristics. Even though sonication process generated smaller vesicles of the thin film hydration method, the process could introduce contaminants into the niosome suspension due to the direct contact with the probe tip as well as generating heat during the process. Results highlighted on the variables and parameters to produce niosomes of desirable and reproducible vesicle sizes for predictable formulation performance. Through direct encapsulation, the drug property was found mainly affecting the encapsulation process in the manufacturing method. On the other hand, the release of encapsulated drug

In microfluidic-based niosomes, a higher hydrophobic drug (cinnarizine) encapsulation and a lower hydrophilic drug (methylene blue) encapsulation was found with both vesicles size less than 200 nm. The encapsulation of cinnarizine was found two-fold increase with microfluidic method compared to the conventional method. Unlike cinnarizine, the encapsulation of methylene blue into niosomes manufactured using both methods showed similar drug loading. Overall, niosomes prepared by microfluidic

method showed high reproducibility and storage stability compared to the niosome formulations of the same composition prepared by thin film hydration method with sonication. As the manufacturing process parameters are closely linked to the formulation parameters, a higher surfactant/lipid concentration (more than 20 mg/mL) was found to limit the mixing efficiency throughout the microfluidic channels, producing niosomes with lower drug encapsulation efficiency at the chosen total flow rate (12 mL/min) and flow rate ratio (4:1 aqueous: organic) in the microfluidic method. This work presented the manufacturing of niosomes using the staggered herringbone structure micromixer (SHM) where it generates controlled chaotic advection for a rapid miscible fluid mixing and drug loading with nanoprecipitation process simultaneously with the production of the vesicles.

7.2. Mucoadhesion

Consistent release of drug in order to enhance drug absorption is important for drug with variable absorption and/or narrow absorption site upon oral administration. Cinnarizine has a narrow absorption window in the stomach generally shows slow and variable absorption that resulted in low and erratic bioavailability, owing to its low aqueous solubility as a weakly basic drug. Increased solubilisation of cinnarizine achieved through encapsulation into niosomes as a drug carrier system followed by incorporation with mucoadhesive biopolymer in order to prolong gastric retention for enhanced absorption in the stomach. The interactions between the mucoadhesive formulations and the gastric mucin were explored as well as gastric mucosa retention to assess and understand the mucoadhesion mechanism. Drug release results showed enhanced gastric retention to allow enhanced rate and extent of absorption, in order to achieve consistent drug plasma profiles with reduced administration frequency.

Future works are to investigate the influence of pH and gelation of biopolymer upon administration on mucoadhesive properties, and also the diffusion and penetration across the mucus layer into circulation.

7.3. Recovery study for microfluidic-based niosomes

High reproducibility was found in non-ionic surfactant vesicles that manufactured by microfluidic method. Apart from the characterisation studies on vesicle size distribution and encapsulation efficiency, there is a need for quantification method of the formulation systems in order to assess the manufacturing process and efficiency based on the recovery of the formulation composition component. Here, a modified HPLC-ELSD method was used to separate, detect and quantify the amount of Span® 60 and cholesterol compounds within mixtures and disrupted vesicles as recovery studies. These recovery studies were important to identify any inconsistent output in order to assess manufacturing process and efficiency that potential surfactant/lipid loss occurred due to adsorption onto microfluidic cartridge matrix (Roces et al., 2016). Furthermore, the studies on recovered cholesterol showed high reproducibility and feasibility of using the quantification method despite of low recoveries obtained.

7.4. Potential future works

This research has shown the feasibility of niosomes on the delivery of poorly water-soluble drug (cinnarizine) to the stomach for enhanced absorption. Through the studies in this work on both niosome manufacturing methods, these method parameters can be applied on to more other hydrophobic drugs.

For longer term of storage, incorporation of charge-inducing agents as a stabiliser might be explored as well as the effectiveness of retain encapsulated drug throughout storage period.

Future work on verification of the quantification method in the recovery study based on ELSD detection on non-UV compounds such as non-ionic surfactant in this work. Potential use of the quantification method on other non-ionic and non-UV compounds.

Chapter Eight: References

8. References

Abdel-Hamid, M., Shahba, A., Mohsin, K. and Alanazi, F. (2012) 'Ultra performance liquid chromatography assay for cinnarizine in lipid-based formulations', *Asian J. Chem.*, 24(2), p. 6.

Abdelkader, H., Alani, A. W. G. and Alany, R. G. (2014) 'Recent advances in non-ionic surfactant vesicles (niosomes): self-assembly, fabrication, characterization, drug delivery applications and limitations', *Drug Delivery*, 21(2), pp. 87–100. doi: 10.3109/10717544.2013.838077.

Abed, O. S. A., Mulkala, S., Sharif, I., Abdin, A. M. and Alkordy, A. A. (2021) 'Lyophilization-free proliposomes for sustained release oral delivery of hydrophobic drug (cinnarazine): a comparative study', *Pharmaceutical Technology in Hospital Pharmacy*. De Gruyter, 6(1). doi: 10.1515/pthp-2021-0002.

Adeoye, O. and Cabral-Marques, H. (2017) 'Cyclodextrin nanosystems in oral drug delivery: A mini review', *International Journal of Pharmaceutics*, 531(2), pp. 521–531. doi: 10.1016/j.ijpharm.2017.04.050.

Ag Seleci, D., Seleci, M., Walter, J.-G., Stahl, F. and Scheper, T. (2016) 'Niosomes as nanoparticulate drug carriers: fundamentals and recent applications', *Journal of Nanomaterials*, 2016, pp. 1–13. doi: 10.1155/2016/7372306.

Ahad, A., Raish, M., Al-Jenoobi, F. I. and Al-Mohizea, A. M. (2018) 'Sorbitane Monostearate and Cholesterol based Niosomes for Oral Delivery of Telmisartan', *Current Drug Delivery*, 15(2), pp. 260–266. doi: 10.2174/1567201814666170518131934.

Ahadian, S., Finbloom, J. A., Mofidfar, M., Diltemiz, S. E., Nasrollahi, F., Davoodi, E., Hosseini, V., Mylonaki, I., Sangabathuni, S., Montazerian, H., Fetah, K., Nasiri, R., Dokmeci, M. R., Stevens, M. M., Desai, T. A. and Khademhosseini, A. (2020) 'Micro and nanoscale technologies in oral drug delivery', *Advanced Drug Delivery Reviews*, p. S0169409X2030096X. doi: 10.1016/j.addr.2020.07.012.

Akhter, S., Kushwaha, S., Warsi, M. H., Anwar, M., Ahmad, M. Z., Ahmad, I., Talegaonkar, S., Khan, Z. I., Khar, R. K. and Ahmad, F. J. (2012) 'Development and evaluation of nanosized niosomal dispersion for oral delivery of Ganciclovir', *Drug Development and Industrial Pharmacy*, 38(1), pp. 84–92. doi: 10.3109/03639045.2011.592529.

Alam, M. I., Paget, T. and Elkordy, Amal. A. (2016) 'Characterization of furazolidone-chitosan based spray dried microparticles regarding their drug release and mucin adsorptive properties', *Powder Technology*, 295, pp. 175–179. doi: 10.1016/j.powtec.2016.03.026.

- Alani, A. W. G., Rao, D. A., Seidel, R., Wang, J., Jiao, J. and Kwon, G. S. (2010) 'The effect of novel surfactants and Solutol® HS 15 on paclitaxel aqueous solubility and permeability across a caco-2 monolayer', *Journal of Pharmaceutical Sciences*, 99(8), pp. 3473–3485. doi: 10.1002/jps.22111.
- Ali, M. H., Kirby, D. J., Mohammed, A. R. and Perrie, Y. (2010) 'Solubilisation of drugs within liposomal bilayers: alternatives to cholesterol as a membrane stabilising agent', *Journal of Pharmacy and Pharmacology*, 62(11), pp. 1646–1655. doi: 10.1111/j.2042-7158.2010.01090.x.
- Ali, M. H., Moghaddam, B., Kirby, D. J., Mohammed, A. R. and Perrie, Y. (2013) 'The role of lipid geometry in designing liposomes for the solubilisation of poorly water soluble drugs', *International Journal of Pharmaceutics*. (Poorly Soluble Drugs), 453(1), pp. 225–232. doi: 10.1016/j.ijpharm.2012.06.056.
- Amidon, G. L., Lennernäs, H., Shah, V. P. and Crison, J. R. (1995) 'A theoretical basis for a biopharmaceutic drug classification: the correlation of in vitro drug product dissolution and in vivo bioavailability', *Pharmaceutical Research*, 12(3), pp. 413–420. doi: 10.1023/A:1016212804288.
- Attia, I. A., El-Gizawy, S. A., Fouda, M. A. and Donia, A. M. (2007) 'Influence of a niosomal formulation on the oral bioavailability of acyclovir in rabbits', *AAPS PharmSciTech*, 8(4), pp. 206–212. doi: 10.1208/pt0804106.
- Aulton, M. E. and Taylor, K. M. G. (2017) *Aulton's Pharmaceutics E-Book: The Design and Manufacture of Medicines*. London, UNITED KINGDOM: Elsevier. Available at: <http://ebookcentral.proquest.com/lib/sunderland/detail.action?docID=5253018> (Accessed: 3 July 2020).
- Authimoolam, S. P. and Dziubla, T. D. (2016) 'Biopolymeric mucin and synthetic polymer analogs: their structure, function and role in biomedical applications', *Polymers*. Multidisciplinary Digital Publishing Institute, 8(3), p. 71. doi: 10.3390/polym8030071.
- Azmin, M. N., Florence, A. T., Handjani-Vila, R. M., Stuart, J. F. B., Vanlerberghe, G. and Whittaker, J. S. (1985) 'The effect of non-ionic surfactant vesicle (niosome) entrapment on the absorption and distribution of methotrexate in mice', *Journal of Pharmacy and Pharmacology*, 37(4), pp. 237–242. doi: 10.1111/j.2042-7158.1985.tb05051.x.
- Babadi, D., Dadashzadeh, S., Osouli, M., Abbasian, Z., Daryabari, M. S., Sadrai, S. and Haeri, A. (2021) 'Biopharmaceutical and pharmacokinetic aspects of nanocarrier-mediated oral delivery of poorly soluble drugs', *Journal of Drug Delivery Science and Technology*, 62, p. 102324. doi: 10.1016/j.jddst.2021.102324.
- Baillie, A. J., Florence, A. T., Hume, L. R., Muirhead, G. T. and Rogerson, A. (1985) 'The preparation and properties of niosomes—non-ionic surfactant vesicles', *Journal of Pharmacy and Pharmacology*, 37(12), pp. 863–868. doi: 10.1111/j.2042-7158.1985.tb04990.x.

- Bansal, S., Aggarwal, G., Chandel, P. and Harikumar, S. L. (2013) 'Design and development of cefdinir niosomes for oral delivery', *Journal of Pharmacy & Bioallied Sciences*, 5(4), pp. 318–325. doi: 10.4103/0975-7406.120080.
- Bansil, R., Cao, X., Bhaskar, K. R. and Lamont, J. T. (1996) 'Gelation and aggregation of mucin in relation to the stomach's protective barrier', *Macromolecular Symposia*, 109(1), pp. 105–113. doi: <https://doi.org/10.1002/masy.19961090110>.
- Bayindir, Z. S. and Yuksel, N. (2010) 'Characterization of niosomes prepared with various nonionic surfactants for paclitaxel oral delivery', *Journal of Pharmaceutical Sciences*, 99(4), pp. 2049–2060. doi: 10.1002/jps.21944.
- Bear, G. R. (1988) 'Universal detection and quantitation of surfactants by high-performance liquid chromatography by means of the evaporative light-scattering detector'. doi: 10.1016/S0021-9673(01)82019-7.
- Belliveau, N. M., Huft, J., Lin, P. J., Chen, S., Leung, A. K., Leaver, T. J., Wild, A. W., Lee, J. B., Taylor, R. J., Tam, Y. K., Hansen, C. L. and Cullis, P. R. (2012) 'Microfluidic synthesis of highly potent limit-size lipid nanoparticles for in vivo delivery of siRNA', *Molecular Therapy - Nucleic Acids*, 1, p. e37. doi: 10.1038/mtna.2012.28.
- Beri, C. L., Sood, R. and Gupta, A. (2013) 'Stomach specific mucoadhesive microspheres as controlled drug delivery system-a review', in.
- Berlin, M., Przyklenk, K.-H., Richtberg, A., Baumann, W. and Dressman, J. B. (2014) 'Prediction of oral absorption of cinnarizine – a highly supersaturating poorly soluble weak base with borderline permeability', *European Journal of Pharmaceutics and Biopharmaceutics*, 88(3), pp. 795–806. doi: 10.1016/j.ejpb.2014.08.011.
- Berthelsen, R., Holm, R., Jacobsen, J., Kristensen, J., Abrahamsson, B. and Müllertz, A. (2015) 'Kolliphor surfactants affect solubilization and bioavailability of fenofibrate. Studies of in vitro digestion and absorption in rats', *Molecular Pharmaceutics*, 12(4), pp. 1062–1071. doi: 10.1021/mp500545k.
- Bhat, P., Flanagan, D. and Donovan, M. (1996) 'Drug binding to gastric mucus glycoproteins', *International Journal of Pharmaceutics*, 134(1–2), pp. 15–25. doi: 10.1016/0378-5173(95)04333-0.
- Biswal, S., Murthy, P. N., Sahu, J., Sahoo, P. and Amir, F. (2008) 'Vesicles of non-ionic surfactants (niosomes) and drug delivery potential', *International Journal of Pharmaceutical Sciences and Nanotechnology*, 1(1), p. 8.
- Box, K. and Comer, J. (2008) 'Using measured pKa, LogP and solubility to investigate supersaturation and predict BCS class', *Current Drug Metabolism*, 9(9), pp. 869–878. doi: 10.2174/138920008786485155.
- Boyd, B. J., Bergström, Christel A.S., Vinarov, Z., Kuentz, M., Brouwers, J., Augustijns, P., Brandl, M., Bernkop-Schnürch, A., Shrestha, N., Pr at, V., Müllertz, A., Bauer-Brandl, A. and Jannin, V. (2019) 'Successful oral delivery of poorly water-soluble drugs both depends on the intraluminal behavior of drugs and of appropriate advanced drug delivery systems', *European Journal of Pharmaceutical Sciences*, 137, p. 104967. doi: 10.1016/j.ejps.2019.104967.

Boyd, B. J., Bergström, Christel A. S., Vinarov, Z., Kuentz, M., Brouwers, J., Augustijns, P., Brandl, M., Bernkop-Schnürch, A., Shrestha, N., Prémat, V., Müllertz, A., Bauer-Brandl, A. and Jannin, V. (2019) 'Successful oral delivery of poorly water-soluble drugs both depends on the intraluminal behavior of drugs and of appropriate advanced drug delivery systems', *European Journal of Pharmaceutical Sciences*, 137, p. 104967. doi: 10.1016/j.ejps.2019.104967.

British Pharmacopoeia (2020) Part II

Brouwers, J. F., Gadella, B. M., van Golde, L. M. and Tielens, A. G. (1998) 'Quantitative analysis of phosphatidylcholine molecular species using HPLC and light scattering detection', *Journal of Lipid Research*, 39(2), pp. 344–353.

Cairns, D.(ed.) (2012) *Essentials of pharmaceutical chemistry*. 4. ed. London: Pharmaceutical Press.

Capretto, L., Carugo, D., Mazzitelli, S., Nastruzzi, C. and Zhang, X. (2013) 'Microfluidic and lab-on-a-chip preparation routes for organic nanoparticles and vesicular systems for nanomedicine applications', *Advanced Drug Delivery Reviews*. (Design production and characterization of drug delivery systems by Lab-on-a-Chip technology), 65(11), pp. 1496–1532. doi: 10.1016/j.addr.2013.08.002.

Castaneda Hernandez, G., Vargas Alvarado, Y., Aguirre, F. and Flores Murrieta, F. J. (1993) 'Pharmacokinetics of cinnarizine after single and multiple dosing in healthy volunteers', *Arzneimittel-Forschung*, 43(5), pp. 539–42.

Celli, J., Gregor, B., Turner, B., Afdhal, N. H., Bansil, R. and Erramilli, S. (2005) 'Viscoelastic properties and dynamics of porcine gastric mucin', *Biomacromolecules*, 6(3), pp. 1329–1333. doi: 10.1021/bm0493990.

Celli, J. P., Turner, B. S., Afdhal, N. H., Ewoldt, R. H., McKinley, G. H., Bansil, R. and Erramilli, S. (2007) 'Rheology of gastric mucin exhibits a pH-dependent sol-gel transition', *Biomacromolecules*. American Chemical Society, 8(5), pp. 1580–1586. doi: 10.1021/bm0609691.

Chakraborty, S., Shukla, D., Mishra, B. and Singh, S. (2009) 'Lipid – An emerging platform for oral delivery of drugs with poor bioavailability', *European Journal of Pharmaceutics and Biopharmaceutics*, 73(1), pp. 1–15. doi: 10.1016/j.ejpb.2009.06.001.

Chen, D., Love, K. T., Chen, Y., Eltoukhy, A. A., Kastrup, C., Sahay, G., Jeon, A., Dong, Y., Whitehead, K. A. and Anderson, D. G. (2012) 'Rapid discovery of potent siRNA-containing lipid nanoparticles enabled by controlled microfluidic formulation', *Journal of the American Chemical Society*, 134(16), pp. 6948–6951. doi: 10.1021/ja301621z.

Chhabra, R. P. (2010) 'Non-Newtonian Fluids: An Introduction', in Krishnan, J. M., Deshpande, A. P., and Kumar, P. B. S. (eds) *Rheology of Complex Fluids*. New York, NY: Springer New York, pp. 3–34. doi: 10.1007/978-1-4419-6494-6_1.

- Cho, N.-J., Hwang, L. Y., Solandt, J. J. R. and Frank, C. W. (2013) 'Comparison of extruded and sonicated vesicles for planar bilayer self-assembly', *Materials*, 6(8), pp. 3294–3308. doi: 10.3390/ma6083294.
- Chu, B. and Liu, T. (2000) 'Characterization of nanoparticles by scattering techniques', *Journal of Nanoparticle Research*, 2(1), pp. 29–41. doi: 10.1023/A:1010001822699.
- Cinnarizine 15 mg Tablets - Summary of Product Characteristics (SmPC) - (emc)* (no date). Available at: <https://www.medicines.org.uk/emc/product/2607/smpc#gref> (Accessed: 20 September 2021).
- Correia, M. G. S., Briuglia, M. L., Niosi, F. and Lamprou, D. A. (2017) 'Microfluidic manufacturing of phospholipid nanoparticles: stability, encapsulation efficacy, and drug release', *International Journal of Pharmaceutics*, 516(1), pp. 91–99. doi: 10.1016/j.ijpharm.2016.11.025.
- D'Addio, S. M. and Prud'homme, R. K. (2011) 'Controlling drug nanoparticle formation by rapid precipitation', *Advanced Drug Delivery Reviews*, 63(6), pp. 417–426. doi: 10.1016/j.addr.2011.04.005.
- Damiati, S., Kompella, U. B., Damiati, S. A. and Kodzius, R. (2018) 'Microfluidic devices for drug delivery systems and drug screening', *Genes*, 9(2). doi: 10.3390/genes9020103.
- Dan, N. (2017) 'Chapter 2 - Core-shell drug carriers: liposomes, polymersomes, and niosomes', in Andronescu, E. and Grumezescu, A. M. (eds) *Nanostructures for Drug Delivery*. Elsevier (Micro and Nano Technologies), pp. 63–105. doi: 10.1016/B978-0-323-46143-6.00002-6.
- Dhawan, S., Singla, A. K. and Sinha, V. R. (2004) 'Evaluation of mucoadhesive properties of chitosan microspheres prepared by different methods', *AAPS PharmSciTech*, 5(4), pp. 122–128. doi: 10.1208/pt050467.
- Di Marzio, L., Esposito, S., Rinaldi, F., Marianecchi, C. and Carafa, M. (2013) 'Polysorbate 20 vesicles as oral delivery system: In vitro characterization', *Colloids and Surfaces B: Biointerfaces*, 104, pp. 200–206. doi: 10.1016/j.colsurfb.2012.10.036.
- Dimov, N., Kastner, E., Hussain, M., Perrie, Y. and Szita, N. (2017) 'Formation and purification of tailored liposomes for drug delivery using a module-based micro continuous-flow system', *Scientific Reports*, 7(1), p. 12045. doi: 10.1038/s41598-017-11533-1.
- Eloy, J. O., Claro de Souza, M., Petrilli, R., Barcellos, J. P. A., Lee, R. J. and Marchetti, J. M. (2014) 'Liposomes as carriers of hydrophilic small molecule drugs: Strategies to enhance encapsulation and delivery', *Colloids and Surfaces B: Biointerfaces*, 123, pp. 345–363. doi: 10.1016/j.colsurfb.2014.09.029.
- Essa, E. (2010) 'Effect of formulation and processing variables on the particle size of sorbitan monopalmitate niosomes', *Asian Journal of Pharmaceutics*, 4(4), p. 227. doi: 10.4103/0973-8398.76752.

- Essa, E. A., Elebyary, T. T., Abdelquader, M. M., El Maghraby, G. M. and Elkordy, A. A. (2021) 'Smart liquids for oral controlled drug release: An overview of alginate and non-alginate based systems', *Journal of Drug Delivery Science and Technology*, 61, p. 102211. doi: 10.1016/j.jddst.2020.102211.
- Fan, Y., Marioli, M. and Zhang, K. (2021) 'Analytical characterization of liposomes and other lipid nanoparticles for drug delivery', *Journal of Pharmaceutical and Biomedical Analysis*, 192, p. 113642. doi: 10.1016/j.jpba.2020.113642.
- Filipović-Grcić, J., Skalko-Basnet, N. and Jalsenjak, I. (2001) 'Mucoadhesive chitosan-coated liposomes: characteristics and stability', *Journal of Microencapsulation*, 18(1), pp. 3–12. doi: 10.1080/026520401750038557.
- Forbes, N., Hussain, M. T., Briuglia, M. L., Edwards, D. P., Horst, J. H. ter, Szita, N. and Perrie, Y. (2019) 'Rapid and scale-independent microfluidic manufacture of liposomes entrapping protein incorporating in-line purification and at-line size monitoring', *International Journal of Pharmaceutics*, 556, pp. 68–81. doi: 10.1016/j.ijpharm.2018.11.060.
- Garg, S., Heuck, G., Ip, S. and Ramsay, E. (2016) 'Microfluidics: a transformational tool for nanomedicine development and production', *Journal of Drug Targeting*, 24(9), pp. 821–835. doi: 10.1080/1061186X.2016.1198354.
- George, M. and Abraham, T. E. (2006) 'Polyionic hydrocolloids for the intestinal delivery of protein drugs: Alginate and chitosan — a review', *Journal of Controlled Release*, 114(1), pp. 1–14. doi: 10.1016/j.jconrel.2006.04.017.
- Ghafelehbashi, R., Akbarzadeh, I., Tavakkoli Yarak, M., Lajevardi, A., Fatemizadeh, M. and Heidarpour Saremi, L. (2019) 'Preparation, physicochemical properties, in vitro evaluation and release behavior of cephalixin-loaded niosomes', *International Journal of Pharmaceutics*, 569, p. 118580. doi: 10.1016/j.ijpharm.2019.118580.
- Ghasemiyeh, P. and Mohammadi-Samani, S. (2018) 'Solid lipid nanoparticles and nanostructured lipid carriers as novel drug delivery systems: applications, advantages and disadvantages', *Research in Pharmaceutical Sciences*, 13(4), pp. 288–303. doi: 10.4103/1735-5362.235156.
- Grießinger, J., Dünnhaupt, S., Cattoz, B., Griffiths, P., Oh, S., Gómez, S. B. i, Wilcox, M., Pearson, J., Gumbleton, M., Abdulkarim, M., Pereira de Sousa, I. and Bernkop-Schnürch, A. (2015) 'Methods to determine the interactions of micro- and nanoparticles with mucus', *European Journal of Pharmaceutics and Biopharmaceutics*, 96, pp. 464–476. doi: 10.1016/j.ejpb.2015.01.005.
- Griffiths, P. R. and De Haseth, J. A. (2007) *Fourier transform infrared spectrometry*. 2nd ed. Hoboken, N.J: Wiley-Interscience (Chemical analysis, v. 171).
- Guinedi, A. S., Mortada, N. D., Mansour, S. and Hathout, R. M. (2005) 'Preparation and evaluation of reverse-phase evaporation and multilamellar niosomes as ophthalmic carriers of acetazolamide', *International Journal of Pharmaceutics*, 306(1), pp. 71–82. doi: 10.1016/j.ijpharm.2005.09.023.

- Gurrapu, A., Jukanti, R., Bobbala, S. R., Kanuganti, S. and Jeevana, J. B. (2012) 'Improved oral delivery of valsartan from maltodextrin based proniosome powders', *Advanced Powder Technology*, 23(5), pp. 583–590. doi: 10.1016/j.appt.2011.06.005.
- Han, H.-K., Shin, H.-J. and Ha, D. H. (2012) 'Improved oral bioavailability of alendronate via the mucoadhesive liposomal delivery system', *European Journal of Pharmaceutical Sciences*, 46(5), pp. 500–507. doi: 10.1016/j.ejps.2012.04.002.
- Handjani-Vila, R. M., Ribier, A., Rondot, B. and Vanlerberghie, G. (1979) 'Dispersions of lamellar phases of non-ionic lipids in cosmetic products', *International Journal of Cosmetic Science*, 1(5), pp. 303–314. doi: 10.1111/j.1467-2494.1979.tb00224.x.
- Hao, Y., Zhao, F., Li, N., Yang, Y. and Li, K. (2002) 'Studies on a high encapsulation of colchicine by a niosome system', *International Journal of Pharmaceutics*, 244(1–2), pp. 73–80. doi: 10.1016/S0378-5173(02)00301-0.
- Hao, Y.-M. and Li, K. (2011) 'Entrapment and release difference resulting from hydrogen bonding interactions in niosome', *International Journal of Pharmaceutics*, 403(1), pp. 245–253. doi: 10.1016/j.ijpharm.2010.10.027.
- Hassan, E. E. and Gallo, J. M. (1990) 'A simple rheological method for the in vitro assessment of mucin-polymer bioadhesive bond strength', *Pharmaceutical Research*, 7(5), pp. 491–495. doi: 10.1023/A:1015812615635.
- He, H., Lu, Y., Qi, J., Zhu, Q., Chen, Z. and Wu, W. (2019) 'Adapting liposomes for oral drug delivery', *Acta Pharmaceutica Sinica B*, 9(1), pp. 36–48. doi: 10.1016/j.apsb.2018.06.005.
- He, J., Wang, L., Wei, Z., Yang, Y., Wang, C., Han, X. and Nie, Z. (2013) 'Vesicular self-assembly of colloidal amphiphiles in microfluidics', *ACS Applied Materials & Interfaces*, 5(19), pp. 9746–9751. doi: 10.1021/am4028839.
- Hirayama, F. and Uekama, K. (1999) 'Cyclodextrin-based controlled drug release system', *Advanced Drug Delivery Reviews*. (Cyclodextrins in Drug Delivery System), 36(1), pp. 125–141. doi: 10.1016/S0169-409X(98)00058-1.
- Hong, L., Dong, Y.-D. and Boyd, B. J. (2019) 'Preparation of nanostructured lipid drug delivery particles using microfluidic mixing', *Pharmaceutical Nanotechnology*, 7(6), pp. 484–495. doi: 10.2174/2211738507666191004123545.
- Hong, Z., Chasan, B., Bansil, R., Turner, B. S., Bhaskar, K. R. and Afdhal, N. H. (2005) 'Atomic force microscopy reveals aggregation of gastric mucin at low pH', *Biomacromolecules*, 6(6), pp. 3458–3466. doi: 10.1021/bm0505843.
- Hörter, D. and Dressman, J. B. (2001) 'Influence of physicochemical properties on dissolution of drugs in the gastrointestinal tract', *Advanced Drug Delivery Reviews*. (Special issue dedicated to Dr. Eric Tomlinson, Advanced Drug Delivery Reviews, A Selection of the Most Highly Cited Articles, 1991-1998), 46(1), pp. 75–87. doi: 10.1016/S0169-409X(00)00130-7.

Huang, X. M., Caddell, R., Yu, B., Xu, S. L., Theobald, B., Lee, L. J. and Lee, R. J. (2010) 'Ultrasound-enhanced microfluidic synthesis of liposomes', *Anticancer research*, 30(2), pp. 463–466.

Ibrahim, Y. H.-E. Y., Regdon, G., Hamedelniei, E. I. and Sovány, T. (2019) 'Review of recently used techniques and materials to improve the efficiency of orally administered proteins/peptides', *DARU Journal of Pharmaceutical Sciences*, 28(1), pp. 403–416. doi: 10.1007/s40199-019-00316-w.

Jadon, P. S., Gajbhiye, V., Jadon, R. S., Gajbhiye, K. R. and Ganesh, N. (2009) 'Enhanced oral bioavailability of griseofulvin via niosomes', *AAPS PharmSciTech*, 10(4). doi: 10.1208/s12249-009-9325-z.

Jain, S., Sharma, R. K. and Vyas, S. P. (2006) 'Chitosan nanoparticles encapsulated vesicular systems for oral immunization: preparation, in-vitro and in-vivo characterization', *Journal of Pharmacy and Pharmacology*, 58(3), pp. 303–310. doi: 10.1211/jpp.58.3.0003.

Johansson, M. E. V., Sjövall, H. and Hansson, G. C. (2013) 'The gastrointestinal mucus system in health and disease', *Nature reviews. Gastroenterology & hepatology*, 10(6), pp. 352–361. doi: 10.1038/nrgastro.2013.35.

Jones, D. S. (2016) *Pharmaceutics dosage form and design*. London: Pharmaceutical Press.

Joshi, S., Hussain, M. T., Roces, C. B., Anderluzzi, G., Kastner, E., Salmaso, S., Kirby, D. J. and Perrie, Y. (2016) 'Microfluidics based manufacture of liposomes simultaneously entrapping hydrophilic and lipophilic drugs', *International Journal of Pharmaceutics*. (In Honour of Professor Alexander T. Florence), 514(1), pp. 160–168. doi: 10.1016/j.ijpharm.2016.09.027.

Junyaprasert, V. B., Teeranachaideekul, V. and Supaperm, T. (2008) 'Effect of charged and non-ionic membrane additives on physicochemical properties and stability of niosomes', *AAPS PharmSciTech*, 9(3). doi: 10.1208/s12249-008-9121-1.

Kalepu, S. and Nekkanti, V. (2015) 'Insoluble drug delivery strategies: review of recent advances and business prospects', *Acta Pharmaceutica Sinica B*, 5(5), pp. 442–453. doi: 10.1016/j.apsb.2015.07.003.

Kamboj, S., Saini, V. and Bala, S. (2014) 'Formulation and characterization of drug loaded nonionic surfactant vesicles (niosomes) for oral bioavailability enhancement', *The Scientific World Journal*, 2014, p. e959741. doi: 10.1155/2014/959741.

Kastner, E., Kaur, R., Lowry, D., Moghaddam, B., Wilkinson, A. and Perrie, Y. (2014) 'High-throughput manufacturing of size-tuned liposomes by a new microfluidics method using enhanced statistical tools for characterization', *International Journal of Pharmaceutics*, 477(1), pp. 361–368. doi: 10.1016/j.ijpharm.2014.10.030.

Kastner, E., Verma, V., Lowry, D. and Perrie, Y. (2015) 'Microfluidic-controlled manufacture of liposomes for the solubilisation of a poorly water soluble drug', *International Journal of Pharmaceutics*, 485(1–2), pp. 122–130. doi: 10.1016/j.ijpharm.2015.02.063.

- Kaukonen, A. M., Boyd, B. J., Porter, C. J. H. and Charman, W. N. (2004) 'Drug solubilization behavior during in vitro digestion of simple triglyceride lipid solution formulations', *Pharmaceutical Research*, 21(2), pp. 245–253. doi: 10.1023/B:PHAM.0000016282.77887.1f.
- Kawabata, Y., Wada, K., Nakatani, M., Yamada, S. and Onoue, S. (2011) 'Formulation design for poorly water-soluble drugs based on biopharmaceutics classification system: basic approaches and practical applications', *International Journal of Pharmaceutics*, 420(1), pp. 1–10. doi: 10.1016/j.ijpharm.2011.08.032.
- Kazi, K. M., Mandal, A. S., Biswas, N., Guha, A., Chatterjee, S., Behera, M. and Kuotsu, K. (2010) 'Niosome: a future of targeted drug delivery systems', *Journal of Advanced Pharmaceutical Technology & Research*, 1(4), pp. 374–380. doi: 10.4103/0110-5558.76435.
- Khoee, S. and Yaghoobian, M. (2017) 'Chapter 6 - Niosomes: a novel approach in modern drug delivery systems', in *Nanostructures for Drug Delivery*. Elsevier, pp. 207–237.
- Kimura, T. and Higaki, K. (2002) 'Gastrointestinal transit and drug absorption', 25(2), p. 16.
- Kumar, G. P. and Rajeshwarrao, P. (2011) 'Nonionic surfactant vesicular systems for effective drug delivery—an overview', *Acta Pharmaceutica Sinica B*, 1(4), pp. 208–219. doi: 10.1016/j.apsb.2011.09.002.
- Lai, S. K., Wang, Y.-Y., Wirtz, D. and Hanes, J. (2009) 'Micro- and macrorheology of mucus', *Advanced Drug Delivery Reviews*, 61(2), pp. 86–100. doi: 10.1016/j.addr.2008.09.012.
- Lam, C. and Jefferis, S. A. (2014) 'Interpretation of viscometer test results for polymer support fluids', in *Tunneling and Underground Construction*. Shanghai, China: American Society of Civil Engineers, pp. 439–449. doi: 10.1061/9780784413449.043.
- Lapinski, M. M., Castro-Forero, A., Greiner, A. J., Ofoli, R. Y. and Blanchard, G. J. (2007) 'Comparison of liposomes formed by sonication and extrusion: rotational and translational diffusion of an embedded chromophore', *Langmuir*, 23(23), pp. 11677–11683. doi: 10.1021/la7020963.
- Larsen, A. T., Åkesson, P., Juréus, A., Saaby, L., Abu-Rmaileh, R., Abrahamsson, B., Østergaard, J. and Müllertz, A. (2013) 'Bioavailability of cinnarizine in dogs: Effect of SNEDDS loading level and correlation with cinnarizine solubilization during in vitro lipolysis', *Pharmaceutical Research*, 30(12), pp. 3101–3113. doi: 10.1007/s11095-013-1145-x.
- Lasic, D. D. (1988) 'The mechanism of vesicle formation', *Biochemical Journal*, 256(1), pp. 1–11. doi: 10.1042/bj2560001.
- Liang, Y., Kashdan, T., Sterner, C., Dombrowski, L., Petrick, I., Kröger, M. and Höfer, R. (2015) 'Algal Biorefineries', in *Industrial Biorefineries & White Biotechnology*. Elsevier, pp. 35–90. doi: 10.1016/B978-0-444-63453-5.00002-1.

- Lo, C. T., Jahn, A., Locascio, L. E. and Vreeland, W. N. (2010) 'Controlled self-assembly of monodisperse niosomes by microfluidic hydrodynamic focusing', *Langmuir*, 26(11), pp. 8559–8566. doi: 10.1021/la904616s.
- Lock, J. Y., Carlson, T. L. and Carrier, R. L. (2018) 'Mucus models to evaluate the diffusion of drugs and particles', *Advanced Drug Delivery Reviews*. (Technological strategies to overcome the mucus barrier in mucosal drug delivery), 124, pp. 34–49. doi: 10.1016/j.addr.2017.11.001.
- Loh, Z. H., Samanta, A. K. and Sia Heng, P. W. (2015) 'Overview of milling techniques for improving the solubility of poorly water-soluble drugs', *Asian Journal of Pharmaceutical Sciences*, 10(4), pp. 255–274. doi: 10.1016/j.ajps.2014.12.006.
- Lu, Y., Zhang, E., Yang, J. and Cao, Z. (2018) 'Strategies to improve micelle stability for drug delivery', *Nano research*, 11(10), pp. 4985–4998. doi: 10.1007/s12274-018-2152-3.
- MacAdam, A. (1993) 'The effect of gastro-intestinal mucus on drug absorption', *Advanced Drug Delivery Reviews*. (Relevance of Mucus to Advanced Drug Delivery), 11(3), pp. 201–220. doi: 10.1016/0169-409X(93)90010-2.
- Maeki, M., Fujishima, Y., Sato, Y., Yasui, T., Kaji, N., Ishida, A., Tani, H., Baba, Y., Harashima, H. and Tokeshi, M. (2017) 'Understanding the formation mechanism of lipid nanoparticles in microfluidic devices with chaotic micromixers', Choi, J. (ed.) *PLOS ONE*, 12(11), p. e0187962. doi: 10.1371/journal.pone.0187962.
- Maeki, M., Saito, T., Sato, Y., Yasui, T., Kaji, N., Ishida, A., Tani, H., Baba, Y., Harashima, H. and Tokeshi, M. (2015) 'A strategy for synthesis of lipid nanoparticles using microfluidic devices with a mixer structure', *RSC Advances*, 5(57), pp. 46181–46185. doi: 10.1039/C5RA04690D.
- Mahale, N. B., Thakkar, P. D., Mali, R. G., Walunj, D. R. and Chaudhari, S. R. (2012) 'Niosomes: novel sustained release nonionic stable vesicular systems — an overview', *Advances in Colloid and Interface Science*, 183–184, pp. 46–54. doi: 10.1016/j.cis.2012.08.002.
- Makary, P. (2014) 'Principles of salt formation', *UK Journal of Pharmaceutical Biosciences*, 2(4), p. 1. doi: 10.20510/ukjpb/2/i4/91101.
- Manosroi, A., Wongtrakul, P., Manosroi, J., Sakai, H., Sugawara, F., Yuasa, M. and Abe, M. (2003) 'Characterization of vesicles prepared with various non-ionic surfactants mixed with cholesterol', *Colloids and Surfaces B: Biointerfaces*, 30(1–2), pp. 129–138. doi: 10.1016/S0927-7765(03)00080-8.
- Mantle, M. and Allen, A. (1978) 'A colorimetric assay for glycoproteins based on the Periodic Acid/Schiff stain', *Biochemical Society Transactions*, 6(3), pp. 607–609. doi: 10.1042/bst0060607.
- Marianecchi, C., Di Marzio, L., Rinaldi, F., Celia, C., Paolino, D., Alhaique, F., Esposito, S. and Carafa, M. (2014) 'Niosomes from 80s to present: the state of the art', *Advances in Colloid and Interface Science*, 205, pp. 187–206. doi: 10.1016/j.cis.2013.11.018.

- Martínez Rivas, C. J., Tarhini, M., Badri, W., Miladi, K., Greige-Gerges, H., Nazari, Q. A., Galindo Rodríguez, S. A., Román, R. Á., Fessi, H. and Elaissari, A. (2017) 'Nanoprecipitation process: from encapsulation to drug delivery', *International Journal of Pharmaceutics*, 532(1), pp. 66–81. doi: 10.1016/j.ijpharm.2017.08.064.
- Marwa, A., Omaima, S., Hanaa, E.-G. and Mohammed, A.-S. (2013) 'Preparation and in-vitro evaluation of diclofenac sodium niosomal formulations', *International Journal of Pharmaceutical Sciences and Research*, 4(5), p. 9.
- Michelon, M., Oliveira, D. R. B., de Figueiredo Furtado, G., Gaziola de la Torre, L. and Cunha, R. L. (2017) 'High-throughput continuous production of liposomes using hydrodynamic flow-focusing microfluidic devices', *Colloids and Surfaces B: Biointerfaces*, 156, pp. 349–357. doi: 10.1016/j.colsurfb.2017.05.033.
- Moghassemi, S. and Hadjizadeh, A. (2014) 'Nano-niosomes as nanoscale drug delivery systems: An illustrated review', *Journal of Controlled Release*, 185, pp. 22–36. doi: 10.1016/j.jconrel.2014.04.015.
- Moghassemi, S., Hadjizadeh, A. and Omidfar, K. (2017) 'Formulation and Characterization of Bovine Serum Albumin-Loaded Niosome', *AAPS PharmSciTech*, 18(1), pp. 27–33. doi: 10.1208/s12249-016-0487-1.
- Moghassemi, S., Parnian, E., Hakamivala, A., Darzianiazizi, M., Vardanjani, M. M., Kashanian, S., Larijani, B. and Omidfar, K. (2015) 'Uptake and transport of insulin across intestinal membrane model using trimethyl chitosan coated insulin niosomes', *Materials Science and Engineering: C*, 46, pp. 333–340. doi: 10.1016/j.msec.2014.10.070.
- Mohammed, A. R., Weston, N., Coombes, A. G. A., Fitzgerald, M. and Perrie, Y. (2004) 'Liposome formulation of poorly water soluble drugs: optimisation of drug loading and ESEM analysis of stability', *International Journal of Pharmaceutics*, 285(1–2), pp. 23–34. doi: 10.1016/j.ijpharm.2004.07.010.
- Mohsin, K. (2012) 'Design of lipid-based formulations for oral administration of poorly water-soluble drug fenofibrate: effects of digestion', *AAPS PharmSciTech*, 13(2), pp. 637–646. doi: 10.1208/s12249-012-9787-2.
- Mokhtar, M., Sammour, O. A., Hammad, M. A. and Megrab, N. A. (2008) 'Effect of some formulation parameters on flurbiprofen encapsulation and release rates of niosomes prepared from proniosomes', *International Journal of Pharmaceutics*, 361(1), pp. 104–111. doi: 10.1016/j.ijpharm.2008.05.031.
- Möschwitzer, J. and Müller, R. H. (2006) 'New method for the effective production of ultrafine drug nanocrystals', *Journal of Nanoscience and Nanotechnology*, 6(9–10), pp. 3145–3153. doi: 10.1166/jnn.2006.480.
- Mozafari, M. R. (2010) 'Nanoliposomes: preparation and analysis', in Weissig, V. (ed.) *Liposomes: Methods and Protocols, Volume 1: Pharmaceutical Nanocarriers*. Totowa, NJ: Humana Press (Methods in Molecular Biology), pp. 29–50. doi: 10.1007/978-1-60327-360-2_2.

- Müller, R. H. and Peters, K. (1998) 'Nanosuspensions for the formulation of poorly soluble drugs: I. Preparation by a size-reduction technique', *International Journal of Pharmaceutics*, 160(2), pp. 229–237. doi: 10.1016/S0378-5173(97)00311-6.
- Müller, R. H., Radtke, M. and Wissing, S. A. (2002) 'Solid lipid nanoparticles (SLN) and nanostructured lipid carriers (NLC) in cosmetic and dermatological preparations', *Advanced Drug Delivery Reviews*. (Human skin: the Medium of Touch), 54, pp. S131–S155. doi: 10.1016/S0169-409X(02)00118-7.
- Mullineux, G. (2008) 'Non-linear least squares fitting of coefficients in the Herschel–Bulkley model', *Applied Mathematical Modelling*, 32(12), pp. 2538–2551. doi: 10.1016/j.apm.2007.09.010.
- Murgia, X., Loretz, B., Hartwig, O., Hittinger, M. and Lehr, C.-M. (2018) 'The role of mucus on drug transport and its potential to affect therapeutic outcomes', *Advanced Drug Delivery Reviews*. (Technological strategies to overcome the mucus barrier in mucosal drug delivery), 124, pp. 82–97. doi: 10.1016/j.addr.2017.10.009.
- Nasr, M. (2010) 'In vitro and in vivo evaluation of proniosomes containing celecoxib for oral administration', *AAPS PharmSciTech*, 11(1), pp. 85–89. doi: 10.1208/s12249-009-9364-5.
- Nasseri, B. (2005) 'Effect of cholesterol and temperature on the elastic properties of niosomal membranes', *International Journal of Pharmaceutics*, 300(1–2), pp. 95–101. doi: 10.1016/j.ijpharm.2005.05.009.
- Nguyen, A. T., Lewin, P. A. and Wrenn, S. P. (2015) 'Hydrophobic drug concentration affects the acoustic susceptibility of liposomes', *Biochimica et Biophysica Acta (BBA) - General Subjects*, 1850(4), pp. 667–672. doi: 10.1016/j.bbagen.2014.11.001.
- Obeid, M. A., Gebiril, A. M., Tate, R. J., Mullen, A. B. and Ferro, V. A. (2017) 'Comparison of the physical characteristics of monodisperse non-ionic surfactant vesicles (NISV) prepared using different manufacturing methods', *International Journal of Pharmaceutics*, 521(1), pp. 54–60. doi: 10.1016/j.ijpharm.2017.02.007.
- Obeid, M. A., Khadra, I., Albaloushi, A., Mullin, M., Alyamani, H. and Ferro, V. A. (2019) 'Microfluidic manufacturing of different niosomes nanoparticles for curcumin encapsulation: Physical characteristics, encapsulation efficacy, and drug release', *Beilstein Journal of Nanotechnology*, 10, pp. 1826–1832. doi: 10.3762/bjnano.10.177.
- Obeid, M. A., Khadra, I., Mullen, A. B., Tate, R. J. and Ferro, V. A. (2017) 'The effects of hydration media on the characteristics of non-ionic surfactant vesicles (NISV) prepared by microfluidics', *International Journal of Pharmaceutics*, 516(1), pp. 52–60. doi: 10.1016/j.ijpharm.2016.11.015.
- Ong, S. G. M., Ming, L. C., Lee, K. S. and Yuen, K. H. (2016) 'Influence of the encapsulation efficiency and size of liposome on the oral bioavailability of griseofulvin-loaded liposomes', *Pharmaceutics*. Multidisciplinary Digital Publishing Institute, 8(3), p. 25. doi: 10.3390/pharmaceutics8030025.
- Ottino, J. M. (1990) 'Mixing, chaotic advection, and turbulence', 22, p. 48.

- Pearson, J. P., Allen, A. and Hutton, D. A. (2000) 'Rheology of mucin', in Corfield, A. P. (ed.) *Glycoprotein Methods and Protocols*. Totowa, NJ: Humana Press, pp. 99–109. doi: 10.1385/1-59259-048-9:099.
- Peppas, N. A. and Huang, Y. (2004) 'Nanoscale technology of mucoadhesive interactions', *Advanced Drug Delivery Reviews*, 56(11), pp. 1675–1687. doi: 10.1016/j.addr.2004.03.001.
- Peppas, N. A., Thomas, J. B. and McGinty, J. (2009) 'Molecular aspects of mucoadhesive carrier development for drug delivery and improved absorption', *Journal of Biomaterials Science, Polymer Edition*, 20(1), pp. 1–20. doi: 10.1163/156856208X393464.
- Pinto, J. F. (2010) 'Site-specific drug delivery systems within the gastro-intestinal tract: from the mouth to the colon', *International Journal of Pharmaceutics*, 395(1–2), pp. 44–52. doi: 10.1016/j.ijpharm.2010.05.003.
- Prego, C., Torres, D. and Alonso, M. J. (2005) 'The potential of chitosan for the oral administration of peptides', *Expert Opinion on Drug Delivery*. Taylor & Francis, 2(5), pp. 843–854. doi: 10.1517/17425247.2.5.843.
- Prescott, L. F. (1974) 'Gastric emptying and drug absorption', *British Journal of Clinical Pharmacology*, 1(3), pp. 189–190. doi: 10.1111/j.1365-2125.1974.tb00234.x.
- Raina, S. A., Van Eerdenbrugh, B., Alonzo, D. E., Mo, H., Zhang, G. G. Z., Gao, Y. and Taylor, L. S. (2015) 'Trends in the precipitation and crystallization behavior of supersaturated aqueous solutions of poorly water-soluble drugs assessed using synchrotron radiation', *Journal of Pharmaceutical Sciences*, 104(6), pp. 1981–1992. doi: 10.1002/jps.24423.
- Ravalika, V. and Sailaja, A. K. (2017) 'Formulation and evaluation of etoricoxib niosomes by thin film hydration technique and ether injection method', *Nano Biomedicine and Engineering*, 9(3), pp. 242–248. doi: 10.5101/nbe.v9i3.p242-248.
- Rinaldi, F., Hanieh, P. N., Imbriano, A., Passeri, D., Del Favero, E., Rossi, M., Marianecchi, C., De Panfilis, S. and Carafa, M. (2020) 'Different instrumental approaches to understand the chitosan coated niosomes/mucin interaction', *Journal of Drug Delivery Science and Technology*, 55, p. 101339. doi: 10.1016/j.jddst.2019.101339.
- Roces, C. B., Christensen, D. and Perrie, Y. (2020) 'Translating the fabrication of protein-loaded poly(lactic-co-glycolic acid) nanoparticles from bench to scale-independent production using microfluidics', *Drug Delivery and Translational Research*. doi: 10.1007/s13346-019-00699-y.
- Roces, C. B., Kastner, E., Stone, P., Lowry, D. and Perrie, Y. (2016) 'Rapid quantification and validation of lipid concentrations within liposomes', *Pharmaceutics*, 8(3). doi: 10.3390/pharmaceutics8030029.
- Roger, E., Lagarce, F., Garcion, E. and Benoit, J.-P. (2010) 'Biopharmaceutical parameters to consider in order to alter the fate of nanocarriers after oral delivery', *Nanomedicine*, 5(2), pp. 287–306. doi: 10.2217/nnm.09.110.

Rossi, S., Bonferoni, M. C., Lippoli, G., Bertoni, M., Ferrari, Fr., Caramella, C. and Conte, U. (1995) 'Influence of mucin type on polymer-mucin rheological interactions', *Biomaterials*, 16(14), pp. 1073–1079. doi: 10.1016/0142-9612(95)98903-R.

Salazar, J., Müller, R. H. and Möschwitzer, J. P. (2014) *Combinative particle size reduction technologies for the production of drug nanocrystals*, *Journal of Pharmaceutics*. Hindawi. doi: <https://doi.org/10.1155/2014/265754>.

Sarmiento, B., Ribeiro, A., Veiga, F., Sampaio, P., Neufeld, R. and Ferreira, D. (2007) 'Alginate/chitosan nanoparticles are effective for oral insulin delivery', *Pharmaceutical Research*, 24(12), pp. 2198–2206. doi: 10.1007/s11095-007-9367-4.

Sassene, P. J., Mosgaard, M. D., Löbmann, K., Mu, H., Larsen, F. H., Rades, T. and Müllertz, A. (2015) 'Elucidating the molecular interactions occurring during drug precipitation of weak bases from lipid-based formulations: a case study with cinnarizine and a long chain self-nanoemulsifying drug delivery system', *Molecular Pharmaceutics*. American Chemical Society, 12(11), pp. 4067–4076. doi: 10.1021/acs.molpharmaceut.5b00498.

Schultz, H. B., Meola, T. R., Thomas, N. and Prestidge, C. A. (2020) 'Oral formulation strategies to improve the bioavailability and mitigate the food effect of abiraterone acetate', *International Journal of Pharmaceutics*, 577, p. 119069. doi: 10.1016/j.ijpharm.2020.119069.

Sebaaly, C., Greige-Gerges, H., Stainmesse, S., Fessi, H. and Charcosset, C. (2016) 'Effect of composition, hydrogenation of phospholipids and lyophilization on the characteristics of eugenol-loaded liposomes prepared by ethanol injection method', *Food Bioscience*, 15, pp. 1–10. doi: 10.1016/j.fbio.2016.04.005.

Sezgin-Bayindir, Z., Antep, M. N. and Yuksel, N. (2014) 'Development and characterization of mixed niosomes for oral delivery using candesartan cilexetil as a model poorly water-soluble drug', *AAPS PharmSciTech*, 16(1), pp. 108–117. doi: 10.1208/s12249-014-0213-9.

Shabir, G. A. (2005) 'Step-by-step analytical methods validation and protocol in the quality system compliance industry', p. 11.

Shaikh, R., Raj Singh, T. R., Garland, M. J., Woolfson, A. D. and Donnelly, R. F. (2011) 'Mucoadhesive drug delivery systems', *Journal of Pharmacy and Bioallied Sciences*, 3(1), pp. 89–100. doi: 10.4103/0975-7406.76478.

Shalaev, E., Wu, K., Shamblin, S., Krzyzaniak, J. F. and Descamps, M. (2016) 'Crystalline mesophases: Structure, mobility, and pharmaceutical properties', *Advanced Drug Delivery Reviews*. (Amorphous pharmaceutical solids), 100, pp. 194–211. doi: 10.1016/j.addr.2016.04.002.

Shehata, T. M., Abdallah, M. H. and Ibrahim, M. M. (2015) 'Proniosomal oral tablets for controlled delivery and enhanced pharmacokinetic properties of acemetacin', *AAPS PharmSciTech*, 16(2), pp. 375–383. doi: 10.1208/s12249-014-0233-5.

- Shilakari Asthana, G., Sharma, P. K. and Asthana, A. (2016) 'In vitro and in vivo evaluation of niosomal formulation for controlled delivery of clarithromycin', *Scientifica*. Hindawi, 2016, p. e6492953. doi: 10.1155/2016/6492953.
- Sigurdsson, H. H., Kirch, J. and Lehr, C.-M. (2013) 'Mucus as a barrier to lipophilic drugs', *International Journal of Pharmaceutics*. (Poorly Soluble Drugs), 453(1), pp. 56–64. doi: 10.1016/j.ijpharm.2013.05.040.
- Singh, B. N. and Kim, K. H. (2000) 'Floating drug delivery systems: an approach to oral controlled drug delivery via gastric retention', *Journal of Controlled Release*, 63(3), pp. 235–259. doi: 10.1016/S0168-3659(99)00204-7.
- Siqueira, S. D. V. S., Müllertz, A., Gräeser, K., Kasten, G., Mu, H. and Rades, T. (2017) 'Influence of drug load and physical form of cinnarizine in new SNEDDS dosing regimens: in vivo and in vitro evaluations', *The AAPS Journal*, 19(2), pp. 587–594. doi: 10.1208/s12248-016-0038-4.
- Sogias, I. A., Williams, A. C. and Khutoryanskiy, V. V. (2008) 'Why is chitosan mucoadhesive?', *Biomacromolecules*, 9(7), pp. 1837–1842. doi: 10.1021/bm800276d.
- Sonia, T. A. and Sharma, C. P. (2011) 'Chitosan and its derivatives for drug delivery perspective', in Jayakumar, R., Prabakaran, M., and Muzzarelli, R. A. A. (eds) *Chitosan for Biomaterials I*. Berlin, Heidelberg: Springer Berlin Heidelberg, pp. 23–53. doi: 10.1007/12_2011_117.
- Stroock, A. D. (2002) 'Chaotic Mixer for Microchannels', *Science*, 295(5555), pp. 647–651. doi: 10.1126/science.1066238.
- Strous, G. J. and Dekker, J. (1992) 'Mucin-type glycoproteins', *Critical Reviews in Biochemistry and Molecular Biology*, 27(1–2), pp. 57–92. doi: 10.3109/10409239209082559.
- Takeuchi, H., Yamamoto, H. and Kawashima, Y. (2001) 'Mucoadhesive nanoparticulate systems for peptide drug delivery', *Advanced Drug Delivery Reviews*. (Nanoparticulate Systems for Improved Drug Delivery), 47(1), pp. 39–54. doi: 10.1016/S0169-409X(00)00120-4.
- Tan, A., Hong, L., Du, J. D. and Boyd, B. J. (2019) 'Self-Assembled Nanostructured Lipid Systems: Is There a Link between Structure and Cytotoxicity?', *Advanced Science*, 6(3), p. 1801223. doi: 10.1002/advs.201801223.
- Taymouri, S. and Varshosaz, J. (2016) 'Effect of different types of surfactants on the physical properties and stability of carvedilol nano-niosomes', *Advanced Biomedical Research*, 5(1), p. 48. doi: 10.4103/2277-9175.178781.
- Tokumura, T., Ichikawa, T., Sugawara, N., Tatsuishi, K., Kayano, M., Machida, Y., Hoshida, H. and Nagai, T. (1985) 'Kinetics of degradation of cinnarizine in aqueous solution', *Chem. Pharm. Bull.*, 33(5), pp. 2069–2072.
- Trenkenschuh, E. and Friess, W. (2021) 'Freeze-drying of nanoparticles: How to overcome colloidal instability by formulation and process optimization', *European*

Journal of Pharmaceutics and Biopharmaceutics, 165, pp. 345–360. doi: 10.1016/j.ejpb.2021.05.024.

Uchegbu, I. F. and Florence, A. T. (1995) 'Non-ionic surfactant vesicles (niosomes): physical and pharmaceutical chemistry', *Advances in colloid and interface science*, 58(1), pp. 1–55.

Uchegbu, I. F. and Vyas, S. P. (1998) 'Non-ionic surfactant based vesicles (niosomes) in drug delivery', *International Journal of Pharmaceutics*, 172(1–2), pp. 33–70. doi: 10.1016/S0378-5173(98)00169-0.

Uthaiwat, P., Priprem, A., Puthongking, P., Daduang, J., Nukulkit, C., Chio-Srichan, S., Boonsiri, P. and Thapphasaraphong, S. (2021) 'Characteristic evaluation of gel formulation containing niosomes of melatonin or its derivative and mucoadhesive properties using ATR-FTIR spectroscopy', *Polymers. Multidisciplinary Digital Publishing Institute*, 13(7), p. 1142. doi: 10.3390/polym13071142.

Varshosaz, J., Pardakhty, A., Hajhashemi, V. and Najafabadi, A. R. (2003) 'Development and physical characterization of sorbitan monoester niosomes for insulin oral delivery', *Drug Delivery*, 10(4), pp. 251–262. doi: 10.1080/drd_10_4_251.

de Waard, H., Frijlink, H. W. and Hinrichs, W. L. J. (2011) 'Bottom-up preparation techniques for nanocrystals of lipophilic drugs', *Pharmaceutical Research*, 28(5), pp. 1220–1223. doi: 10.1007/s11095-010-0323-3.

Wang, Z. and Fingas, M. (1994a) 'Analysis of sorbitan ester surfactants. Part I: High performance liquid chromatography', *Journal of High Resolution Chromatography*, 17(1), pp. 15–19.

Wang, Z. and Fingas, M. (1994b) 'Analysis of sorbitan ester surfactants. Part II: Capillary supercritical fluid chromatography', *Journal of High Resolution Chromatography*, 17(2), pp. 85–90. doi: 10.1002/jhrc.1240170208.

Wilson, C. G. and Washington, N. (1989) 'The stomach: its role in oral drug delivery', in *Physiological pharmaceutical: biological barriers to drug absorption*. 1st ed. Ellis Horwood, pp. 47–70.

Wu, L., Zhang, J. and Watanabe, W. (2011) 'Physical and chemical stability of drug nanoparticles', *Advanced Drug Delivery Reviews*. (Nanodrug Particles and Nanoformulations for Drug Delivery), 63(6), pp. 456–469. doi: 10.1016/j.addr.2011.02.001.

Xu, X., Khan, M. A. and Burgess, D. J. (2011) 'A quality by design (QbD) case study on liposomes containing hydrophilic API: I. Formulation, processing design and risk assessment', *International Journal of Pharmaceutics*, 419(1), pp. 52–59. doi: 10.1016/j.ijpharm.2011.07.012.

Xu, X., Khan, M. A. and Burgess, D. J. (2012) 'Predicting hydrophilic drug encapsulation inside unilamellar liposomes', *International Journal of Pharmaceutics*, 423(2), pp. 410–418. doi: 10.1016/j.ijpharm.2011.12.019.

- Xu, Z., Lu, C., Riordon, J., Sinton, D. and Moffitt, M. G. (2016) 'Microfluidic manufacturing of polymeric nanoparticles: comparing flow control of multiscale structure in single-phase staggered herringbone and two-phase reactors', *Langmuir*, 32(48), pp. 12781–12789. doi: 10.1021/acs.langmuir.6b03243.
- Yeo, L., Chaw, C. and Elkordy, A. (2019) 'The effects of hydration parameters and co-surfactants on methylene blue-loaded niosomes prepared by the thin film hydration method', *Pharmaceuticals*, 12(2), p. 46. doi: 10.3390/ph12020046.
- Yoshioka, T., Sternberg, B. and Florence, A. T. (1994) 'Preparation and properties of vesicles (niosomes) of sorbitan monoesters (Span 20, 40, 60 and 80) and a sorbitan triester (Span 85)', *International Journal of Pharmaceutics*, 105(1), pp. 1–6. doi: 10.1016/0378-5173(94)90228-3.
- Yu, L. X. and Amidon, G. L. (1999) 'A compartmental absorption and transit model for estimating oral drug absorption', *International Journal of Pharmaceutics*, 186(2), pp. 119–125. doi: 10.1016/S0378-5173(99)00147-7.
- Zheng, C., Li, Y., Peng, Z., He, X., Tao, J., Ge, L., Sun, Y. and Wu, Y. (2020) 'A composite nanocarrier to inhibit precipitation of the weakly basic drug in the gastrointestinal tract', *Drug Delivery*, 27(1), pp. 712–722. doi: 10.1080/10717544.2020.1760402.
- Zhigaltsev, I. V., Belliveau, N., Hafez, I., Leung, A. K. K., Huft, J., Hansen, C. and Cullis, P. R. (2012) 'Bottom-up design and synthesis of limit size lipid nanoparticle systems with aqueous and triglyceride cores using millisecond microfluidic mixing', *Langmuir*, 28(7), pp. 3633–3640. doi: 10.1021/la204833h.
- Zhong, Z., Ji, Q. and Zhang, J. A. (2010) 'Analysis of cationic liposomes by reversed-phase HPLC with evaporative light-scattering detection', *Journal of Pharmaceutical and Biomedical Analysis*, 51(4), pp. 947–951. doi: 10.1016/j.jpba.2009.10.001.